

Dissertation zur Erlangung des Doktorgrades
der Fakultät für Chemie und Pharmazie
der Ludwig-Maximilians-Universität München

Regulation of Viral and Cellular Gene Expression upon Lytic Murine Cytomegalovirus Infection



Lisa Kristina Marcinowski

aus Ludwigshafen am Rhein, Deutschland

2012

Erklärung

Diese Dissertation wurde im Sinne von §7 der Promotionsordnung vom 28. November 2011 von Herrn Prof. Koszinowski betreut und von Herrn Prof. Förstemann von der Fakultät für Chemie und Pharmazie vertreten.

Ehrenwörtliche Versicherung

Diese Dissertation wurde eigenständig und ohne unerlaubte Hilfe erarbeitet.

München, den

.....
(Unterschrift des Autors)

Dissertation eingereicht am:
Erstgutachter: Prof. Dr. Klaus Förstemann
Zweitgutachter: Prof. Dr. Ulrich Koszinowski
Tag der mündlichen Prüfung: 13.06.2012

Contents

Acknowledgements	IV
Summary	VI
Publications	VIII
General Introduction	9
I.1 Cytomegalovirus	9
I.1.1 Life cycle.....	9
I.1.2 Gene expression cascade	10
I.1.3 Modulation of host cell gene expression.....	11
I.2 Gene expression profiling	12
I.2.1 Problems of standard gene expression analysis	12
I.2.2 Metabolic labeling of newly transcribed RNA.....	13
I.3 microRNAs.....	14
I.3.1 miRNAs as key regulators of cellular gene expression.....	14
I.3.2 miRNAs and herpesvirus infection	15
I.4 Aims of this thesis	17
Real-time transcriptional profiling of cellular and viral gene expression during lytic cytomegalovirus infection	18
II.1 Introduction	18
II.2 Materials and Methods	21
II.3 Results	26
II.4 Discussion	42
Degradation of cellular miR-27 by a novel, highly abundant viral transcript is important for efficient virus replication in vivo	47
III.1 Introduction	47
III.2 Materials and Methods	50
III.3 Results	58
III.4 Discussion	75
List of figures and tables	79
List of abbreviations	81
References	87

Supplementary Tables.....Appendix

Acknowledgements

Die Zeit der Promotion war für mich ein sehr intensiver, erfahrungs- und lehrreicher Lebensabschnitt. Deshalb möchte ich mich bei den Menschen, die diese ermöglicht haben, die Zeit so interessant und bewegend gemacht haben, sowie mich auf diesem Weg begleitet und unterstützt haben, bedanken.

Als erstes möchte ich mich bei meinem Betreuer Lars Dölken danken. Vielen Dank, dass du mir im Laboralltag so viel Freiheit in der Gestaltung und Planung meiner Projekte gegeben hast und in den richtigen Momenten unterstützend, ermutigend und mit Ratschlägen da warst. Du hast es immer wieder geschafft, mich weiter zu fördern und zu fordern und mir zu helfen mich weiter zu entwickeln. Vielen Dank auch für deine Geduld, mir Ideen näher zu bringen, und dein Vertrauen in meine Arbeit.

Bei meinem Doktorvater Ulrich Koszinowski möchte ich mich herzlich für die Begleitung durch meine Doktorarbeit bedanken. Vielen Dank für die Ratschläge und Unterstützung während meiner Doktorarbeit sowie das Teilen von Erfahrungswerten für die Arbeit in der Wissenschaft im Allgemeinen. Vielen Dank, dass ich immer mit Fragen und Wünschen zu Ihnen kommen durfte.

Ich möchte mich bei Zsolt Ruzsics bedanken, dass ich ihn immer um Rat fragen durfte, wenn ich bei meinen Projekten nicht mehr weiter wusste und für die vielen fruchtbaren Diskussionen.

Des Weiteren möchte ich mich bei allen Kooperationspartnern sowie Studenten bedanken, die mitgewirkt haben, dass meine Doktorarbeit so erfolgreich und spannend geworden ist.

Bei meinen Arbeitskollegen, aus der AG Koszinowski sowie Conzelmann, möchte ich mich für die vielen Hilfestellungen, Ratschläge und das gute Arbeitsklima bedanken.

Hierbei möchte ich mich bei einigen persönlich bedanken:

Bernd (Rädle), danke, dass du den Laboralltag so angenehm gemacht hast und wir so viel Spaß im Labor und auch außerhalb des Labors hatten. Stefan (Jordan) und Jens (Bosse), vielen Dank für die vielen Diskussionen und Ideen sowie lustige, unvergessliche Abende!

Simone (Boos), vielen Dank, dass du mir immer wieder gezeigt hast, dass es noch andere

wichtige Dinge im Leben außer den Laboralltag gibt und für entspannte Pausen und wundervolle Gespräche. Ich freue mich schon auf unsere Zeit nach der Doktorarbeit!

Martina (Rieder), vielen Dank für die unzähligen Western Blots! Danke, dass du immer an meiner (linken) Seite warst, für die unvergesslichen Kaffeepausen, dass du immer unterstützende Worte für mich hattest und dass wir so gute Freunde geworden sind!

Michi (Lidschreiber), danke für deine Geduld, mir die Bionformatik näher zu bringen, und dein Interesse ein Projekt mit mir zusammen durchzuziehen und vielen Dank, dass du immer für ein Feierabendbier und tolle Gespräche zu haben bist.

Katja (Fruehauf), vielen Dank, dass du schon so lange mit mir durchs Leben gehst und für mich da bist! Danke, dass du die Zeit der Promotion mit mir durchlebt hast, immer mit objektiven Ratschlägen und Unterstützung an meiner Seite stehst und mir geholfen hast mich weiter zu entwickeln.

Ich möchte mich bei meinen Freunden bedanken, die mir immer so viel Kraft und Energie geben und mir geholfen haben auch mal Abstand von der Arbeit zu bekommen. Danke, dass es euch gibt!

Vor allem möchte ich mich hierbei bei den „Mädels“ bedanken. Vielen Dank Julia, Petra, Becky, Clare, Natalie, Janina und Prisca, dass ihr mir alle auf eure ganz besondere Weise, immer mit eurer Freundschaft Kraft und Unterstützung gebt .

Bei meinen Brüdern möchte ich mich bedanken, dass sie immer an meiner Seite sind, mich auffangen und unterstützen! Es ist so schön, dass es euch gibt!

Bei meinen Eltern möchte ich mich von ganzem Herzen bedanken, dass sie immer hinter mir stehen und mich während meiner Doktorarbeit großartig unterstützt haben.

Zu allerletzt möchte ich noch Dinge betonen, die mir während meiner Doktorarbeit immer Kraft gegeben haben: Musik, die mich immer durch den Laboralltag „getragen“ hat, Reisen, die mir immer neue Energie und Erfahrungen gebracht haben und die wundervolle Stadt München!

Summary

Herpesviruses are large DNA viruses which have evolved in close association with their hosts over millions of years. Following primary infection, they persist in the form of latency posing the constant risk of reactivation and disease. Herpesviruses have developed a multitude of mechanisms to escape antiviral host mechanisms and reprogram cellular gene expression to support efficient virus replication, life-long maintenance (latency) as well as efficient reactivation thereof. Hence, herpesvirus infections are ideal models for studying key cellular mechanisms involved in the regulation of gene expression and innate and adaptive immunity.

This thesis reports on transcriptional and post-transcriptional regulations of cellular and viral gene expression during lytic murine cytomegalovirus infection.

Topic I

Real-time transcriptional profiling of cellular and viral gene expression during lytic cytomegalovirus infection

During lytic viral infection the cellular gene expression profile is subjected to dramatic changes induced by both viral and antiviral mechanisms. Many of these changes are only very transient and thus hard to dissect using standard gene expression analysis on total cellular RNA. We employed metabolic labelling of newly transcribed RNA using 4-thiouridine (4sU-tagging) coupled to quantitative real-time PCR (qRT-PCR), microarray analysis and RNA-Sequencing (RNA-Seq) to study the real-time kinetics of transcriptional activities during lytic murine cytomegalovirus (MCMV) infection. Microarray profiling on newly transcribed RNA during the first six hours of MCMV infection revealed discrete functional clusters of cellular genes regulated with distinct kinetics at surprising temporal resolution. Among others, this included a rapid inflammatory/interferon-response; a transient DNA-damage-response and a delayed endoplasmic reticulum (ER)-stress-response, which were all rapidly counter-regulated by the virus, implying the involvement of novel viral regulators. It is important to note that most of these changes as well as their temporal order (the rapid counter-regulations in particular) were inherently undetectable by conventional total RNA purification. Promoter analysis revealed strong associations of distinct transcription factors with each functional cluster. Furthermore, metabolic labeling and purification of newly transcribed RNA provided access to the real-time kinetics of viral gene expression in the absence of any interfering virion-associated RNA. This revealed three surprising findings. First, both, qRT-PCR and RNA-Seq analysis on newly transcribed RNA derived from various time frames of the whole

lytic virus life cycle revealed a peak of viral transcriptional activity at 1-2 hours post infection (hpi), including transcription of immediate-early, early and even well characterized late genes. Second, this peak of transcription was subject to rapid gene silencing until the onset of DNA replication, indicating the involvement of so far undisclosed molecular mechanism in the regulation of viral gene expression. Finally, transcriptional activity of some viral genes remained remarkably constant or even declined substantially despite the rapid onset of viral DNA replication, highlighting the importance of transcription factor activity and chromatin status rather than DNA copy number in regulating viral gene expression. In summary, this study pioneers real-time transcriptional analysis during lytic herpesvirus infection and highlights numerous novel regulatory aspects of virus host-cell interaction.

Topic II

Degradation of cellular miR-27 by a novel, highly abundant viral transcript is important for efficient virus replication *in vivo*

MicroRNAs (miRNAs) are small non-coding RNAs which regulate expression of various genes on post-transcriptional level. While the mechanism how miRNA repress transcription of their target genes is more and more understood, little is known about mechanisms how miRNA by themselves are regulated and degraded in particular. In this work we studied the mechanism behind rapid degradation of two cellular miRNAs, namely miR-27a/b, we observed during lytic MCMV infection. Using a set of virus deletion mutants, miR-27a and miR-27b were found to be targeted for degradation by a highly abundant viral protein-coding transcript with an additional non-coding RNA function, namely m169. This is mediated via a single miR-27 binding site in its 3' untranslated region (UTR). This function could be efficiently retargeted to other cellular and viral miRNAs by miRNA target site replacement. Furthermore, the degradation of miR-27 was preceded by 3'-tailing and trimming as well as displacement of tailed miRNAs from Argonaute 2 complexes. Despite the rapid degradation of miR-27 by m169 we found this interaction to mutual resulting in miR-27-mediated repression of m169 protein expression. Most importantly, three mutant viruses which were no longer able to target miR-27a/b, either due to miRNA target site disruption or target site replacement, showed significant attenuation in multiple organs as early as 4 days post infection. This indicates that the miR-27/m169 interaction and degradation of miR-27a/b is important for efficient MCMV replication *in vivo*. In summary, these findings describe the degradation of two cellular miRNAs by an abundant viral transcript revealing a novel mechanism by which MCMV alters the host cell miRNA machinery for its own needs.

Publications

Part of this work has been published or is in the process of being published.

Lisa Marcinowski, Michael Lidschreiber, Lukas Windhager, Martina Rieder, Jens B. Bosse, Bernd Rädle, Thomas Bonfert, Ildiko Györy, Olivia Prazeres da Costa, Philip Rosenstiel, Caroline C. Friedel, Ralf Zimmer, Zsolt Ruzsics, Lars Dölken

Real-time transcriptional profiling of cellular and viral gene expression during lytic cytomegalovirus infection.

Plos Pathogen (submitted) (2012).

Lisa Marcinowski^{*}, Mélanie Tanguy^{*}, Astrid Krmpotic^{*}, Bernd Rädle, Vanda J Lisnić, Lee Tuddenham, Béatrice Chane-Woon-Ming, Zsolt Ruzsics, Florian Erhard, Corinna Benkartek, Marina Babic, Ralf Zimmer, Joanne Trgovcich, Ulrich Koszinowski, Stipan Jonjic, Sébastien Pfeffer, Lars Dölken (2012).

Degradation of cellular miR-27 by a novel, highly abundant viral transcript is important for efficient virus replication *in vivo*.

Plos Pathogen 8(2):e1002510.

Further publications related to the thesis:

Miller C, Schwalb B, Maier K, Schulz D, Dümcke S, Zacher B, Mayer A, Sydow J, **Marcinowski L**, Dölken L, Martin DE, Tresch A, Cramer P. 2011. Dynamic transcriptome analysis measures rates of mRNA synthesis and decay in yeast. *Mol Syst Biol*, 7:458

Dölken L, Krmpotic A, Kothe S, Tuddenham L, Tanguy M, **Marcinowski L**, Ruzsics Z, Elefant N, Altuvia Y, Margalit H, Koszinowski UH, Jonjic S, Pfeffer S. 2010. Cytomegalovirus microRNAs facilitate persistent virus infection in salivary glands. *PLoS Pathogen*, 6 (10)

Dölken L, Malterer G, Erhard F, Kothe S, Friedel CC, Suffert G, **Marcinowski L**, Motsch N, Barth S, Beitzinger M, Lieber D, Bailer SM, Hoffmann R, Ruzsics Z, Kremmer E, Pfeffer S, Zimmer R, Koszinowski UH, Grässer F, Meister G, Haas J. 2010. Systematic analysis of viral and cellular microRNA targets in cells latently infected with human gamma-herpesvirus by RISC immunoprecipitation assay. *Cell Host Microbe*, 7 (4)

Buck AH, Perot J, Chisholm MA, Kumar DS, Tuddenham L, Cognat V, **Marcinowski L**, Dölken L, Pfeffer S. 2010. Post-transcriptional regulation of miR-27 in murine cytomegalovirus infection. *RNA*, 16 (2)

General Introduction

I.1 Cytomegalovirus

Herpesviridae represent a family of large double-stranded DNA viruses which can be subdivided into alpha-, beta- and gamma-herpesvirinae based on biological properties, such as host range and length of reproductive cycle [1]. The human Cytomegalovirus (HCMV) is the best-studied member of the beta-herpesvirinae. Like all other herpesviruses, HCMV shares the ability to persist for life in the human host in latent form with the risk for reactivation and disease. While primary infection is usually asymptomatic, reactivation may result in life-threatening disease in immunocompromised patients and for the fetus during pregnancy. Due to its broad cell tropism HCMV reactivation is able to affect almost every organ of the body with pneumonia, colitis, retinitis (in AIDS patients) and deafness (following congenital infection) being the most common clinical presentations (reviewed in [2]).

I.1.1 Life cycle

The lifecycle of CMV can be divided into a lytic and a latent phase. In the lytic phase a plethora of viral proteins and new infectious particles are produced, in the latent phase viral production ceases and only a very small set of viral latency-associated genes are expressed.

In general, CMV binds to specific cell surface receptors and the viral envelope fuses with cellular membranes leading to the release of capsids into the cytoplasm. These capsids are then transferred into the nucleus, facilitated by cytoplasmic microtubules [3]. In the nucleus, the cellular and viral protein machineries manufacture new viral DNA and proteins. After autocatalytic assembly of the capsids in the nucleus, newly synthesized viral genomes are encapsidated. The nucleocapsid is then translocated to the cytoplasm by budding through the inner nuclear membrane. Together with the fusion of the primary envelope with the outer membrane and the release of the nucleocapsid into the cytoplasm, this process is called nuclear egress. In a next step, tegumentation and secondary envelopment take place. This includes a complex interaction of cytoplasmatic tegument proteins with the nucleocapsid and the future envelope resulting in infectious virions (reviewed in [4]).

After a primary acute infection, herpesviruses can persist for a lifetime in their hosts in the

form of latency. During this latency, the lytic transcription program is suppressed, no infectious virus particles are produced and viral transcription is restricted to the expression of a few latency-associated transcripts [5]. Latency is interrupted by episodes of virus reactivation resulting in the biosynthesis and release of new virus particles. Extrinsic signals and conditions, such as immune cell depletion, allogenic transplantation and inflammatory disease states can trigger reactivation posing the risk of potentially life-threatening disease [6].

One critical step for the establishment of latency and reactivation into the lytic phase is the regulation of the viral MIE promoter (MIEP). This promoter region controls the expression of the major viral immediate early (IE) genes. Hence, activation and silencing of this promoter is a credible mechanism to control viral lytic gene expression since the IE genes are crucial for the activation of all other viral genes upon lytic infection [7]. Multiple cellular transcription factors regulate the MIEP. While, among others, NF- κ B, AP-1 and Sp1 have been shown to activate the MIEP, other cellular transcription factors like YY1 and ERF have been shown to repress the MIEP (reviewed in [8]). Interestingly, some of the transcriptional repressors, including YY1 and ERF, are transcription factors known to mediate transcriptional repression by recruitment of co-factors involved in post-translational modification of histones [9,10]. Hence, it is not surprising that ChIP assays showed the transcriptionally inactive MIEP, in latency, to be associated with markers of repressed chromatin and in contrast, the active MIEP with histone markers of transcriptional activation [11,12]. However, the mechanisms involved in the establishment of latency and the induction of reactivation are still not fully understood.

I.1.2 Gene expression cascade

Traditionally, CMV gene expression is categorized based on the time of synthesis during infection, thereby defining immediate early, early and late genes [13]. Once the viral DNA has entered the nucleus, transcription of immediate early genes, which require no protein synthesis for their expression, is initiated. As mentioned above, the MIEP controls the production of mRNAs encoding the viral major immediate early (IE) proteins. Furthermore, tegument proteins from the incoming particles act as viral transcription factors and can modulate IE gene expression [14]. The IE proteins then induce the expression of early genes which are in general transcribed prior to DNA replication. Proteins translated by that time are mainly important to modulate the host cell to favor and to establish viral replication [15]. Following the initiation of viral DNA replication, late gene expression is started. There are

two groups of late genes, the leaky-late genes expressed at low levels in early infection and dramatically up-regulated at late times and the “true” late genes expressed exclusively after viral DNA replication. These genes are required for assembly and egress and result in the production and release of infectious virus particles [16]. The mechanisms restricting viral late gene expression to after DNA replication is still poorly understood. One major reason is the difficulty to recapitulate the appropriate kinetic regulation of late genes in cell culture. However, improvements and novel methods in the field of gene expression analysis will give rise to a more accurate picture of the complexity of CMV late gene regulation.

I.1.3 Modulation of host cell gene expression

Compared to other herpesviruses, the infection cycle of CMV is slow and no host shut-off takes place. Thus, viral modulation of the cell has to be very effective. Hence, especially in the first hours of lytic CMV infection, various modulations of the cell take place. Following attachment to the cell the virus is subjected to recognition by pattern-recognition receptors (PRRs) resulting in an innate immune response by activation of various cellular signal transduction pathways and proinflammatory cytokine production (reviewed in [17]). CMV has gained the ability to manipulate this early host inflammatory response towards its own needs. Thereby, one important example of modulation of the host cell response by the virus is the interaction with the NF- κ B pathway. First, CMV activates the NF- κ B response resulting in favorable conditions for viral replication. However, later in infection CMV inhibits the NF- κ B response, thereby dampening the inflammatory host response [18,19]. In this context, it was recently shown that the MCMV M45 protein plays a role in inhibiting the NF- κ B response by proteasome-independent degradation of the NF- κ B essential modulator (NEMO) leading to a novel mechanism of overcoming the host immune response [20]. As additional means of the virus, it has been hypothesized that stimulation of transcription factors by CMV in early infection is important for the subsequent viral replication. This is supported by a plethora of responsive DNA elements in the promoter/enhancer regions of CMV genes [21–25].

Like many other viruses, CMV dysregulates the host cell cycle machinery to its advantage. As such, CMV stimulates pro-proliferative cellular pathways, but once the infected cells reach the G1/S transition, the CMV IE2 protein inhibits further cell cycle progression by specifically blocking cellular DNA synthesis [26]. However, only DNA synthesis and cell division are blocked while other features of S-phase cells, such as an active nucleotide

metabolism and the expression of replication factors, are still induced [27]. At the same time, cell cycle checkpoints are by-passed [28,29] preventing apoptosis. All together this results in sufficient time for the virus to replicate in a favorable environment. CMV also encodes proteins to target apoptosis and thus to prevent cell death directly [30–32]. These anti-apoptotic effects of CMV may permit prolonged viral infection and perhaps also facilitate chronic inflammation.

During and after viral replication the cell is reprogrammed to support production and release of infectious viral particles. However, viral modulations of the host at late times of infection also lag far behind the understanding of viral-host interactions during early phase of infection.

I.2 Gene expression profiling

Gene expression profiling has enabled the simultaneous measurement of expression levels of thousands of genes in one RNA sample. Thereby, this analysis provides a genome-wide picture of the regulation of genes and pathways involved in many biological processes. RNA levels are determined by the interplay of tightly regulated processes for RNA production (transcription), processing (e.g. poly-adenylation or splicing) and degradation, resulting in a fine-tuned balance between RNA synthesis and decay which has to be considered when studying gene expression.

I.2.1 Problems of standard gene expression analysis

Numerous genome wide analyses have been performed on the progress of the cellular transcriptional response using total RNA. However, standard gene expression analyses on total RNA represent a static picture by only evaluating RNA abundance levels. This causes a number of problems. First, it is not easily possible to distinguish whether differentially expressed genes are regulated due to changes in transcription rate, RNA decay or a combination of both [33]. Second, fold changes detectable in total RNA do not reflect changes in RNA synthesis but are strongly dependent on transcript turnover rates, i.e. RNA half-lives. Therefore, the temporal resolution of gene expression studies on total RNA is rather low. To increase the detection level in standard gene expression, changes in total RNA levels are usually only analyzed hours after the initial stimulus was applied. Following such prolonged exposure, primary effects can no longer be distinguished from secondary

downstream effects [33]. In case short-term changes in gene expression are analyzed these are heavily biased for the detection of up-regulation of short-lived transcripts. As short-lived transcripts commonly encode for proteins with regulatory function substantial bias is introduced to all subsequent bioinformatics analyses.

In consequence, the fundamental character of the alteration analyzing total RNA often remains elusive unless studied by additional means. Drugs, such as Actinomycin D [34], or thermal inactivation of temperature sensitive RNA Polymerase II [35] can be employed to inhibit transcriptional activity and thus, to study RNA decay. However, these methods affect cell growth and are inherently cell invasive, resulting again in substantial experimental bias.

I.2.2 Metabolic labeling of newly transcribed RNA

Direct measurements of RNA production rates are required to overcome these problems. Metabolic labeling of RNA with 4-thiouridine (4sU), termed 4sU-tagging, allows the purification of newly transcribed RNA from total RNA. Transcriptional activities become directly accessible in a non-disruptive way by introducing 4sU, a naturally occurring uridine derivative, into newly transcribed RNA utilizing salvage pathways. Following isolation of total cellular RNA, it is thiol-specifically biotinylated allowing separation of newly transcribed RNA from the total RNA [36]. 4sU-tagging is applicable to a broad range of organisms allowing a very sensitive and unbiased detection of differentially expressed genes [36–38]. In this context, work of this PhD thesis contributed, in cooperation with the group of Prof. Cramer, to the establishment of 4sU-tagging in yeast [39].

By analyzing total RNA and newly transcribed RNA, e.g. by microarray or RNA-Seq, changes in gene expression can then be contributed to RNA synthesis or decay [40]. Alterations in newly transcribed RNA levels, which may not be visible in the total RNA at the same time, indicate changes in transcription rates, while changes in total RNA without a corresponding change in newly transcribed RNA are indicative of altered RNA stability [36]. Therefore, the temporal kinetics of the cell response to stimuli and to changes in conditions, such as viral infection, can now be properly studied. We thus applied 4sU-tagging to detail cellular and viral gene expression upon lytic infection of fibroblasts with the murine cytomegalovirus (MCMV).

I.3 MicroRNAs

MicroRNAs (miRNAs) are a large family of endogenous ~22-nt non-coding RNAs. These regulatory RNAs provide a unique level of post-transcriptional gene regulation by binding to mRNAs in a sequence-specific manner. First identified in *Caenorhabditis elegans*, miRNAs are expressed by all metazoans and plants as well as by several DNA viruses and modulate a range of fundamental cellular processes such as development, differentiation, growth, stress response, apoptosis and immune activation (reviewed in [41]). To date, more than 15,000 miRNAs have been annotated in over 140 species [42]. More than 45,000 miRNA target sites are computationally predicted in the 3' untranslated regions (UTRs) of human mRNAs, indicating that miRNAs control the activity of ~60 % of all protein-coding genes. Furthermore, a single miRNA can potentially target over 300 different transcripts [43]. Taken together, this illustrates the influence miRNAs can have on regulation of gene expression.

I.3.1 MicroRNAs as key regulators of cellular gene expression

MicroRNA biogenesis typically begins with the nuclear transcription of a long primary miRNA (pri-miRNA), which is either transcribed by RNA polymerase II from an independent gene or represents an intron of a protein-coding gene [44]. Pri-miRNAs contain a 5' cap, are polyadenylated and fold to produce one or more ~80-nt RNA hairpin structures. The hairpin structure is recognized and cleaved by the RNase III enzyme Droscha and its cofactor DGR8 to the precursor miRNA (pre-miRNA) in the nucleus. This pre-miRNA contains a 2-nt 3' overhang which is recognized by Exportin 5 leading to the transport of the pre-miRNA to the cytoplasm. There, the same overhang is recognized by another RNase III enzyme, Dicer, and its cofactor TRBP producing a ~22 bp miRNA duplex intermediate flanked by 2-nt 3' overhangs at each end [45,46]. The mature miRNA strand, the one which is less tightly base-paired at the 5' end, is then loaded into the RNA-induced silencing complex (RISC). The passenger strand, termed miRNA*, is degraded in the majority of cases. The RISC complex which is minimally composed of a mature miRNA and one of four Argonaute proteins (Ago1-4) then functions to target mRNAs. For the targeting the 2nd to 7th 5' nucleotides of the mature miRNA are important, termed the seed. Typically, the mature miRNA binds to complementary sequences found in the 3' UTRs of target mRNAs (reviewed in [41]). The base-pairing of the miRNA with the target sequence inhibits protein synthesis either by repressing translation or promoting mRNA deadenylation and decay [47].

MicroRNAs are subjected to ingenious control themselves. In the last few years, several reports have shown that miRNA biogenesis is heavily regulated. Hence, miRNAs regulate their own gene expression by autoregulatory feedback loops with specific transcription factors [48]. Furthermore, miRNA processing can be regulated by regulation of Drosha, Dicer and their co-factors. For example Dicer gets destabilized by dephosphorylation of its co-factor TRBP resulting in inhibition of pre-miRNA processing [49]. MicroRNA stability can also be affected. For example post-transcriptional addition of non-genome encoded nucleotides to the 3' end of either pre- or mature miRNAs results in protection or induction of degradation of miRNAs [50,51].

Downstream of miRNA biogenesis, on the level of miRNA function, the miRNA pathway is also extensively controlled. These regulations mainly occur on effector steps of repression by miRNAs, especially by regulation of the RISC complex core components. In this context, the Ago proteins are the most obvious targets for regulation. For example Ago2 is stabilized by the heat shock protein Hsp90 under certain conditions resulting in impaired miRNA silencing [52]. In contrast to the mentioned options to regulate the miRNA pathway, turnover of miRNAs and mechanisms to regulate decay of miRNAs are still poorly understood and under strong investigation.

I.3.2 MicroRNAs in herpesvirus infections

In contrast to viral proteins, miRNAs are non-immunogenic, require little coding capacity and can evolve rapidly to target new transcripts. Thus, miRNAs are ideal tools for viruses to modulate gene expression. In 2004, virally encoded miRNAs were discovered in members of the herpesvirus family [53]. So far, viral miRNAs have been identified in 6 human herpesviruses, including HCMV, Epstein-Barr-Virus (EBV), Kaposi's sarcoma-associated herpesvirus (KSHV), herpes simplex virus 1 and 2 (HSV-1/-2) and human herpesvirus 6B (HHV6B) as well as in many animal models including the two murine herpesviruses MCMV and murine herpesvirus 68 (MHV68) [54–59]. Thereby, work of this PhD thesis contributed to the first miRNA target atlas of the two human gamma-herpesviruses, Kaposi-Sarkoma-Virus and Epstein-Barr-Virus [60] as well as to the first functional phenotype of a viral miRNA knock-out virus [61].

The sequence-specific regulation of viral transcripts is easily achieved by herpesviruses through expression of antisense miRNAs. Hence, several latently expressed miRNAs upon HSV-1 infection are, for example, transcribed antisense to ICP0, which is a key immediate-

early HSV-1 transcriptional activator and probably inhibited by these miRNAs during latency [62].

Recently, the first direct and transcriptome-wide analyses of cellular herpesvirus miRNA targets were performed using Photoactivatable-Ribonucleoside-Enhanced Crosslinking and Immunoprecipitation (PAR-CLIP). For EBV and KSHV infection this resulted in the identification of several cellular pathways directly relevant for viral infection [63,64]. These studies and others showed that viral miRNAs target several cellular genes involved in cell proliferation, stress responses and antiviral defense pathways to favor the cellular environment for their needs. For KSHV it was for example shown that inhibition of apoptosis is supported by KSHV encoded miRNAs targeting caspase 3, important for apoptosis induction [65]. Interestingly, caspase 3 is not only targeted by one but by three KSHV encoded miRNAs indicating that cooperativity of viral miRNAs plays a role in targeting cellular mRNAs. MICB, another cellular protein, is targeted by several herpesvirus miRNAs, namely HCMV miR-UL112-1, KSHV miR-K7 and EBV miR-BART2, leading to a reduction on NK-cell mediated killing of infected cells [66,67]. MICB is the first gene found to be targeted by several herpesvirus miRNAs, which have no apparent sequence homology. Furthermore, HCMV miR-UL112-1 not only targets MICB but was also shown to have the potential to attenuate lytic replication of HCMV by targeting the IE72/IE1 transactivator [68], making it the first viral miRNA known to target both viral and cellular mRNAs.

Besides expressing their own miRNAs, these viruses also learned to utilize cellular miRNAs to aid their needs. Wang et al. showed that infection with HCMV results in a down-regulation of miR-100 and miR-101 which play an important role in mTOR-signaling regulation [69]. This manipulation of cellular miRNA expression favors the cellular environment for viral replication.

Recently, we reported on two cellular miRNAs, namely miR-27a and -b, to be targeted for degradation during lytic MCMV infection. Together with collaborators, we not only made the surprising observation that a viral gene is responsible for this function but that this interaction (m169 and miR-27) is indeed important for efficient virus replication *in vivo* [70]. During the course of this study the group of Joan Steitz reported *herpesvirus samirii*, an oncogenic monkey gamma-herpesvirus, to employ one of its non-coding RNA to specifically target the same two miRNAs, namely miR-27a/b, for degradation [71]. Elucidating why a murine beta-herpesvirus and an oncogenic gamma-herpesvirus independently learned to target the same two cellular miRNAs for degradation will certainly provide important insights into herpesvirus biology.

I.4 Aims of this thesis

CMV has acquired an extraordinary capacity to adapt to its host and has evolved numerous mechanisms to counteract the antiviral host defenses. Thus, CMV infection is an excellent model to study virus-host interactions. In this thesis the regulation of cellular and viral gene expression was studied at transcriptional and post-transcriptional level.

4sU-tagging was established for lytic MCMV infection of fibroblasts and coupled to qRT-PCR, microarray analysis and RNA-Seq to detail infection-induced changes in cellular transcription rates as well as rapid viral counter-regulation. As expected, due to the increase in temporal resolution, this revealed discrete functional networks of genes regulated with distinct kinetics and allowed an unbiased analysis of viral gene expression in absence of virion-associated RNAs.

There is increasing evidence that manipulation of cellular gene expression by both cellular and viral miRNAs is important in herpesvirus infections. At the beginning of this thesis, together with the labs of Sébastien Pfeffer and Amy Buck, we reported on the degradation of two cellular miRNAs, namely miR-27a/b, during lytic MCMV infection [70]. We hypothesized that this would be mediated by a viral gene product and thus screened large deletion mutants for the responsible gene. Once we had identified the gene, work focused on the underlying molecular mechanisms and the relevance of this interaction *in vivo*.

Real-time transcriptional profiling of cellular and viral gene expression during lytic cytomegalovirus infection

II.1 Introduction

Herpesviruses are large DNA viruses, which cause a broad range of disease ranging from the common cold sore to cancer. They all share the ability to establish a life-long, latent infection, leaving the infected individual at constant risk of reactivation and subsequent disease. The human cytomegalovirus (HCMV) poses a severe threat to immunocompromised patients and represents the most common infective cause of congenital disorders affecting about 1 in 1,000 newborns [72]. Like all herpesviruses, cytomegaloviruses (CMV) have co-evolved with their animal and human hosts for millions of years. During this time, they have mastered host-cell modulation to facilitate their needs and thus provide ideal tools to study many fundamental cellular processes.

Numerous signaling events are triggered during the first few hours of infection. As such, binding of CMV particles to the cell membrane and virus entry result in the activation of cellular signaling pathways, some of which, *e.g.* NF- κ B signaling, play an important role in initiating lytic viral infection [73–75]. Concomitantly, viral pathogen-associated molecular patterns are recognized by pattern-recognition receptors, resulting in robust activation of an innate immune response. Virion-associated proteins as well as the advent of viral gene expression then counteract intrinsic and arising host cell defense [15]. Several high-throughput studies addressed the transcriptional response of the cell to lytic CMV infection by analyzing temporal changes in total RNA levels [18,76–80]. These studies revealed lytic CMV infection altered expression of numerous cellular genes involved in a variety of processes including inflammation, innate immunity, cell cycle progression, cellular metabolism and cell adhesion.

One of the earliest events upon entry of the viral DNA into the nucleus is the deposition of viral genomes at nuclear domain (ND10) bodies [81,82]. This appears to be part of an intrinsic antiviral defense mechanism suppressing the expression of foreign DNA entering the nucleus [83]. In part, this is mediated by chromatin-remodeling enzymes recruited to these structures [84–86]. In HCMV infection, this intrinsic host defense is overcome by the viral tegument protein pp71 [87,88]. In lytic murine cytomegalovirus (MCMV) infection,

dispersion of ND10 bodies seems to be predominately mediated by the IE1 protein [89] and reviewed in [90]. In addition to disruption of ND10 body-mediated antiviral defense, the immediate-early proteins initiate the lytic replication cycle by facilitating the transcription of early genes [91,92]. The latter then modulate host cell environment, disarm the arising immune response, and establish the viral replication machinery. Upon viral DNA replication, viral late gene expression is initiated, culminating in the production and release of infectious virus particles [16].

The analysis of *de novo* early viral gene expression has been substantially hindered by large amounts of so called ‘virion-associated RNA’, unspecifically bound by the virus particles and delivered to the newly infected cell [93–96]. Chromatin immunoprecipitation (ChIP) has thus been employed to study the kinetics of viral transcriptional activity by looking at markers of active and inactive chromatin associated with the viral promoters. Immediately upon infection of permissive fibroblasts (at ‘pre-IE’ times of infection, using low multiplicities of infection) HCMV genomes become associated with markers of repressed chromatin [97]. As infection progresses, the chromatin status of viral promoters reflects the cascade of viral immediate-early, early and late gene expression [98,99].

Standard gene expression analysis (using total RNA) to study kinetics of transcriptional regulation has several limitations. First, short-term changes in total RNA levels do not match changes in transcription rates but are inherently dependent on the RNA half-life of the respective transcripts [36]. This strongly favors the detection of up-regulation of short-lived transcripts, commonly encoding for transcription factors and genes with regulatory function. This, in turn, may result in substantial bias in downstream bioinformatics analyses. Second, the temporal resolution - particularly for down-regulated genes - is rather low due to the relatively long median RNA half-life (5-10 h) in mammalian cells [33,100]. The same is true for detecting (viral) counter-regulation of cellular genes induced earlier in infection. Third, alterations in RNA synthesis rates cannot be differentiated from changes in RNA decay rates. Finally, transcriptional activity of the incoming CMV genomes cannot be definitively studied due to the presence of virion-associated RNA introduced to the newly infected cells by the incoming virus particles [95,101].

Recently, we developed an approach termed 4-thiouridine-(4sU)-tagging to purify newly transcribed RNA from total cellular RNA [36]. This is applicable to a broad range of organisms including vertebrates, drosophila and yeast [37,39]. In short, cells are cultured in presence of 4sU resulting in metabolic thiol-labeling of newly transcribed RNA. After isolation of total cellular RNA, RNA-incorporated 4sU is thiol-specifically biotinylated.

Labeled newly transcribed RNA is then efficiently purified from total RNA using streptavidin-coated magnetic beads. All three RNA fractions, *i.e.* total, newly transcribed and unlabeled pre-existing RNA, are suitable for quantitative RT-PCR (qRT-PCR), microarray analysis and next-generation sequencing [36,38,40,102]. In the present study, we employed this approach to lytic murine cytomegalovirus (MCMV) infection of fibroblasts to study the real-time kinetics of cellular and viral gene expression using qRT-PCR, microarray analysis and RNA-Sequencing (RNA-Seq). We show that this approach circumvents all the caveats mentioned above, thereby providing intriguing new insights into cytomegalovirus host-cell modulation and regulation of viral gene expression.

II.2 Materials and Methods

Cell culture and virus infection

Murine NIH-3T3 fibroblasts were cultured in DMEM (Gibco) supplemented with 5% fetal calf serum. Cells were seeded overnight to 80% confluence followed by infection with BAC-derived MCMV Smith strain. Infection was performed at an MOI of 10 using centrifugal enhancement (30 min, 2000 rpm) or an MOI of 0.5. The time point after centrifugation was marked as time point '0 min' in all experiments. To block RNA polymerase II transcription, Actinomycin-D (Sigma) was used at a final concentration of 5 µg/ml. UV irradiation of virus stocks was performed with 1500 J/m² UV light using a UV-Crosslinker (Vilber Loumart). Standard plaque assays were performed as described [103] to analyze the influence of 4sU on productive virus infection and to confirm the efficiency of UV-inactivation.

Metabolic labeling and purification of newly transcribed RNA

RNA labeling was started by adding 200 µM 4-thiouridine (4sU, Sigma) to cell culture media for 1 h at different times of infection. At the end of labeling, total cellular RNA was isolated using Trizol reagent (Invitrogen). Biotinylation and purification of 4sU-tagged RNA (newly transcribed RNA) as well as dot blot analysis were performed as described previously [36]. For all samples subjected to qRT-PCR analysis, DNase I (Fermentas) treatment was performed on total RNA according to the manufacturer's instructions before biotinylation. RNA was recovered using the RNeasy Mini Kit (Qiagen).

Reverse transcription and quantitative PCR

Reverse transcription was carried out in 20 µl reactions using Superscript III (Invitrogen) and Oligo-dT primers (Invitrogen) following the manufacturer's instruction. Samples were diluted 1:5 with H₂O before performing qRT-PCRs on a Light Cycler (Roche Molecular Biochemicals) as described in Dölken et al. [36]. Relative quantification was performed in relation to uninfected controls normalized to the housekeeping gene Lbr (Lamin B receptor). Primers were designed using the online Roche Universal Probe Library primer design tool spanning exon-exon junctions. All primers are listed in Table 1.

Table 1. All PCR primers used for qRT-PCR are shown

Primer	Sequence
LBR-for	5'-GGA AGT TTG TTG AGG GTG AAG TGG T-3'
LBR-rev	5'-CCA GTT CGG TGC CAT CTT TGT ATT T-3'
Nfkbia-for	5'-ACG AGC AAA TGG TGA AGG AG-3'
Nfkbia-rev	5'-ATG ATT GCCAAG TGC AGG A-3'
Ifit1-for	5'-TCT AAA CAG GGC CTT GCA G-3'
Ifit1-rev	5'-GCA GAG CCC TTT TTG ATA ATG T-3'
Gadd45a-for	5'-AGA GCA GAA GAC CGA AAG GA-3'
Gadd45a-rev	5'-CGT AAT GGT GCG CTG ACT C-3'
Herpud1-for	5'-ACC TGA GCC GAG TCT ACC C-3'
Herpud1-rev	5'-AAC AGC AGC TTC CCA GAA TAA A-3'
Lamb1-1-for	5'-TTG CGT GTG TTT GTG ATC CT-3'
Lamb1-1-rev	5'-ATC CAG AGG CAC AGT CAT CA-3'
Top2a-for	5'-CAA AAG AGT CAT CCC CCA AG-3'
Top2a-rev	5'-GGG GTA CCC TCA ACG TTT TC-3'
ie1-for	5'-TCA GCC ATC AAC TCT GCT ACC AAC-3'
ie1-rev	5'-ATC TGA AAC AGC CGT ATA TCA TCT TG-3'
m152-for	5'-CCC GCT CAT CCT CGA ATA-3'
m152-rev	5'-CTC ATA AAC CGA GGC GAG AC-3'
m169-for	5'-CAG GCA GAC ATC CGA AGG GAC TT-3'
m169-rev	5'-TCT CCC CCC GTC CGT GAT CT-3'
m129/131-for	5'-CCA CGT ACA TCA TGT CGG CG-3'
m129/131-rev	5'-GGG ATG AGG GTG TGC GCT A-3'
m94-for	5'-ACT GTG TCC TGC GAG GCC GA-3'
m94-rev	5'-GCG TGT TCG CAC CGT CTT CC-3'

Microarray analysis, data processing and statistical analysis

For the microarray analysis, 200 ng RNA of each sample was amplified and labeled using the Affymetrix Whole-Transcript (WT) Sense Target Labeling Protocol without rRNA reduction. Affymetrix GeneChip Mouse Gene 1.0 ST arrays were hybridized, washed, stained, and scanned according to the protocol described in WT Sense Target Labeling Assay Manual. Microarray data were assessed for quality and normalized with RMA. All microarray data are available at Gene Expression Omnibus (GEO) record GSE35919.

Quality control, normalization, filtering, statistical testing

Data were analyzed using R and Bioconductor [104]. Only „present“ genes (*i.e.* expression values greater than 20 in at least 2 out of the total number of arrays for each RNA type) were included in downstream analysis. In the total RNA data set, $n = 9,022$ genes passed this filter; in the newly transcribed RNA data set, $n = 9,399$ genes passed. To better compare fold-

changes between the total and newly transcribed data, the set union of genes ($n = 10,071$) was used. Differentially expressed genes were identified separately for the total RNA and newly transcribed RNA data sets using the LIMMA package. Differential expression was defined as having an estimated fold-change of at least 2 (calculated as the fold-change of the average expression in the triplicate measurements after infection compared to uninfected status) and a p-value smaller than 0.05 (adjusted for multiple testing using the Benjamini and Hochberg method [105]) (gene list see Table S1a).

Grouping of differentially expressed genes into co-regulatory modules and gene-ontology (GO) analysis

Newly transcribed transcripts, which showed differential expression in at least one condition, were grouped into clusters based on their fold-changes upon MCMV infection. Five clusters were defined (for details see Table S1c). Gene Ontology analysis for each cluster was performed using the DAVID bioinformatics analysis suite (<http://david.abcc.ncifcrf.gov/>; release 6.7).

Identification of over-represented transcription factor binding sites (TFBSs) in promoter regions

For all probe sets with a mapped Ensembl ID, the core promoter sequence (-500 to +100 bp relative to the transcriptional start site (TSS)) was retrieved using the Regulatory Sequence Analysis Tools (RSAT; <http://rsat.ulb.ac.be/>) *retrieve Ensembl seq* function. In case of alternative transcripts the most 5' TSS was chosen. Over-represented TFBSs for each cluster were predicted using Transcription Factor Matrix (TFM) Explorer (<http://bioinfo.lifl.fr/TFM/TFME/>; release 2.0) [106]. Weight matrices modeling putative TFBSs were taken from TRANSFAC (version 6.0 public; vertebrate matrices only). P-value thresholds to define locally over-represented TFBSs were set to 0.0001 and 0.00001 for clusters of less or more than 100 genes, respectively.

Immunoblotting and immunofluorescence

For immunoblotting, NIH-3T3 infected with MCMV were harvested in 500 μ l cell lysis buffer (62.5 mM Tris, 2% SDS, 10% glycerol, 6 M urea, 5% β -mercaptoethanol, 0.01% bromophenol blue, 0.01% phenol red) at several time points of infection. Following heat denaturation (95 $^{\circ}$ C, 5 min), 50 μ l of the lysates were subjected to SDS-PAGE. Proteins were transferred to a nitrocellulose membrane (Schleicher & Schuell) using a semidry blotter (Peq-

Lab) (2 h, 400 mA). Membranes were blocked in PBS + 2.5 % milk powder and subsequently incubated with primary antibody (o/n, 4 °C). After incubation with horseradish peroxidase-conjugated secondary antibody (1 h, RT) the proteins were visualized by the ECL system (Perkin Elmer) in the Fusion FX device (Vilber Lourmat).

For indirect immunofluorescence NIH-3T3 cells were seeded onto fibronectin-coated glass cover-slips in 24-well plates and infected with MCMV. At various time points of infection, cells were fixed with 4 % paraformaldehyde in DPBS (w/v) for 10 min at 37° C. The fixative solution was replenished twice with DPBS and the cells were permeabilized for 10 minutes with a solution of 0.1% Triton X-100 in DPBS. After extensive washing with DPBS, the cells were blocked using 3 % (w/v) BSA in DPBS (blocking solution) for 1 h at room temperature (RT). Primary antibodies were applied in blocking solution and incubated with the cells at RT for 1 h followed by three DPBS washing steps and 1 h incubation at RT with 1:1,000 dilutions of Alexa Fluor-conjugated, specific secondary antibodies (Invitrogen) in blocking solution. After a final washing step with DPBS, the preparations were mounted on glass slides with Prolong Gold including DAPI (Invitrogen) and analyzed using an LSM 710 (Zeiss) confocal laser scanning microscope with 405 nm, 488 nm and 561 nm laser excitation and appropriate filter sets.

The following primary antibodies were used for immunoblotting and -fluorescence: mouse anti-IE1 (CROMA101; kindly provided by S. Jonjic, University of Rijeka, Rijeka, Croatia), rabbit anti-GAPDH (mAbcam 9484) from Abcam, rabbit anti-RelA (A) and mouse anti-I κ B- α (H4) from Santa Cruz Biotechnology.

Luciferase assays

To monitor the activity of c-Myc-regulated signal transduction pathway, cells were transfected in a 6-well format using the Cignal c-Myc-Reporter (luc) Kit from Qiagen. 6 hours post transfection cells were seeded in 96-well plates (10,000 cells / well). 48 hours after seeding, the transfected cells were infected with MCMV (n=3). At various times of infection, cells were lysed in 100 μ l lysis buffer and luciferase firefly activity was determined according to the manufacturer's (Promega) instructions.

Next Generation Sequencing

RNA was subjected to WTAK library construction to generate transcriptomic fragment libraries (50 bp, SOLiD™ (Life Technologies, Foster City, CA, USA) Total RNA-Seq Kit V3) that preserve strandedness information of the reads. Molecular barcoding was used in

order to pool several libraries in a single sequencing reaction according to the manufacturer's protocol. Sequencing was performed using the SOLiD™ 3 system (Life Technologies). Potential sequencing errors were corrected using the SOLiD Accuracy Enhancement Tool (solidsoftwaretools.com/gt/project/saet). All sequencing data are available at Gene Expression Omnibus (GEO) at GSE35833.

Short-read alignment, MCMV read coverage

Between 26 and 42 million 50 nt reads were obtained per sample (Table S2). Reads were aligned in a 4-step process using the Bowtie alignment program. First, all reads were aligned to mouse transcripts (Ensembl version 63). Remaining unaligned reads were aligned to the mouse genome (mm9, NCBI Build 37). Remaining reads were aligned to MCMV coding sequences and finally to the full MCMV genomic sequence. Reads with ambiguous base calls, non-unique alignment positions or more than 4 mismatches were discarded. Reads were classified as exon-exon and exon-intron junction reads, respectively, if they overlapped an exon-exon or an exon-intron junction by ≥ 1 nt. MCMV genome coverage was scaled before plotting. Scaling factors were derived using DESeq based on reads aligned to mouse exons.

II.3 Results

Establishment of 4sU-tagging for lytic MCMV infection

Upon its addition to the cell culture medium, 4-thiouridine (4sU) is rapidly taken up by cells, phosphorylated and incorporated into newly transcribed RNA in a concentration-dependent manner [36]. To establish 4sU-tagging for MCMV infection, we first analyzed the effect of lytic MCMV infection on 4sU-incorporation. NIH-3T3 fibroblasts were infected with MCMV at a multiplicity of infection (MOI) of 10. At different times of infection, 200 μ M 4sU was added to the cell culture medium for 1 h. Total RNA was prepared and subjected to thiol-specific biotinylation. 4sU-(biotin)-incorporation was quantified by dot blot (Figure 1A). At all times of infection, 4sU-incorporation was at least as efficient as in uninfected cells, ensuring efficient purification of newly transcribed RNA at all times of infection. Interestingly, from 5 to 24 hours post infection (hpi) the extent of 4sU-incorporation into cellular RNA was about 20-fold greater than in uninfected cells. By 47-48 hpi this had returned to levels found in uninfected cells. These data are consistent with increased transcriptional activity as well as enhanced nucleoside metabolism during lytic CMV infection [107].

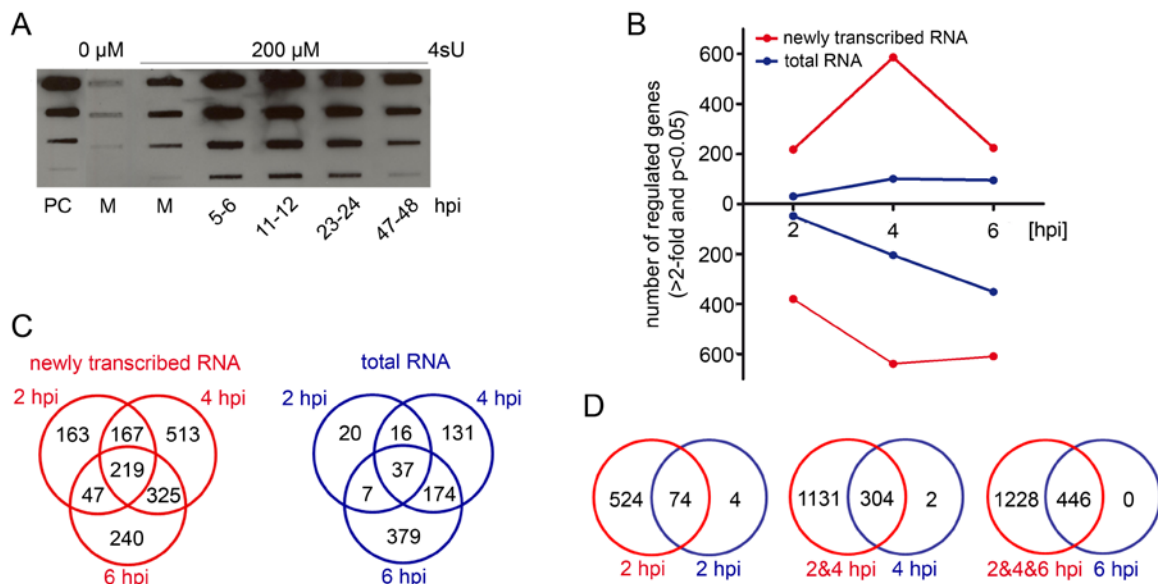


Figure 1. Establishment of 4sU-tagging for lytic MCMV infection

(A) Incorporation of 4sU throughout MCMV infection. Cells were infected with MCMV at an MOI of 10 and exposed to 200 μ M 4sU for 1 h at different times of infection before total RNA was isolated. Thiol-specifically biotinylated RNA was subjected to dot blot analysis in 10-fold dilutions (1 μ g down to 1 ng). A biotinylated oligonucleotide of 81 nt (PC, 100 ng down to 0.1 ng) was used to quantify 4sU-incorporation; M = mock control. (B)-(D) Comparison of genes identified to be regulated in newly transcribed RNA to genes regulated in total RNA. (B) Numbers of genes up- and down-regulated (>2-fold, p<0.05) at different times of infection are shown for newly transcribed RNA and total RNA. (C) Venn diagrams of all genes regulated >2-fold more than 2-fold in newly transcribed RNA and total RNA. (D) Venn diagrams showing genes regulated >2-fold in total RNA at 2, 4 and 6 hpi and in newly transcribed RNA at and prior to the indicated time point of infection; red = newly transcribed RNA, blue = total RNA.

Metabolic labeling of newly transcribed RNA with 4sU has negligible polar effects on eukaryotic cells [36,108]. To exclude gross adverse effects of 4sU-labeling on MCMV replication, we applied 1h of 200 μ M 4sU-treatment to NIH-3T3 cells at different times of infection. No effect of 4sU exposure on virus titers, determined at 48 hpi, was observed (Figure 2). We therefore decided to use 1h of 200 μ M 4sU in all following experiments.

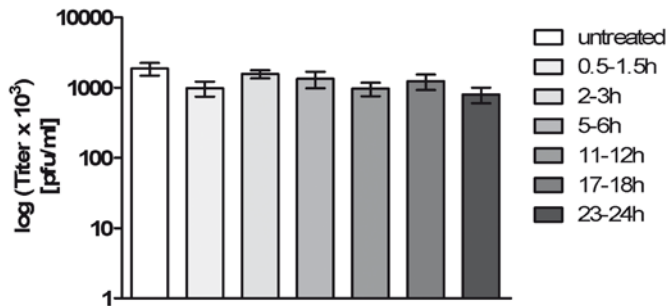


Figure 2. No effect of 1 h 200 μ M 4sU treatment on virus replication

NIH-3T3 fibroblasts were infected with MCMV at an MOI of 10 for 48 h. Samples were exposed to 200 μ M 4sU for 1 h at different time points of infection or left untreated. Supernatants were harvested and titrated at 48 hpi. Shown are the means \pm SD of three biological replicates.

Kinetics of transcriptional activity of cellular genes during early MCMV infection

To detail transcriptional changes in host gene expression during early MCMV infection we infected NIH-3T3 fibroblasts with MCMV at an MOI of 10 and labeled newly transcribed RNA from 1-2, 3-4 and 5-6 hpi. Three replicates of both total and newly transcribed RNA were subjected to Affymetrix Gene ST 1.0 arrays. After Robust Multichip Average (RMA) normalization, we identified all genes significantly regulated ($p \leq 0.05$) by at least 2-fold compared to uninfected cells in any condition. This resulted in the identification of 1,674 probe sets showing differential expression (Table S1a). With the exception of 4 genes, all differentially expressed genes were either exclusively up- or down-regulated during the first 6 h of infection. The number of genes with differential expression detectable in total RNA only represented 13 % (at 2 hpi), 25 % (at 4 hpi) and 54 % (at 6 hpi) of those identified in newly transcribed RNA. As predicted, down-regulation only started to become detectable in total RNA with substantial delay, i.e. at 4 hpi (Figure 1B). Furthermore, a peak of MCMV-induced and rapidly counter-regulated gene expression was apparent in newly transcribed RNA at 3-4 hpi. This was invisible in total RNA. The overlap of differential gene expression detectable at different times of infection was substantially greater for newly transcribed RNA (Figure 1C). Notably, we found all genes induced or repressed by at least 2-fold in total RNA at 6 hpi to show concordant regulation in newly transcribed RNA (Figure 1D). In addition, only 3 probe

sets showed more than 2-fold greater regulation in total RNA than in newly transcribed RNA (genes listed in Table S1b). Hence, the vast majority of differential gene expression during the first six hours of MCMV infection is the result of alterations in transcription rates and not due to changes in RNA decay rates. We therefore decided to focus all our subsequent analyses on newly transcribed RNA.

4sU-tagging details discrete functional gene clusters regulated with distinct kinetics

Clustering genes based on >2-fold differences in regulation at different times of infection, we identified 5 clusters of genes characterized by distinct kinetic profiles (Figure 3A; for details and genes represented in each cluster see Table S1c). MCMV-induced genes peaked at 1-2 (Cluster 1), 3-4 (Cluster 2) or 5-6 hpi (Cluster 3). Of these, Cluster 2 was not detectable in total cellular RNA at all. Rapid and rather constant down-regulation was characteristic of genes in Cluster 4, while genes in Cluster 5 showed delayed down-regulation. To look for functional characteristics of these five gene clusters, we performed Gene Ontology (GO) analysis. Interestingly, all five clusters were associated with distinct GO terms (see Figure 3B). Genes in Cluster 1 were involved in immune and inflammatory processes as well as apoptosis. Genes in Cluster 2 mainly played a role in p53 signaling and cell cycle progression. Delayed induction was observed for genes involved in the ER stress response (Cluster 3). Rapid and sustained down-regulation was observed for genes involved in cell proliferation and differentiation, focal adhesion as well as actin filament-based processes (Cluster 4). Finally, delayed down-regulation was characteristic of genes with a role in chromatin assembly and cell cycle processes (Cluster 5). Due to the delayed visibility of down-regulation in total RNA (see Figure 1B), Cluster 4 and 5 could only be differentiated using newly transcribed RNA. This approach thus allowed dissecting differential gene expression into discrete functional clusters regulated with distinct kinetics. These provided us with ideal templates to elucidate the underlying transcription factors and molecular mechanisms using *in silico* promoter analysis.

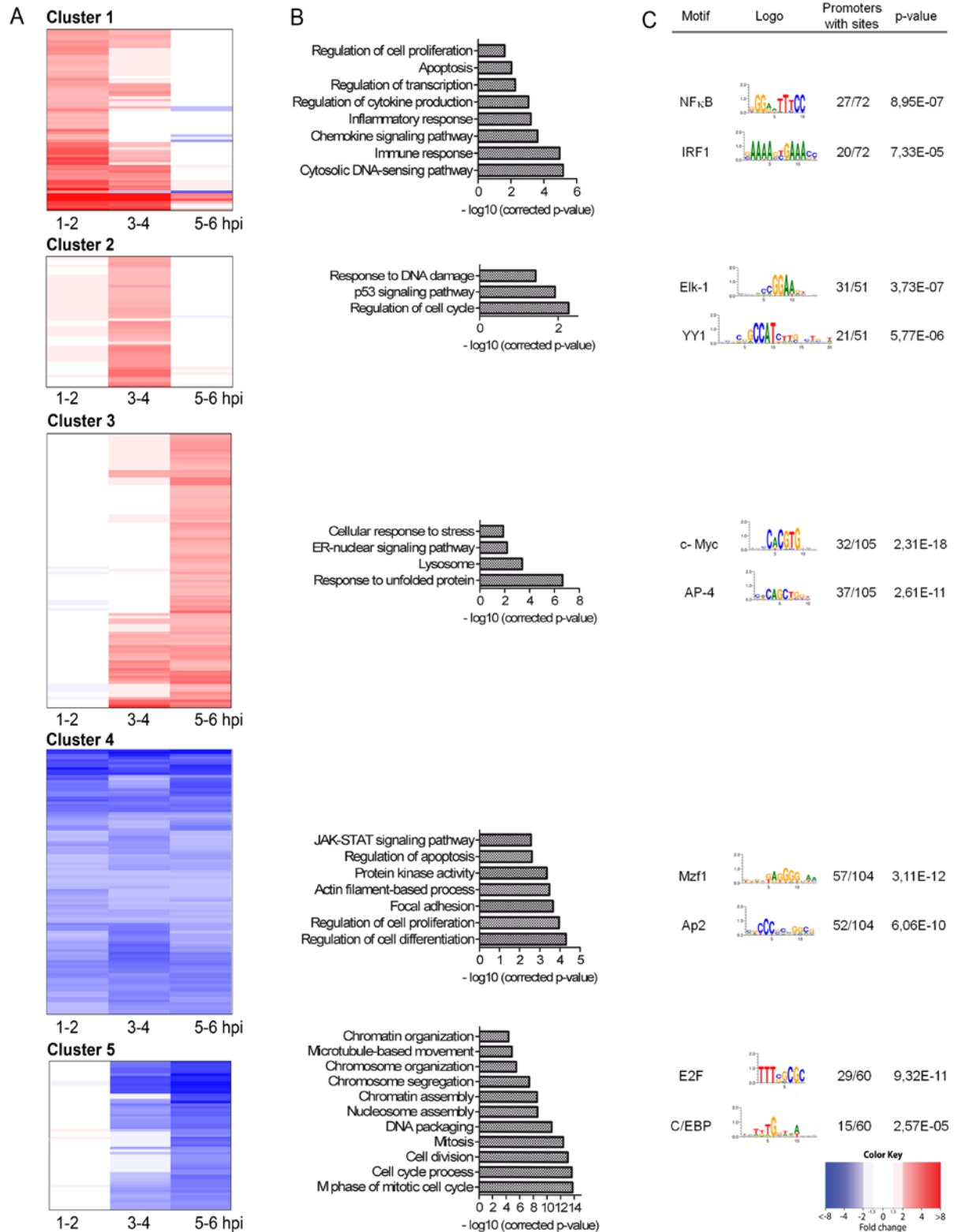


Figure 3. Gene expression kinetics define distinct functional clusters

(A) Heat-maps indicating the fold-changes are shown as matrices with rows representing genes and columns representing the time points post infection. Red represents up-regulation, blue down-regulation (>2-fold, $p \leq 0.05$) in newly transcribed RNA relative to uninfected cells. Ordering of genes in the heat-maps was determined using non-supervised hierarchical clustering. Shown are the 5 clusters of genes we identified. (B) All clusters are associated with distinct functional annotations. Gene Ontology analyses are shown for each of the five clusters with the most significant ($p \leq 0.05$) categories displayed in the graphs as bars, sorted from bottom (most significant) to top. (C) Specific transcription factor binding sites correlate with functional clusters. Shown are exemplary transcription factors with over-represented binding sites unique for the different clusters. Illustrated are the transcription factor weight matrices, the percentage of promoters with sites and p-value.

Promoter analysis associates distinct transcription factors with each individual gene cluster

We performed promoter analysis on the five clusters to identify cellular transcription factors (TFs) involved in their regulation. Proximal promoter regions (PPR) ranging from -500 to +100 bp from the transcription start site (TSS) were analyzed for over-represented transcription factor binding motifs. While a number of transcription factor binding motifs were significantly over-represented in the five clusters (for complete list and data see Table S3), we observed distinct transcription factor binding sites to be uniquely over-represented in each of the individual clusters (see Figure 3C). These correlated very well with the functional annotations of the associated clusters.

Two exemplary TFs were chosen for further validation. As a proof-of-principle TF, we decided to look at NF- κ B to see whether its well-described rapid induction and counter-regulation during CMV infection [43–45] would precisely reflect the transcriptional changes we observed in newly transcribed RNA under our experimental conditions. NF- κ B-dimers of the NF- κ B- (p105 and p100) and Rel-subfamily (c-Rel, RelB and RelA) are present in inactive I κ B-bound complexes in the cytoplasm. I κ K-mediated phosphorylation induces degradation of the inhibitor I κ B α , enabling translocation of the NF- κ B dimers to the nucleus and enhanced transcription of NF- κ B target genes (reviewed in [111]). To look for degradation of the inhibitor I κ B α during the first 12 h of MCMV infection, we performed immunoblotting (Figure 4A). In addition, immunofluorescence analysis was performed to reveal the shift of RelA into the nucleus (Figure 4B). Results from both experiments demonstrated the kinetics of transcriptional regulation of genes in Cluster 1 to precisely mirror NF- κ B activation, highlighting the ability of 4sU-tagging to detail real-time transcription factor activity.

In addition, we looked at a representative TF of Cluster 3, namely c-Myc. c-Myc is a proto-oncogene which drives cell cycle progression and apoptosis, whereas cellular differentiation and cell adhesion are negatively influenced [112]. c-Myc forms a heterodimer with Max, followed by its binding to target genes [113]. Furthermore, phosphorylation of two amino acids at the NH₂-terminal domain is important for transactivation of c-Myc [114]. Hagemeyer et al. showed that HCMV IE1 and IE2 can transactivate the c-Myc promoter [115]. We performed luciferase assays using a c-Myc-specific reporter construct transfected into NIH-3T3 cells 48 h prior to infection to analyze c-Myc activation. Luciferase activity started to significantly increase at 4 hpi, matching the expression kinetics of genes in Cluster 3 (Figure 4C).

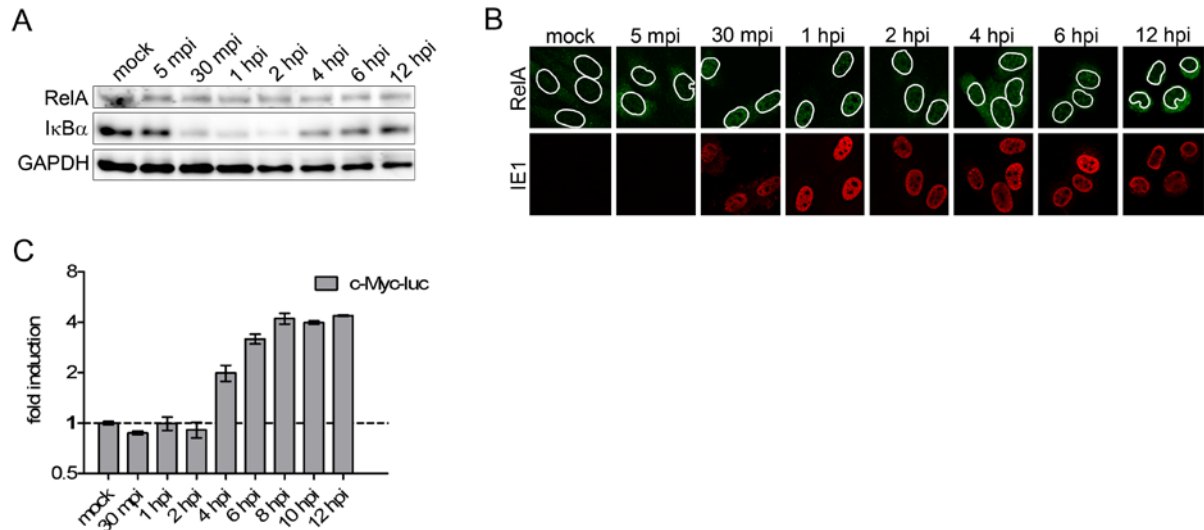


Figure 4. Validation of exemplary transcription factors

NIH-3T3 fibroblasts were infected with MCMV at an MOI of 10 for the indicated time points and lysates were prepared for western blot analysis (A), for immune staining (B) or luciferase assay (C). Western blot analysis was performed on samples prepared from uninfected and infected NIH-3T3 cells probed for RelA and IκBα (A). GAPDH was probed as loading control. For the immunofluorescence staining (B) cells were fixed and stained with the indicated antibodies; white circle indicating nucleus, DAPI nuclear staining; green, RelA; red, viral IE1. For the luciferase assays cells were transfected with a c-Myc-reporter construct (C) and infected 48 hours post transfection with MCMV at an MOI of 10. At the indicated times post infection, Firefly-Luciferase measurements were performed in triplicates. Shown is the mean +/- SD of a representative of three experiment; mpi =minutes post infection, hpi = hours post infection.

Virus-mediated regulation and counter-regulation of host gene expression

We then addressed the role of viral gene expression in the regulation of each cluster using infection with UV-inactivated virus. To provide a more comprehensive picture, we extended the kinetics until 48 hpi. To this end, NIH-3T3 cells were infected with either wild-type (wt) or UV-inactivated virus. RNA was labeled for 1 h at different times of infection and newly transcribed RNA was purified. Transcription rates of exemplary genes of each functional cluster were determined in newly transcribed RNA using quantitative RT-PCR (qRT-PCR). This included NF-κB- (Cluster 1), interferon- (Cluster 1), DNA-damage- (Cluster 2) and ER-stress- (Cluster 3) induced genes as well as MCMV-repressed genes involved in the regulation of cell differentiation (Cluster 4) and cell cycle/chromatin organization (Cluster 5). The housekeeping gene Lbr (Lamin B receptor) was used for normalization.

Cluster 1 contains both NF-κB- as well as interferon-induced genes. We thus chose NF-κBiα (NF-κB-inhibitor alpha), an NF-κB-induced negative regulator of the NF-κB response, as well as Ifit1 (Interferon-induced protein with tetratricopeptide repeats 1) for this analysis. Both NF-κBiα and Ifit1 were rapidly induced and counter-regulated by lytic MCMV infection (Figure 5A, B). Induction of both genes following infection with UV-inactivated virus was comparable to wt-MCMV infection, consistent with previous reports showing that viral gene

expression is not required for induction of both NF- κ B- and interferon-signaling. In both cases, however, counter-regulation was substantially delayed following infection with UV-inactivated virus. While counter-regulation of the NF- κ B response is consistent with the MCMV M45 gene product efficiently targeting NF- κ B- signaling [20] a viral gene product targeting the induction of the interferon response remains to be identified [116].

To monitor DNA-damage response-mediated signaling, we analyzed transcriptional activity of Gadd45a (Growth arrest and DNA damage-inducible protein A), a well characterized DNA damage- induced gene [117]. Consistent with our microarray data, qRT-PCR revealed the same slightly delayed induction at 3-4 hpi, followed by a more protracted counter-regulation than we observed for NF- κ B α and Ifit1. Interestingly, UV-inactivated virus also triggered the induction of Gadd45a with similar kinetics. This was, however, no longer counter-regulated, but continued to increase until 48 hpi (Figure 5C). While these data are indicative of counter-regulation of the underlying DNA-damage response by an MCMV gene product, we cannot exclude that the enhanced response - at least in parts - reflects increased activation by the UV-damaged viral DNA. For HCMV, it was described that Gadd45a interacts with the anti-apoptotic UL37x1 gene product and increases its anti-apoptotic function early in infection [118]. Thus, the induction of Cluster 2 may at least in parts represent an intended action of the virus.

For Cluster 3, expression of Herpud1 (Homocysteine-responsive endoplasmic reticulum-resident ubiquitin-like domain member 1 protein), a gene induced by endoplasmic reticulum (ER) stress [119], was monitored. Delayed induction was observed, which was rapidly counter-regulated. Induction of Herpud1 was lost upon infection with UV-inactivated virus, consistent with viral gene expression being required for the induction of the ER stress response. In summary, these findings indicate that a so far unknown viral gene product counteracts the ER stress response provoked by viral gene expression (Figure 5D). For HCMV, this function is thought to be performed by the viral pUL38 protein [120].

For Clusters 4 and 5 we chose to monitor the transcription kinetics of Lamb1-1 (Laminin beta 1), an important extracellular matrix glycoprotein, and Top2 α (Topoisomerase 2 alpha), which is involved in the control and alteration of the topologic states of DNA during transcription [121,122]. Interestingly, consistent down-regulation of both genes was observed following wt-MCMV, but not UV-MCMV infection, indicating that viral gene expression is required for both their regulation (Figure 5 E, F).

In summary, these data highlight that all cellular signaling pathways we identified to be induced during early MCMV infection are rapidly counter-regulated by the virus later on. In

contrast, down-regulation of defined cellular signaling pathways prevails and thus most likely represents an intentional action of the virus to facilitate its needs.

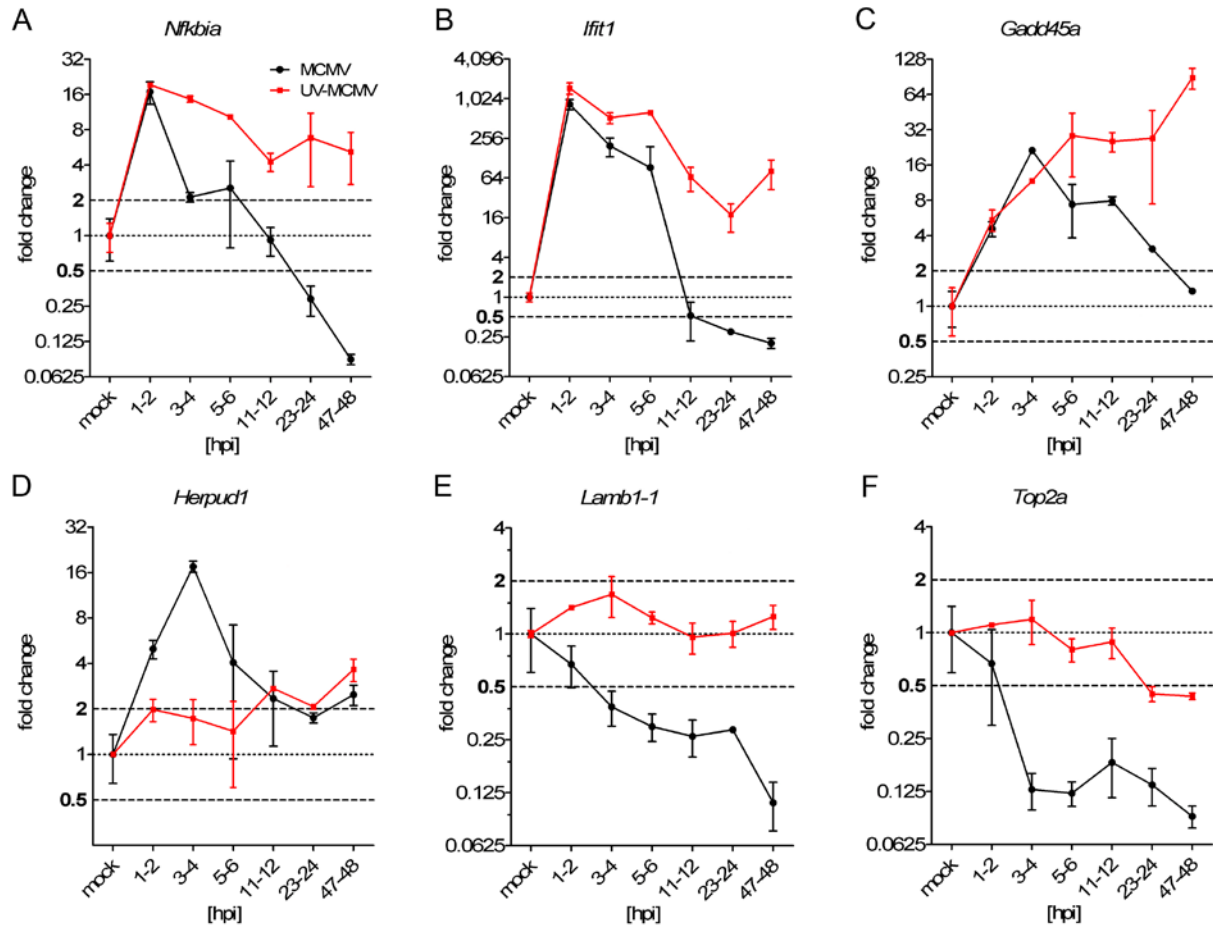


Figure 5. Identification of virus-specific regulation and counter-regulation using UV-inactivated virus

Quantitative RT-PCR was employed to measure transcription rates of exemplary genes of the five gene clusters (A-F). NIH-3T3 were infected with wt- or UV-inactivated (1500J, 15min) MCMV (MOI of 10) for the indicated time points. Displayed are the fold-changes relative to uninfected cells normalized to Lbr. Fold-changes in between 0.5- and 2-fold were considered as non-regulated. Shown are the combined data (means +/- SD) of three independent experiments.

Analysis of newly transcribed RNA allows studying viral gene expression in absence of virion-associated RNA

Cytomegalovirus particles unspecifically incorporate and transfer large amounts of so called ‘virion-associated RNA’ to newly infected cells [95]. This has substantially hindered detailed studies on the kinetics of viral gene expression during the first few hours of infection and in latency. 4sU-tagging allows the removal of virion-associated RNA and thus, the dissection of the regulation of viral gene expression during the initial phase of infection. To show that 4sU-tagged newly transcribed RNA fraction is indeed free of virion-associated RNA, we labeled newly transcribed RNA in MCMV infected NIH-3T3 cells from 1-2, 3-4 and 7-8 hpi in the presence and absence of the RNA polymerase II inhibitor Actinomycin D (Act-D). Act-D

treatment inhibits RNA synthesis and thus prevents 4sU-incorporation into newly transcribed RNA. Following isolation of total RNA, we included a DNase digest prior to biotinylation to further remove viral DNA. Newly transcribed and total RNA samples were subjected to qRT-PCR analysis for the spliced viral *ie1* gene and the cellular housekeeping gene *Lbr*. In total RNA, large amounts of IE1 transcripts were detectable even in presence of Act-D, consistent with large amounts of virion-associated RNA delivered to the infected cells. However, in newly transcribed RNA virtually no IE1 and *Lbr* transcripts (below detection limit of our qRT-PCR assay) were detectable in presence of Act-D, consistent with the complete removal of virion-associated RNA (Figure 6A).

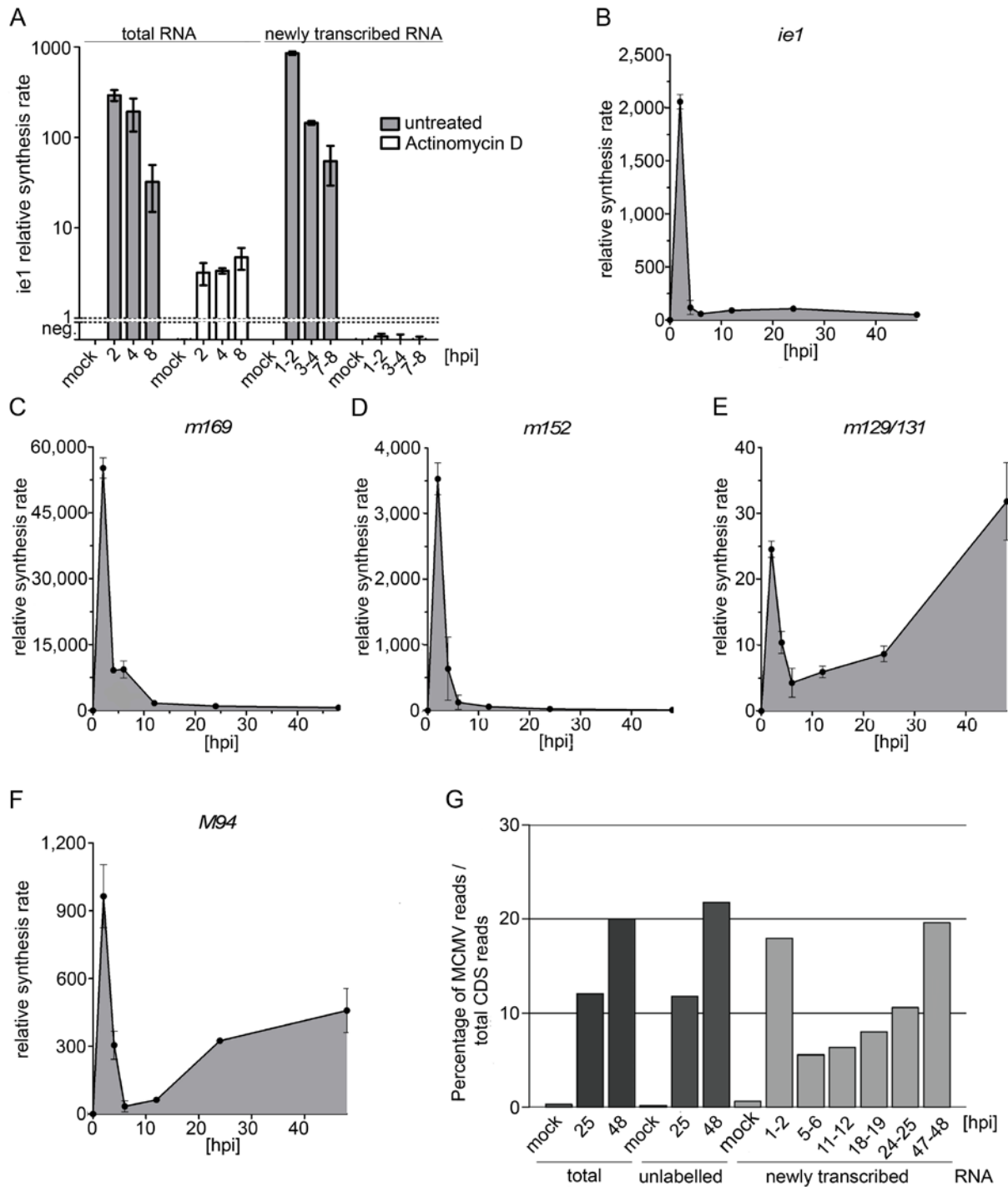


Figure 6. Real-time kinetics of viral gene expression

(A) 4sU-tagging allows efficient removal of viral DNA and virion-associated RNA. Newly transcribed RNA was labeled with 200 μ M 4sU for 1 h in MCMV-infected NIH-3T3 cells at -1 to 0 (mock), 1-2, 3-4 and 7-8 hpi. As a negative control, Actinomycin-D was added to cells prior to infection to block transcription and thus 4sU-incorporation. Total RNA was isolated, treated with DNaseI and newly transcribed RNA was purified. qRT-PCR analysis was performed on newly transcribed RNA for viral IE1 and cellular Lbr. Shown are the combined data (means \pm SD) of three independent experiments. (B-F) Gene expression kinetics of exemplary viral genes. Shown are qRT-PCR measurements of newly transcribed RNA for IE1 (B), the early genes m169 (C) and m152 (D) as well as for the late genes m129/131 (E) and M94 (F). Synthesis rates were normalized to Lbr expression. Shown are the combined data (means \pm SD) of three independent experiments. (G) Contribution of viral transcripts to all coding sequence reads (CDS). RNA-Seq was performed on newly transcribed, total and unlabeled pre-existing RNA samples (n=1). Reads were mapped to both the cellular and viral transcriptome/genome. The contribution of viral reads to all CDS reads at different times of infection is shown.

4sU-tagging reveals a peak of viral gene expression at 1-2 hpi, including immediate-early, early and even late gene expression

We then performed a comprehensive time-course analysis of transcriptional activity during lytic MCMV infection. To study relevant time frames, we first determined the kinetics of viral DNA replication in NIH-3T3 cells infected with wt-MCMV at an MOI of 10. Both qRT-PCR on M54, the catalytic subunit of MCMV DNA polymerase, and southern blot analysis of concatameric DNA revealed viral DNA replication to start at ~15 hpi (Figure 7).

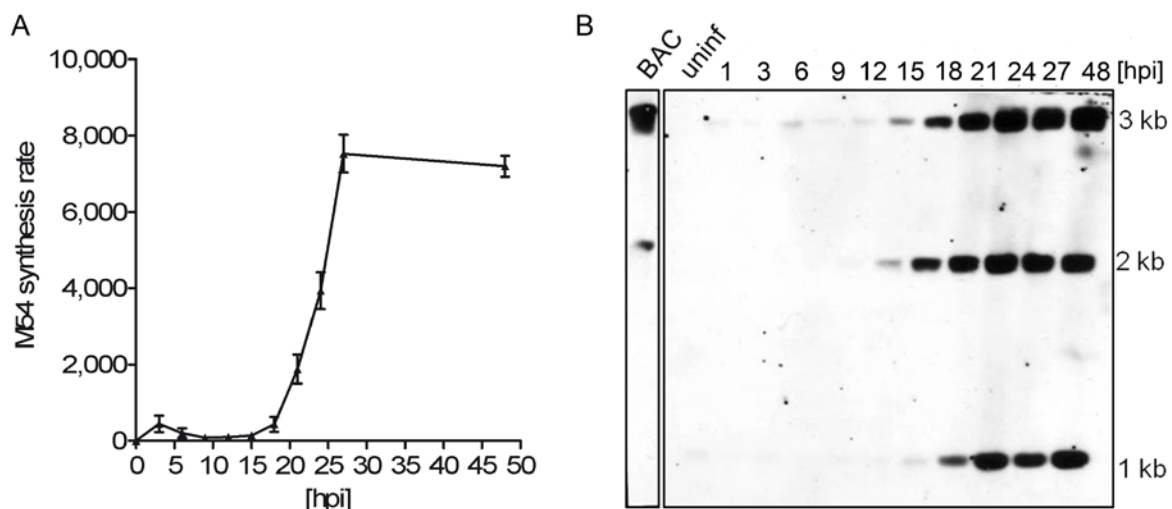


Figure 7. Temporal kinetics of MCMV replication

NIH-3T3 cells were infected with MCMV at an MOI of 10. DNA was isolated at various times of infection using the DNeasy Blood & Tissue Kit (Qiagen) according to the manufacturer's instructions. Prior to amplification, extracted DNA was digested with *PaeI* for 1 h, 37 °C followed by heat inactivation. (A) TaqMan qRT-PCR was performed in triplicates for MCMV M54 and cellular Lbr using the ABI Prism 7700 sequence detector (Applied Biosystems) as described [123]. Synthesis rates were normalized to Lbr. Shown are the means \pm SD of three independent experiments. (B) Southern Blot analysis was performed as described in Popa et al. [124]. Shown is the detection of different genome fragments in DNA isolated from NIH-3T3 cells at various times of infection. MCMV BAC-DNA (BAC) served as a negative control. The 3 kb fragment serves as a measurement of genomic load, the 2 kb fragment for concatameric/circular DNA and the 1 kb fragment for linear, unique length genomic DNA. The appearance of the 1kb DNA fragment indicates the onset of viral DNA replication. Due to its circular form, digested BAC DNA produces only two of the three fragments.

We therefore decided to label newly transcribed RNA at 1-2 hpi, 5-6 hpi, 11-12 hpi (prior to the onset of DNA replication), 18-19 hpi (during DNA replication, but prior to the first release of virus particles), 24-25 hpi (first infectious virus particles starting to be released) and at 47-48 hpi (late stage infection). Following DNase digest and purification of newly transcribed RNA, this was subjected to qRT-PCR analysis for IE1 as well as two genes well characterized to be expressed with either early (m152 and m169) or late (m129/131 and M94) kinetics [125–127]. For the spliced late gene m129/m131 [128] we designed the qRT-PCR to span exon-exon junctions to further eliminate any residual risk of amplifying viral DNA or

transcripts derived from the opposite DNA strand. To our great surprise, we found not only the two early, but also the two late genes to be well expressed during the first few hours of infection peaking at 1-2 hpi followed by a down-regulation at 5-6 hpi (6B-F). It is important to note that we could not detect any specific signals in any assay when qRT-PCR was carried out using non-reverse-transcribed samples or Act-D-treated samples (data not shown). This demonstrated the complete removal of viral DNA and virion-associated RNA from these samples. Expression of M94 was also observed when strand-specific cDNA synthesis was performed, matching the kinetics shown in Figure 6F (data not shown). In addition, agarose electrophoresis on m129/m131-PCR products confirmed a band of the predicted size, thereby excluding amplification of viral DNA or a transcript expressed from the opposite DNA strand (data not shown).

A second unexpected finding was the dramatic drop of transcriptional activity of all viral genes starting 3-4 hpi. For IE1 and m169, transcription dropped >30-fold by 5-6 hpi (compared to 1-2 hpi) and then leveled off (Figure 6B, C). In contrast, transcription rates of m152 continued to drop exceeding 500-fold at 47-48 hpi (Figure 6D). Both late genes, *i.e.* m129/m131 and M94, showed a substantial increase in synthesis rates with the onset of viral DNA replication, consistent with their kinetic class. To rule out that our observations were simply caused by the high MOI, we repeated the experiment using a low MOI of 0.5. As observed with high MOI, IE1 transcription had already peaked by 1-2 hpi. In contrast, transcription rates of both the two early and late genes had not, now peaking at 3-4 hpi (see Figure 8). Nevertheless, transcription rates of all five genes significantly dropped by 5-6 hpi. These data indicate that transient expression of viral late genes during the first few hours of infection is not an artifact of high MOI.

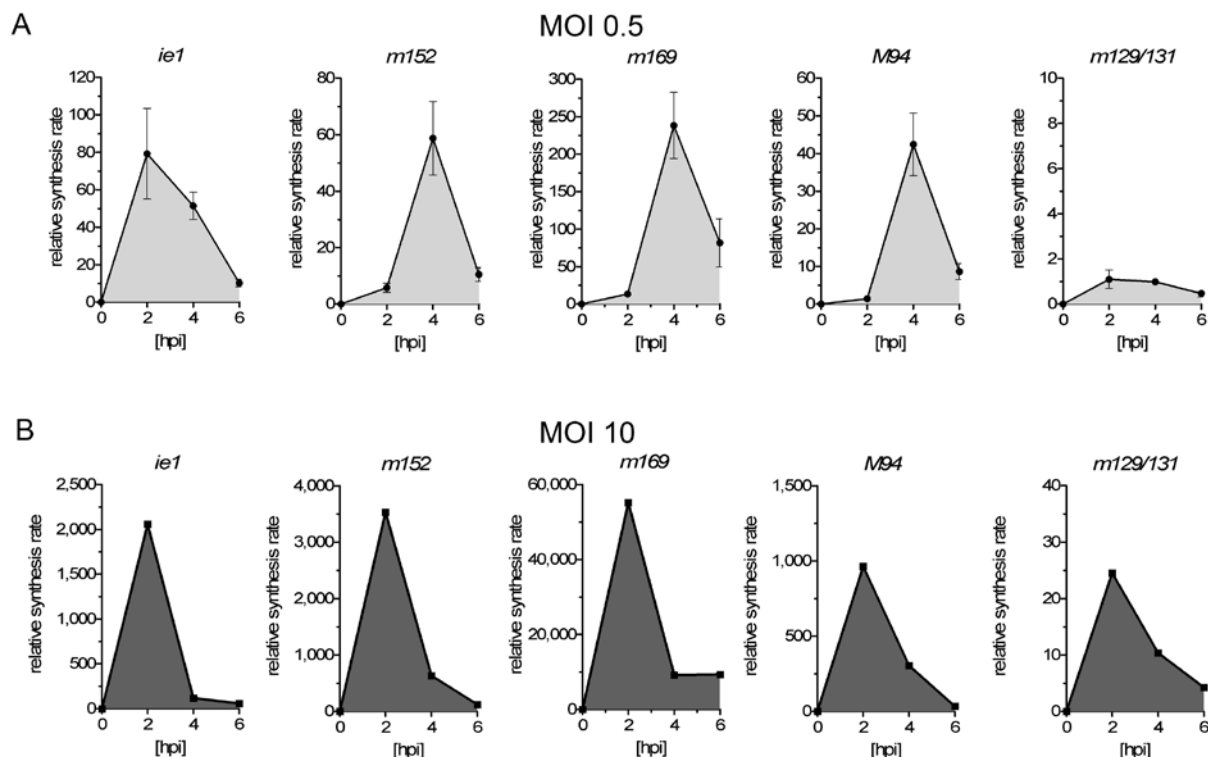


Figure 8. Regulation of viral gene expression following low and high MOI

NIH-3T3 cells were infected with (A) an MOI of 0.5 (low MOI) and (B) an MOI of 10 (high MOI, data taken from Figure 6B-F). Newly transcribed RNA was labeled from -1 to 0 (mock), 1-2, 3-4 and 5-6 hpi. Following purification of newly transcribed RNA, expression levels of IE1, m152, m169, m129/131 and M94 were determined by qRT-PCR normalized for Lbr.

RNA-Seq reveals rapid silencing of viral gene expression after the initiation of early gene expression

To confirm these observations at the whole transcriptome level, we repeated the experiment described above and subjected newly transcribed RNA samples from 7 time points (mock, 1-2, 5-6, 11-12, 18-19, 24-25 and 47-48 hpi) to SOLiD 3 sequencing. In addition, we included samples of total and pre-existing RNA (mock, 25 hpi and 48 hpi). We obtained between 16 and 42 million reads per sample, which were mapped to the mouse transcriptome, mouse genome, MCMV predicted coding sequences and the MCMV genome in the respective order. As expected, introns were substantially over-represented in newly transcribed RNA (Figure 9) reflecting the substantially greater contribution of immature, unspliced nascent transcripts [38].

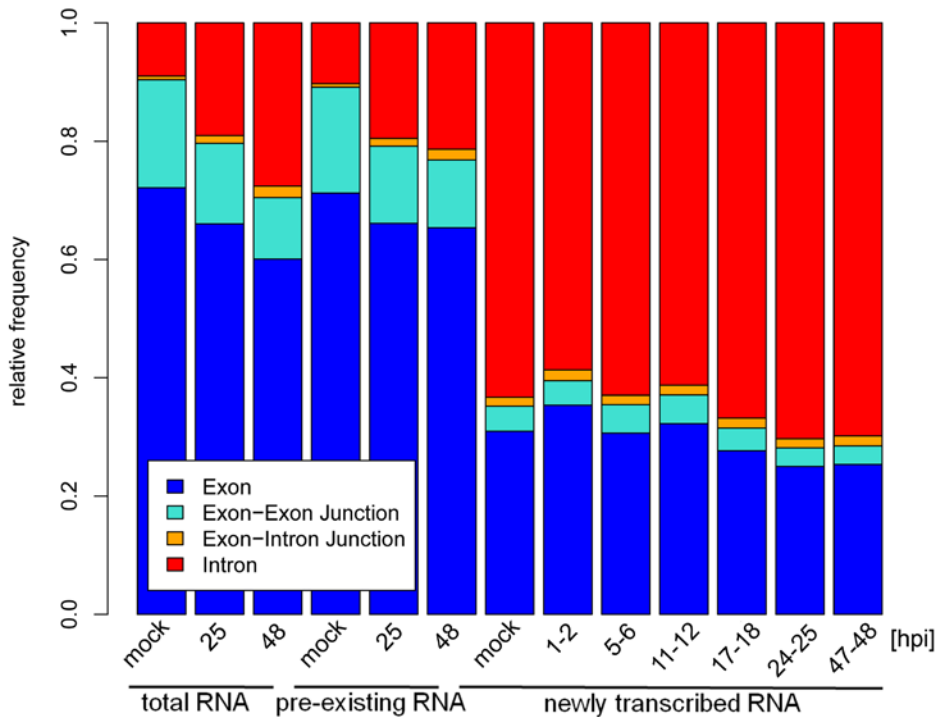


Figure 9. Classification of reads aligned to mouse transcripts and genomic sequence

Reads were classified according to their alignment position in mouse transcripts or genomic sequence as exon, intron, exon-exon junction, or exon-intron junction reads. Shown are the relative frequencies of each class for total, pre-existing, and newly transcribed RNA samples derived from NIH-3T3 cells at various times of infection. The high fraction of intronic reads in newly transcribed RNA samples is consistent with the increased proportion of premature transcripts present in newly transcribed RNA.

When considering only coding sequences, viral transcripts accounted for ~20% of all reads in total RNA at 48 hpi and in newly transcribed RNA at 47-48 hpi (Figure 6G). Interestingly, the extent of viral gene expression in newly transcribed RNA at 1-2 hpi also accounted for ~15% of all reads, dropping to around 5% of all reads at 5-6 hpi. This corroborates our qRT-PCR finding of a burst of viral gene expression at 1-2 hpi, but also highlights that not all viral genes expressed at 1-2 hpi are subject to the same massive down-regulation we observed for m152. A closer look at the distribution of transcription rates across the whole viral genome (direct and complementary strand) revealed viral gene expression arising from multiple loci at 1-2 hpi (Figure 10). By 5-6 hpi, transcription rates of many but not all viral genes dropped substantially. With the onset of viral DNA replication, late gene expression was initiated, accounting for the increasing number of viral reads at 24-25 and 47-48 hpi (although of shifted viral gene subsets compared to 1-2 hpi). At late stages of infection, transcription rates of viral genes stabilized, reflected by the continuous accumulation of the respective viral transcripts in both total and unlabeled pre-existing RNA (Figure 11).

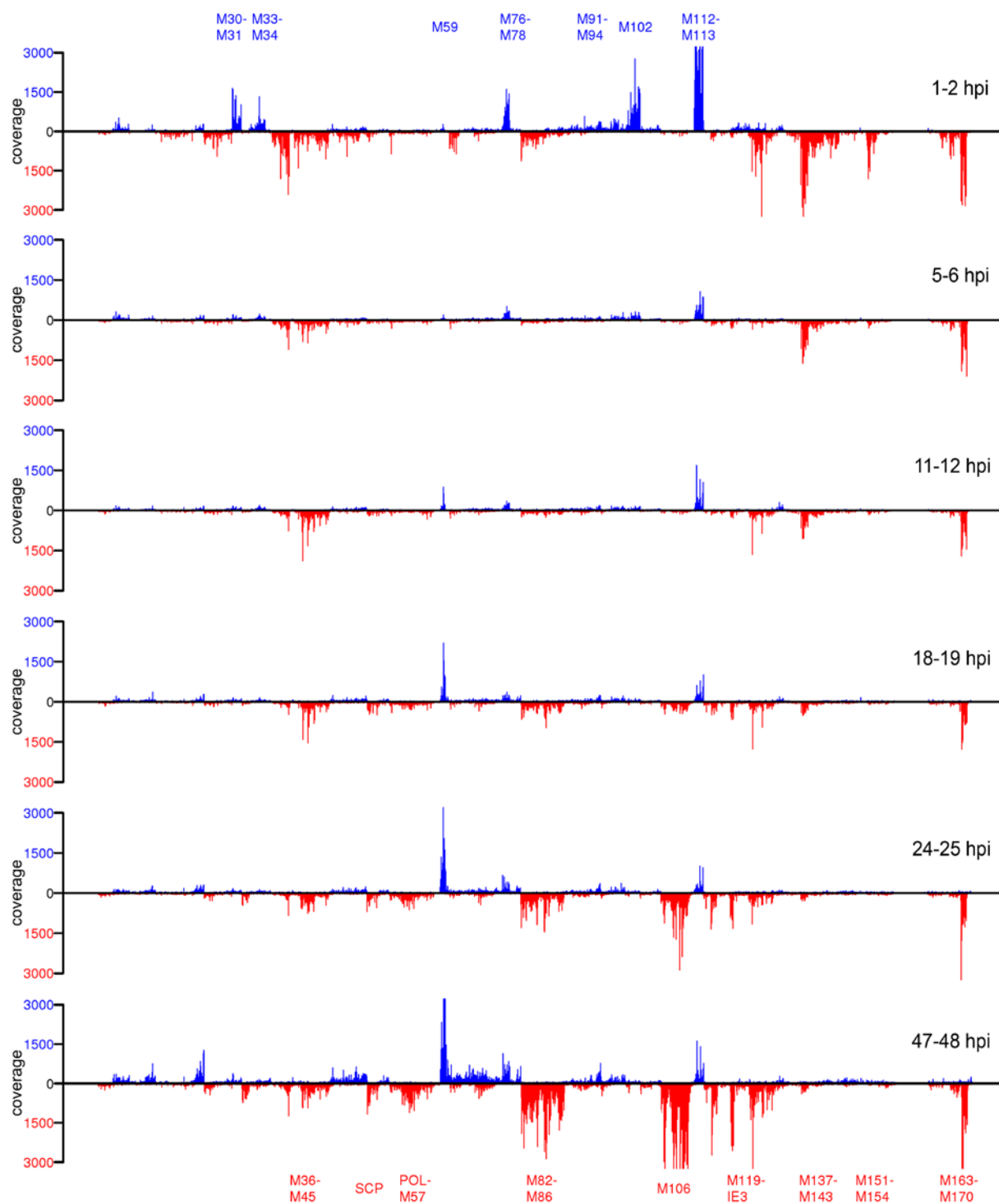


Figure 10. Analysis of MCMV gene expression by RNA-Seq

Shown are the coverages of all viral genes across the MCMV genome obtained by RNA-Seq on newly transcribed RNA from uninfected cells, 1-2 hpi, 5-6 hpi, 11-12 hpi, 18-19 hpi, 24-25 hpi and 47-48 hpi, normalized to the total number of mapped exonic mouse reads. Genomic positions of exemplary genes as well as concordantly regulated gene clusters are marked; SCP = small capsid protein (m48.2), POL = polymerase (M54). Blue represents transcripts matching the direct DNA strand and red the complementary DNA strand.

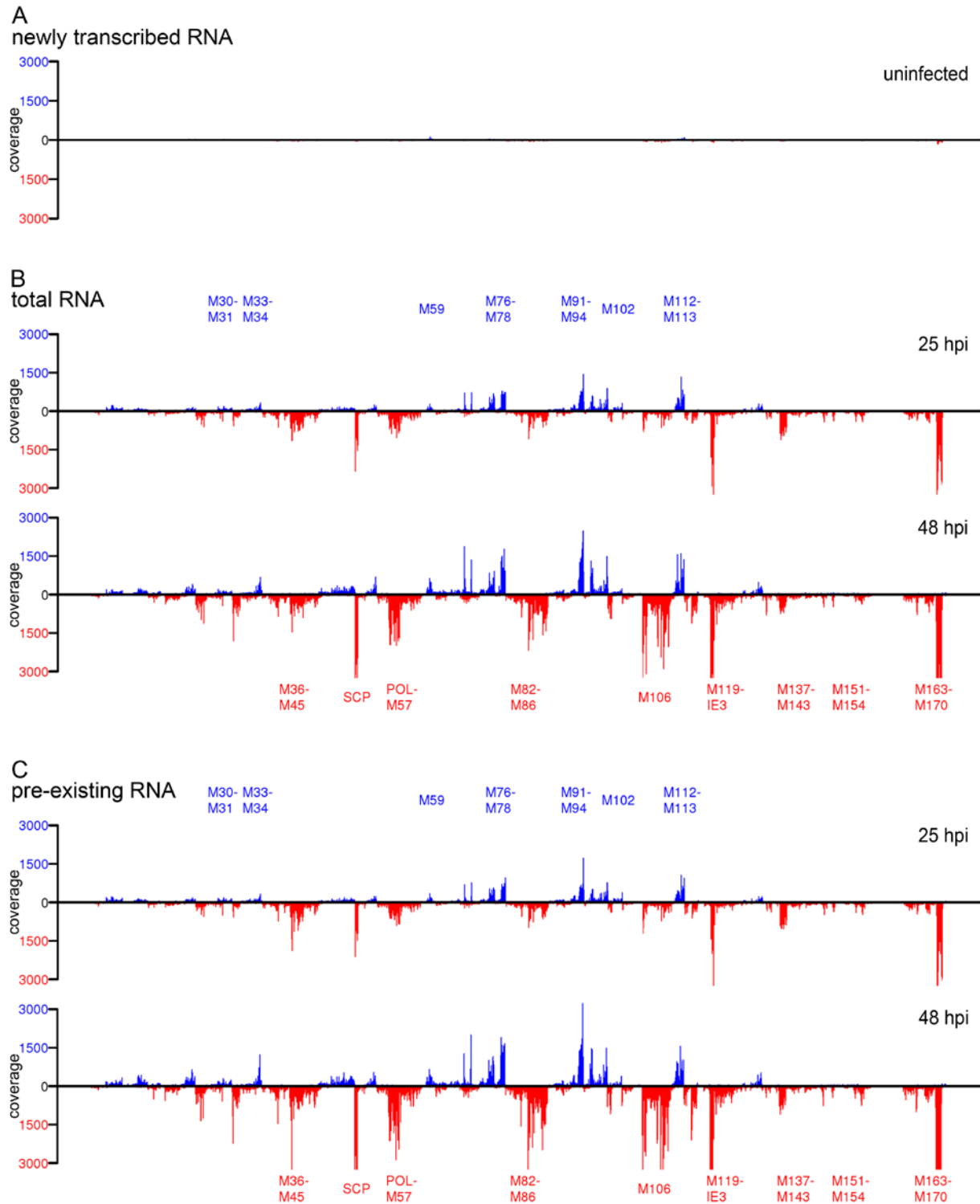


Figure 11. RNA-Seq data on MCMV gene expression using total RNA and unlabeled pre-existing RNA
 Shown are the read coverages of all viral genes across the whole MCMV genome obtained by RNA-Seq for uninfected cells for (A) newly transcribed RNA samples and 25 hpi and 48 hpi for (B) total RNA samples and (C) pre-existing RNA samples normalized to the total number of mapped exonic mouse reads. Positions of exemplary genes as well as representative gene clusters showing concordant regulation are indicated; SCP = small capsid protein (m48.2), POL = polymerase (M54). Blue represent reads matching to the direct DNA strand and red represents reads matching to the complementary DNA strand.

II.4 Discussion

In this work, we first employed 4sU-tagging combined with microarray analysis to study the dynamic changes in transcriptional activity of NIH-3T3 fibroblasts during early MCMV infection. Interestingly, we found virtually all changes in total cellular RNA to be matched by concordant changes in newly transcribed RNA, indicating that alterations in RNA decay rates do not substantially contribute to differential gene expression during early phase of MCMV infection of fibroblasts. This is consistent with previous reports showing that alterations in RNA decay rates do not seem to provide a major contribution during the first 3 h of the response of fibroblasts to type I and II interferons [36] or of dendritic cells to lipopolysaccharides [38]. It is important to note that the high MOI we employed facilitated the initiation of a fast, contemporaneous infection, crucial to dissect the temporal cascade of rapid transcriptional changes during lytic MCMV infection. This approach revealed extensive regulation, which remained undetectable in total cellular RNA. These elements of the host response to lytic infection are of particular interest because they are likely to be subjected to rapid viral counter-regulation. Analysis of newly transcribed RNA combined with the use of UV-inactivated virus detailed such rapid viral counter-regulation for inflammatory-, interferon-, DNA-damage- and ER-stress-induced changes. While numerous MCMV proteins have been shown to counteract the consequences of the induced ER-stress response, *i.e.* the induction of stress-induced natural killer cell activating ligands (reviewed in [129]), little is known about the counter-regulation of ER-stress signaling itself. The same is true for the very transient DNA-damage response we observed. The rapid counter-regulation in transcriptional activity revealed by newly transcribed RNA implies the existence of novel viral factors targeting these important cellular processes. Furthermore, our approach will now allow screening of large deletion mutants for the responsible viral genes.

Analysis of newly transcribed RNA revealed delayed down-regulation of genes involved in chromatin modification as well as down-regulation of genes involved in cell proliferation and actin filament-based processes. Within a few hours of infection, MCMV-infected cells show a profound cytopathic effect. The underlying molecular events remain to be elucidated. It is tempting to speculate that transcriptional down-regulation of genes involved in actin filament-based processes and cell adhesion, which we found to be consistently down-regulated as early as 1-2 hpi, contributes to this phenomenon.

As we exemplified for both NF- κ B and c-Myc, changes in transcriptional activity (as detectable in newly transcribed RNA) directly mirror the changes in the activation status of

the involved transcription factors. In addition, the ability to group the large number of differentially regulated genes (as usually identified when analyzing total RNA changes) into well-defined functional clusters of genes (regulated with distinct kinetics) further aids the subsequent success of *in silico* promoter analyses. Our approach thus provides an ideal mean to obtain insights into the molecular mechanisms/transcription factors involved. It is important to note that most of the transcription factors, implicated by our promoter analysis, have already been associated with the functional annotations of the respective gene clusters. In addition, many of the transcription factors specifically over-represented in the clusters (see Table S3) were consistent with published data on their functional role in lytic CMV infection. Of interest, E2F-sites were significantly over-represented in genes repressed with delayed kinetics (Cluster 5). The E2F family consists of both activating and repressing transcription factors (for review see [130,131]). The activating E2F family members, E2F-1, -2 and -3, are important for the transactivation of target genes involved in G1/S transition and apoptosis. E2F-4 and -5 predominantly have repressive functions, mediating cell-cycle exit and cell differentiation. E2F-6, -7 and -8 also act as transcriptional repressors, but are less well characterized. A caveat of this is that the DNA-binding sites of the E2F-family members cannot be differentiated from each other by bioinformatics means, highlighting the complexity of this regulation. Therefore, the repression of genes in Cluster 5 could either be mediated by repression of activating E2F-family members (E2F-1,-2 and -3) or activation of repressive family members like E2F-4 and -5. Interestingly, the most significantly associated gene ontology for Cluster 5 was not ‘G1/S-phase of the mitotic cell cycle’, as would have been expected in case of E2F-1-associated regulation, but ‘M-phase of the mitotic cell cycle’. Recently, the LIN complex (LINC), which involves the repressive E2F-4 family member, was shown to selectively repress genes involved in G2/M phase [132]. A closer look at the genes of Cluster 5 revealed the presence of numerous genes reported by this and other work [133] to be key marker-genes repressed by the LINC complex (which involves E2F-4). These included Survivin (Birc5), Cyclin B1, Aurkb, Esp11 and Bub1. It is thus tempting to speculate that the repression of genes in Cluster 5 is mediated not by repression of activating E2F-family members, but by activation of repressive E2F-family members (involving LINC). Ongoing work seeks to clarify the role of E2F-family members in this regulation. Lytic HCMV infection has been shown to result in E2F-1 activation by rapid degradation of the under-phosphorylated form of pRB by the HCMV protein pp71 [134,135] and to increase E2F-1 responsive genes [136]. Of note, we did not observe over-representation of E2F sites in any of the MCMV-induced gene clusters. While HCMV can only induce lytic infection in G0/G1

phase, MCMV can also efficiently replicate in cells that have passed through S phase by arresting them in G2 [137]. Differences in shifting cell populations may thus account for the lack of E2F-1 over-representation in our MCMV-induced gene clusters.

4sU-tagging provides the unique opportunity to study the regulation of viral gene expression in real-time without the interference of virion-associated RNAs. Employing 4sU-tagging combined with qRT-PCR and RNA-Seq to lytic MCMV infection, we report on three surprising findings. 1) A peak of viral gene expression including expression of immediate-early, early and even well-characterized late genes at 1-2 hpi at both high and low MOI. 2) The rapid suppression of all three classes of viral gene expression by 5-6 hpi. 3) Very constant levels of viral gene transcription rates (e.g. for IE1 and m169) or even continuously increasing suppression (e.g. m152), despite the onset of extensive viral DNA replication.

Both qRT-PCR and RNA-Seq on newly transcribed RNA revealed a peak of transcriptional activity of viral genes at 1-2 h of lytic MCMV infection, to an extent only reached again at late stages of infection (47-48 hpi). We were surprised to observe that this even included transcription of well-characterized late genes, e.g. m129-131 and M94. Rigorous controls excluded DNA contamination, virion-associated RNA and gene expression from the opposing DNA strand. Furthermore, this transcriptional activity was also observed at low MOI. In this case, however, the peak of both early (m152 and m169) and late (M94 and m129/131) gene expression slightly shifted from 1-2 hpi to 3-4 hpi, thus separating this from the peak of immediate-early gene expression, which still had already peaked at 1-2 hpi. This shift strongly argues against 'leaky' promoters being responsible for this late gene expression, but rather highlights a role of virus-mediated regulation (most likely mediated by IE- or viral tegument-proteins) in facilitating this part of viral gene expression. At present, it is unclear whether the respective transcripts are actually translated. Recent reports indicate regulation occurring at the level of translation to provide a major contribution to overall regulation of mammalian gene expression [102]. It is tempting to speculate that the virus uses additional, so far undisclosed mechanisms, to regulate its gene expression at post-transcriptional level. Of note, previous studies already postulated a role of post-transcriptional regulation in HCMV [138] and expression of some HCMV genes has already been shown to be regulated at post-transcriptional level [139,140].

Interestingly, the peak of viral gene expression we observed at 1-2 hpi was followed by a rapid drop in transcription rates by 6-12 hpi. We were surprised to see this rapid down-regulation of early gene expression. Interestingly, this was sustained or even exaggerated at late times of infection. What is the cause of this down-regulation? Chromatin modifications of

the viral genome are well known to play an important role during productive CMV infection (reviewed in [141]). The ND10 body-associated protein Daxx is known to rapidly repress transcription of incoming viral genomes by inducing repressive chromatin modifications around the HCMV major immediate-early promoter (MIEP) within 3 hpi. Dependent on the MOI of infection, the virus is able to overcome this repression. This results in the inhibition/reversion of HDAC-mediated repression of the viral genomes present in the nucleus and initiates the expression of early genes [89,142]. It is important to note that the peak of early gene expression should thus only occur after ND10 body-mediated repression has already been efficiently disrupted. Our data are fully consistent with this hypothesis. While we observed both immediate-early and early gene expression to peak or already have peaked at 1-2 hpi following high MOI (consistent with rapid disruption of ND-10 bodies), low MOI resulted in a visible delay between the peak of immediate-early and early gene expression. This is consistent with a delayed dispersion of ND-10 body-mediated repression of early gene expression at low MOI. Of note, we observed repression of viral gene expression after the peak of early gene expression, i.e. after ND-10 bodies have already been dispersed. Therefore, this suppression, which we observed by both qRT-PCR and RNA-Seq to occur in between 6 and 12 hpi, is unlikely to be due to the intrinsic antiviral defense known to be mediated by ND-10 bodies.

Interestingly, transcription of some genes, *e.g.* *ie1* and *m169* substantially dropped and then continued at low level despite the onset of viral DNA replication (i.e. a rapid >100-fold increase in viral DNA load). The most likely explanation for this observation is that the DNA architecture of *de novo* synthesized viral genomes does not support transcription of (at least) some viral genes. On the other hand, it is tempting to speculate that these differences in chromatin structure play an important role in initiating viral late gene expression. Interestingly, transcription rates of some viral genes, *e.g.* *m152*, continued to drop (exceeding 500-fold compared to 1-2 hpi) until 47-48 hpi. These observations highlight the importance of transcription factors in the regulation of viral gene expression. Activation or repression of these transcription factors will also influence the expression of the cellular genes they govern. The kinetics of viral gene expression during the first few hours of infection best matches those of cellular genes within the Clusters 1 and 2. This is consistent with the well described presence of binding sites for NF- κ B and even interferon stimulated response elements (ISRE) in many viral promoters [143,144]. The changes in transcription factor activity following the advent of viral DNA replication are less well understood. 4sU-tagging now allows us to properly study the changes in cellular gene expression following the onset of

viral DNA replication. Correlating these with the changes in viral gene expression will substantially enhance our understanding of how these viruses modulate the host-cell machinery for their own needs and pinpoint novel targets for antiviral intervention.

Degradation of cellular miR-27 by a novel, highly abundant viral transcript is important for efficient virus replication in vivo

III.1 Introduction

MicroRNAs (miRNAs) are small non-coding RNA molecules, which are involved in a broad range of biological processes. They represent an evolutionary highly conserved mechanism present in virtually all multicellular organisms ranging from fungi to mammals (reviewed in [145]). MiRNA biogenesis is a stepwise process involving the sequential action of the RNase III enzymes Drosha and Dicer, generating a ~22 nucleotide (nt) miRNA duplex. One strand of the duplex is then loaded into the RNA-induced silencing complex (RISC), while the other strand, known as the passenger strand or star sequence (miRNA*), is often, but not always, actively degraded. Upon assembly into the RISC complex, which invariably contains a member of the Argonaute protein family, they regulate gene expression either *via* translational inhibition, and/or destabilization of the targeted transcript. To date, more than 1,400 miRNAs have been identified in humans [146]. Once incorporated into RISC, the loaded miRNA is thought to be rather stable, with a half-life in the range of days [147].

In the last few years, tremendous progress has been made regarding the functional role of miRNA-mediated regulation of gene expression, resulting in the identification of thousands of miRNA target sites [148–150]. However, much less is known about the regulation of small RNAs themselves. Regulation of miRNA expression levels has been described to occur at the level of transcription, processing, and stability (reviewed in [145]). Nevertheless, the underlying molecular mechanisms are not always clearly understood. As such, it has been reported that the regulation of the maturation step of the let-7 miRNA precursor is subject to regulation *via* the interaction of Lin28 with its terminal loop. After binding to the pre-miRNA, Lin28 recruits the terminal uridylyltransferase Zcchc11, which mediates tailing of the 3' end of the small RNA [151–153]. The modification of small RNAs by nucleotide addition is not only observed for pre-miRNAs, mature miRNAs can also be modified. This was initially reported in the plant model *Arabidopsis thaliana*, whereby miRNAs are usually methylated at their 3' end by the methyl transferase HEN1 [154]. In a HEN1 mutant background, the absence of the 2'-O-methyl group on small RNAs triggers their 3' end tailing, usually by uridylation, to bring

about their degradation [155]. It has thus been proposed that the 2'-O-methylation of plant small RNAs, which also occurs on animal Piwi-interacting RNAs (piRNAs) [156,157] actually functions to protect the small RNAs against uridylation and subsequent degradation. Recently, it was described that the interaction between a small RNA and its target can in some cases (extensive base pairing) also result in the degradation of the miRNA [158]. Interestingly, this was found to be accompanied by 3'-tailing and -trimming of the miRNA. However, the molecular mechanisms involved still remain to be identified.

Regulation of miRNA expression occurs in response to both biotic and abiotic stresses [159]. Among the former, viral infections represent a prominent part and are known to interact extensively with the RNA silencing machinery. In mammals, this is best exemplified by the hijacking of the miRNA machinery by viruses, especially herpesviruses, to express their own miRNAs [160]. The use of small, non-immunogenic RNA molecules to regulate their own, as well as cellular gene expression, is yet another illustration of the extensive adaptation of these viruses to their hosts - the result of millions of years of coevolution [162]. In addition to expressing their own miRNAs, viruses also interact with cellular miRNAs. For example, miR-32 plays an antiviral role upon primate foamy virus infection, and both miR-24 and miR-93 negatively regulate the vesicular stomatitis virus [163]. A recent study revealed a number of cellular miRNAs with apparently intrinsic antiviral properties [164], highlighting the need for viruses to engage in the alteration of the cellular miRNA profile. It is therefore not surprising that the expression levels of some cellular miRNAs are deregulated during viral infection.

Recently, we showed that lytic mouse cytomegalovirus (MCMV) infection, besides expressing large numbers of viral miRNAs [58], results in the dramatic destabilization of two cellular miRNAs, namely miR-27a and miR-27b [70]. MiR-27a is encoded within a miRNA cluster located on chromosome 8, along with miR-23a and miR-24-2. It possesses an isoform located on chromosome 13, miR-27b that is clustered with miR-23b and miR-24-1. Strikingly, only the level of the mature forms of miR-27a and 27b were affected upon MCMV infection, while the levels of miR-27a* and miR-27b* remained unaltered. We thus hypothesized MCMV to encode a transcript targeting miR-27a/b for rapid degradation by a yet to be identified molecular mechanism. Interestingly, during the course of this work Cazalla *et al.* identified the herpesvirus saimiri HSUR1 transcript to bind to, and target miR-27a/b for degradation [71].

Here, we report on the identification of the MCMV transcript, encoded by the m169 gene, which mediates the rapid degradation of both miR-27a and 27b. We found this down-regulation to be accompanied by 3'-tailing and -trimming of the miRNA. Specificity to miR-

27a/b is mediated *via* a single binding site located in the m169 3'-UTR. Replacement of this target site allowed for efficient retargeting of the transcript to other cellular and viral miRNAs. Despite its dramatic effect on miRNA stability, we found this interaction to be mutual, resulting in miR-27a/b-mediated regulation of m169. We thus performed infections of mice with the mutant viruses we generated, which lost the ability to degrade miR-27a/b, but retained regulation by a retargeted cellular or viral miRNA. Results from these experiments reveal that the interplay between the m169 transcript and cellular miRNAs is important during acute MCMV infection *in vivo*.

III.2 Materials and Methods

Ethic statement

All of the protocols used for breeding of mice and different kinds of treatments were approved by the Ethical Committee of the Faculty of Medicine University of Rijeka and were performed in accordance with Croatian Law for the Protection of Laboratory Animals, which has been harmonized with the existing EU legislation (EC Directive 86/609/EEC).

Cell lines

BALB/c murine embryonic fibroblasts (MEFs) and M2-10B4 bone marrow stroma cells (ATCC: CRL-1972) were cultured in DMEM containing 10% fetal calf serum and penicillin/streptomycin. NIH-3T3 fibroblasts (ATCC: CRL-1658) were cultured in DMEM medium containing 5% fetal calf serum and penicillin/streptomycin.

Generation of mutant viruses

Generation of deletion mutants to screen for the gene responsible for miR-27a/b degradation was performed as described previously [165] using the full-length MCMV BAC pSM3fr [166]. All PCR primers are included in Table 2A. Markerless BAC mutagenesis was performed to introduce more subtle changes into the MCMV m169 locus. This was performed according to previously published protocols [167,168]. Briefly, an I-SceI-aphAI cassette was amplified from the plasmid pEPKAN-S by 2-step PCR using the different sets of primers included in Table 2B. In the first Red recombination step these PCR fragments were inserted into pSM3fr, resulting in a BAC carrying a kanamycin resistance cassette flanked by I-SceI restriction sites. The kanamycin resistance cassette was then removed from kanamycin-resistant clones by an arabinose-induced I-SceI digestion and subsequent heat-induced Red recombination, resulting in markerless mutagenesis of the miR-27a/b binding site in m169.

The revertant virus (MCMV-m169-mut-rev) was generated from the m169-mut BAC by completely restoring the wild-type sequence, *i.e.* reverting all three point mutations to wild-type sequence. All mutant BACs were subjected to extensive restriction pattern analysis using at least three different restriction enzymes followed by sequencing of the altered m169 locus. All viruses were reconstituted by transfecting the recombinant BACs into murine embryonic fibroblasts and virus titers were determined on MEFs by standard plaque assay as described [165].

Table 2. List of all primers used for cloning

A. Primers used for generation of MCMV deletion mutants using ET-cloning. **B.** Primers used for generation of MCMV mutants using Markerless mutagenesis [167].

A

Δ 7S.1-gfp	F: 5' AACTGGAAAATATAGTTAGCACCCGTTAGAGAGGGGCGACAGATTCGATCACTACAAGGACGACGACGACA AGTAA 3' R: 5' CGGCGCGAAGACACAGACGTATAGCGCTGTACGTCCTACCGAATCGCGGTGTGACACAGGAACACTTAA GGCTGA 3'
Δ 7S.2-gfp	F: 5' GAAAGCCCCATGTCTATCGGAAACACACTACGGTTCAAGAGAGGGCCCTACTACAAGGACGACGACGACA AGTAA 3' R: 5' GCGGGCGTCCAGAGACAGAGGACTCCGGCGGGCGGACACTAACGATCCGGGGTGTGACACAGGAACACTTAA CGGCTGA 3'
Δ 7S.3-gfp	F: 5' CGAACGTCGATCCAAAACACCCTCTCCGCACGCGCAGCTGCTGGCCCTACTACAAGGACGACGACGAC AAGTAA 3' R: 5' ATGTGCTCGGTTAACGAGTTGGCCCTTCGTCGGCTGTCCGGCAGGACTACGTGACACAGGAACACTTAA CGGCTGA 3'
Δ m167	F: 5' CGAACGTCGATCCAAAACACCCTCTCCGCACGCGCAGCTGCTGGCCCTACTACAAGGACGACGACGACA AGTAA 3' R: 5' ATGCTCACGTGGCAGAGTGTGAAACTTTGACAGCGGATGTTGCGACCCGACAGGAACACTTAACGGCT GA 3'
Δ m168	F: 5' ATGCGAGGACGGACACACGAGGGAAGGATGTATGTGCGTGAAAGAACACGTAGGACGACGACGACAAG TAA 3' R: 5' CGACTGCCCGTCTCCTTCGGAGTAGAAACTCTATCCTCGGAGCGATCCTCGCAGGAACACTTAACGGCT GA 3'
Δ m169	F: 5' GAACACTTTCGGTGACATGAACGATGAAGTGGCGGGAGAAAGTAGCAAGCTCAGGACGACGACGACAAG TAA 3' R: 5' ATGAGCAACGCGGTCCCGTTCGTCGCCCTACGCGGGTATCGGCCACAACCTCAGGAACACTTAACGGCT GA 3'
Δ m170	F: 5' CCTGGTACCTGCGCGGGCGTCAACCCGTAACGCTGTAGCATGCCGGCGGGAGGACGACGACGACAAGT AA 3' R: 5' ATGCTCACGTGGCAGAGTGTGAAACTTTGACAGCGGATGTTGCGACCCGAAGGAACACTTAACGGCTG A 3'

B

Generation of MCMV-m169-mut	
1. PCR	
H5-m169-pepkan	5'-tgaggagaccgttctcaggcagacatccaaggactctttCcaTagTttattattccgcagatcgtctctgggggatA GGATGACGACGATAAGTAGGG-3'
Pepkan rev	5'-CAACCAATTAACCAATTCTGATTAG-3'
2. PCR	
H3-m169-pepkan	5'- CCTCGGAGCGATCCTCGTCCGCCGTCTCCCCCGTCCGTGATCTCCCCCAGA CGACGATCTGCGGAATAATAAACTATGGAAAGAAGTCCCTTCGGATGTCTCAACCAATT AACCAATTCTGATTAG-3'
m169 pepkan-for	5'- TGAGGAGACCGTTCTCAGGCAGAC-3'
Generation of MCMV-m169-rev	
H5-m169-rep	5'-AGTAGCATCTCCCGATGAGGAGACCGTTCTCAGGCAGACATCCGAAGGGAC TTCTTTTCACAGCTTATTATTCGCGAGAT AGGATGACGACGATAAGTAGGG-3'
Pepkan rev	5'-CAACCAATTAACCAATTCTGATTAG-3'
2. PCR	
H3-m169-rep	5'-TCCGCCGTCTCCCCCGTCCGTGATCTCCCCCAGACGACGATCTGCGGAAT AATAAGCTGTGAAAAGAAGTCCCTTCGGACAACCAATTAACCAATTCTGATTAG-5'
m169 pepkan-for	5'- TGAGGAGACCGTTCTCAGGCAGAC-3'

Generation of MCMV-m169-miR-16	
1. PCR	
H5-m169-miR-16-pepkan	5'-tgaggagaccgttctcaggcagacatccgaaggacttcttagcagcaaacctattggcggatcgtcgtctgggggat AGGATGACGACGATAAGTAGGG-3'
Pepkan rev	5'-CAACCAATTAACCAATTCTGATTAG-3'
2. PCR	
H3-m169-miR-16-pepkan	5'-CCTCGGAGCGATCCTCGTCCGCCGTCTCCCCCGTCCGTGATCTCCCCCAGACGACGATCCGCCAATAGGGTTGCTGCTAAGAAGTCCCTTCGGATGTCTCAACCAATTAACCAATTCTGATTAG-3'
m169 pepkan-for	5'-TGAGGAGACCGTTCTCAGGCAGAC-3'
Generation of MCMV-m169-miR-M23-2	
1. PCR	
H5-m169-miR-M23-2-pepkan	5'-tgaggagaccgttctcaggcagacatccgaaggacttctatggggcgctttacaagcgggatcgtcgtctgggggggat AGGATGACGACGATAAGTAGGG-3'
Pepkan rev	5'-CAACCAATTAACCAATTCTGATTAG-3'
2. PCR	
H3-m169-miR-M23-2-pepkan	5'-CCTCGGAGCGATCCTCGTCCGCCGTCTCCCCCGTCCGTGATCTCCCCCAGACGACGATCCCGCTTGTAACGCCCCCATAGAAGTCCCTTCGGATGTCTCAACCAATTAACCAATTCTGATTAG-3'
m169 pepkan-for	5'-TGAGGAGACCGTTCTCAGGCAGAC-3'
Generation of MCMV-m169-PRS-mut	
1. PCR	
H5-m169-bHuR-1 pepkan	5'-ACGGACACACGAGGGAAGGATGTATGTGCGTGAAAGAACACGTTCTCGTTTCTTTCTTCTGCGTATTGCATTCAAGTAGCATCTAGGATGACGACGATAAGTAGGG-3'
Pepkan rev	5'-CAACCAATTAACCAATTCTGATTAG-3'
2. PCR	
m169-bHuR-1-for	5'-ACGGACACACGAGGGAAGGATGT -3'
H3-m169-bHuR-1 pepkan	5'-TCCCTTCGGATGTCTGCCTGAGAACGGTCTCCTCATCGGGAGATGCTACTTGAATGCAATACGCAAGAAGAAAAGAAACGACAACCAATTAACCAATTCTGATTAG-3'

Generation of adenoviruses expressing full-length or parts of m169

Adenoviral vectors expressing either full-length m169, or its 3'-UTR fused to EGFP under control of the cellular EF1-promoter were generated by Sirion Biotech, Martinsried, Germany. An adenovirus expressing mCherry served as control. To increase transduction efficiency of NIH-3T3 cells, TransMAX enhancer reagent (Sirion Biotech) was used following the manufacturer's instruction using an MOI of 50 and 500 (titers derived from infection of HEK-293 cells, corresponding to an MOI of about 5 and 50 in NIH-3T3 cells).

Infection of NIH-3T3 cells

Six-well plates were seeded with 0.5×10^6 cells one day prior to infection in DMEM containing 10% fetal calf serum. Cells were infected with indicated viruses at an MOI of 1

followed by centrifugal enhancement (800 g, 30 min), resulting in an effective MOI of ~10; culture media was replaced following one hour of infection.

Quantifying changes in miRNA levels by qRT-PCR

NIH-3T3 cells were infected with wild-type MCMV or mutant viruses at an MOI of 10. 48 h post infection RNA was prepared using either Trizol reagent (Invitrogen) or miRNeasy columns (Qiagen) following the manufacturers' instructions. cDNA was prepared in a single step reaction for both miRNAs and larger transcripts using the miScript Reverse Transcription kit (Qiagen). Light Cycler qRT-PCR was performed for various cellular and viral miRNAs using the miScript SYBR Green PCR kit (Qiagen) following the manufacturer's instructions. In each case the nucleotide sequence of the mature target miRNA was used to design the miRNA-specific forward primer. The PCR program was composed of a denaturation step at 94°C for 12 min followed by 45 cycles of 95°C for 15 sec (ramp rate 20°C/sec), 55°C for 30 sec (ramp rate 20°C/sec; 60°C for mRNA targets) and 70°C for 1 sec (ramp rate 2°C/sec). A list of all PCR primers is provided in Table 3.

Table 3. List of all primers used for qRT-PCR

miR-27a-for	5'-TTCACAGTGGCTAAGTTCCGC-3'
miR-24-for	5'-TGGCTCAGTTCAGCAGGAACAG-3'
miR-16-for	5'-TAGCAGCACGTAAATATTGGCG-3'
m169-for	5'-CAGGCAGACATCCGAAGGGACTT-3
m169-rev	5'-TCTCCCCCGTCCGTGATCT-3
IE1-for	5'-TCA GCC ATC AAC TCT GCT ACC AAC-3'
IE1-rev	5'-ATC TGA AAC AGC CGT ATA TCA TCT TG-3'
gapdh-for	5'-TGT CAA GCT CAT TTC CTG GTA TGA-3'
gapdh-rev	5'-CTT ACT CCT TGG AGG CCA TGT AG-3'
LBR-for	5'-GGA AGT TTG TTG AGG GTG AAG TGG T-3'
LBR-rev	5'-CCA GTT CGG TGC CAT CTT TGT ATT T-3'
irf1-for	5'-AGA GCC AGA TCC CAA GAC ATG GAA-3'
irf1-rev	5'-ACA GCA GAG CTG CCC TTG TTC CTA-3'

Immunoprecipitation of mouse Argonaute 2 complexes

To determine whether the m169 transcript was recruited to Ago2-complexes, immunoprecipitation of miRNA/target complexes was performed using the recently published antibody to mouse Ago2 [169]. Per replicate, ten large (15 cm) dishes of NIH-3T3 cells were infected with an MOI of 10 for 0, 6 or 12 h with wild-type MCMV. Cells were washed twice

with PBS before lysis in 10 ml lysis buffer, containing 25 mM Tris HCl pH 7.5, 150 mM KCl, 2 mM EDTA, 0.5% NP-40, 0.5 mM DTT, and Complete protease inhibitor (Roche). DTT and protease inhibitors were always prepared freshly and added immediately before use. Lysates were incubated for 30 min at 4°C and cleared by centrifugation at 20,000 g for 30 min at 4°C. Total RNA was prepared from 100 µL of cell lysates using the miRNeasy kit (Qiagen) following the manufacturer's instructions. Ago2-immunoprecipitation was performed as recently described [60]. In short, 6 µg of purified monoclonal mAgo2-antibody (2D4, Wako) or monoclonal BrdU-antibody (Abcam; used as control) was added to 5 mL of RPMI-medium and incubated with 30 µL of Protein-G-Sepharose beads (GE Healthcare) in Pierce centrifuge columns (Thermo Scientific) under constant rotation at 4°C over night. Columns were drained by gravity flow and washed once with the lysis buffer. Beads were subsequently incubated with 5 mL of cell lysates for 2.5 h under constant rotation at 4°C. After incubation, the beads were washed four times with IP wash buffer (300 mM NaCl, 50 mM Tris HCl pH 7.5, 5 mM MgCl₂, 0.1% NP-40, 1 mM NaF) and once with PBS to remove residual detergents. RNA was recovered from the beads by adding 700 µl of Qiazol to the columns. After 5 min the Qiazol lysates were collected from the columns. This step was repeated once and the Qiazol lysates were combined. RNA was prepared using the miRNeasy kit (Qiagen) according to the manufacturer's instructions. RNA samples were eluted in 30 µL of H₂O. Efficiency of the immunoprecipitation was checked by qRT-PCR for miR-16 and let7a.

Northern blot analysis

Small RNAs. RNA was extracted using Trizol and northern blotting was performed on 10 µg of total RNA. Briefly, total RNA was resolved on a 17.5% acrylamide gel of 30 cm in length. RNA was transferred by semi-dry transfer (BioRad TransBlot SD) to a Hybond-NX membrane (GE Healthcare). RNAs were then cross-linked to the membrane by EDC cross-linking as described in Pall and Hamilton [170] with a 90 min incubation step at 65°C. Prehybridization, hybridization, and wash steps were performed at 50°C. Probes either consisted of 5'-³²P-radiolabelled oligodeoxynucleotides only or oligodeoxynucleotides containing Locked Nucleic Acid positions for the detection of tailed forms of miR-27 (Eurogentec). They are perfectly complementary to the miRNA sequence or to part of the U6 snRNA sequence.

m169 transcript. Total RNA samples (1 µg) were mixed with equal volumes of loading dye and heated at 65°C for 10 minutes prior to separation on a 1.2% agarose/formaldehyde gel.

RNA was transferred overnight to a Hybond-NX membrane (GE Healthcare) by standard capillary transfer methods and crosslinked with UV. Membranes were prehybridized for 2 hrs in PerfectHyb™ plus (Sigma) at 50°C. Antisense DNA oligos for m169 (5'-GGACGGGGGAGACGGCGGACGAG) and mouse 18S (5'-CGGAACTACGACGGTATCTG) were 5' end labelled using T4 polynucleotide kinase (Fermentas) with 25 µCi of [γ -32P]dATP. The labelled probe was hybridized to the blot overnight at 50°C. The blot was then washed at 50°C twice for 20 min (5× SSC/0.1% SDS), followed by an additional wash (1× SSC/0.1% SDS) for 20 min.

Northern blots were exposed to phosphorimager plates (Fuji) and scanned using a FLA-5000 series phosphorimager (Fuji).

Small RNA cloning and sequencing

To assess the role of MCMV in the regulation of miR-27, four small RNA libraries were generated, either from total RNA, or from small RNAs immunoprecipitated with Ago2. For libraries generated from total RNA, 10 µg of total RNA was used in the initial step. For libraries generated from small RNAs incorporated into Ago2 containing RISC complexes, a fraction of the mAgo2 IPs from either MCMV infected (6 hpi), or control cells were used. Samples were size fractionated on a 17.5% PAGE gel, and small RNAs between 19 and 33 nt were excised and cloned as previously described [171], except that small RNA PCR products were not concatamerized, and instead sent directly for sequencing. Small RNA libraries were sequenced at the Institut de Génétique et de Biologie Moléculaire et Cellulaire (IGBMC, Illkirch, France) using an Illumina Genome Analyzer IIX with a read length of 36 nt.

Deep-sequencing data analysis

Short sequences generated by the Illumina platform were pre-processed and annotated using an in-house pipeline, specifically designed to detect miRNA variants. We first applied the Dustmasker program [172] to filter out low complexity reads, before removing the 3' adaptor from the remaining sequences using the FASTX-Toolkit (http://hannonlab.cshl.edu/fastx_toolkit). Trimmed reads of 15 to 32 nt in length were then selected to be mapped simultaneously to the mouse (UCSC repository - assembly version mm9) and the MCMV (RefSeq database - accession number NC_004065.1) genomes using Bowtie [173] by permitting up to 1 mismatch in the first 15 read nucleotides and no limit beyond. Reads that could map to more than 20 loci were discarded and a post-filtering was applied to keep only the best alignment(s) of each small RNA sequence provided this (these)

alignment(s) did not exceed a total number of 9 mismatches compared to the reference genome. From there, all known mature and star miRNAs derived from *Mus musculus* and MCMV (miRBase v.17) were annotated by comparing their genomic coordinates to that of the reads, and by keeping reads with at least 50% of their length inside the genomic feature. By doing so, we were able to inventory and quantify all miRNA forms: full length, 3'-trimmed, 3'-tailed, 5'-trimmed, 5'-tailed and every possible combination (5'-trimmed+3'-trimmed, 5'-trimmed+3'-tailed, 5'-tailed+3'-trimmed and 5'-tailed+3'-tailed), may they be identical or different to the template sequence. During the quantification process, multiple mapped reads were weighted by a factor $1/n$, n being the number of alignments they were respectively involved in. To determine the nature of the modifications affecting miR-27a and miR-27b upon infection, these two miRNAs were more precisely analyzed and manually curated to redistribute the few sequences that were mis-annotated between the two forms. These mis-annotations were most probably due to the poor constraints applied on the 3' ends during the mapping step.

The data discussed in this publication have been deposited in NCBI's Gene Expression Omnibus and are accessible through GEO Series accession number GSE34475

For the generation of sequence logo representations and for the comparison of libraries, sequencing data were normalized per million miRNA reads. In addition, only sequences that were cloned at least once per 1×10^6 miRNA reads were considered to produce Figure 14D, Table S4 and Table S5. For Figure 14E and Figure 15, we first determined the 100 most abundant miRNAs in each library before selecting those that were common to all four libraries. We then extracted their respective tailed (only non-template additions were considered) and trimmed sequences, and in both cases we only kept modified miRNAs that were represented by at least 1 read per million miRNA reads in all four libraries. Finally, we calculated the sequence ratios for each selected miRNA between MCMV and mock infected libraries, and generated boxplot graphs. For Table S6, raw sequences of miR-27a and b prior to any filter were taken into account.

Mice

BALB/c (H-2^d) and SCID BALB/c (H-2^d) mice were housed and bred under specific-pathogen-free conditions at the Central Animal Facility, Faculty of Medicine, University of Rijeka.

Luciferase assays

HeLa WS cells were seeded in 48-well plates at 25,000 cells/well and then incubated for 24 h. Cells were then co-transfected using Lipofectamine 2000 (Invitrogen) with 25 ng of the reporter constructs, 250 ng of carrier pUC19 DNA and 10 nM of miRNA mimic (cel-miR-67 as a control or miR-27a). After 24 h, cells were then washed in PBS and lysed with 65 μ L of passive lysis buffer (Promega), and 10 μ L were assayed for Firefly and Renilla luciferase activity, using the dual-luciferase reporter assay system (Promega) and a luminescence module (Glomax, Promega). The relative reporter activity was obtained by first normalizing to the transfection efficiency with the Renilla activity, and then, to the firefly activity obtained for the empty control reporter, in presence of the miR-27 mimic or control mimic, to normalize for the effect of transfection of these oligonucleotides. Finally, the ratios of the values obtained for miR-27 and control mimics were calculated.

Infection conditions and detection of infectious MCMV in tissues, depletion of lymphocyte subsets and statistical evaluation

Mice were injected intravenously with 1×10^5 PFU of tissue culture-grown wild-type MCMV or recombinant viruses in 0.5 mL of diluent. Organs were collected either 4 or 14 days after infection and virus titers were determined by a standard plaque-forming assay [174]. *In vivo* depletion of B and T cells was performed by intraperitoneal injection of the mAbs to CD4 (YTS191.1), to CD8 (YTS 169.4) molecules [175]. Statistical significance of the difference between experimental groups was determined by the Mann-Whitney exact rank test.

Accession numbers of genes

The following murine genes were mentioned in the text: Glyceraldehyde-3-phosphate dehydrogenase (GAPDH; NM_008085.1), Lamin B receptor (LBR; NM_133815.2), Interferon regulatory factor 1 (IRF1; NM_008390.2), mmu-miR-27a (MIMAT0000537), mmu-miR-27b (MIMAT0000126), mmu-miR-24 (MIMAT0000219), mmu-miR-16 (MIMAT0000527).

III.3 Results

Degradation of miR-27a/b is mediated by a single binding site in the MCMV m169 transcript

Upon lytic infection with the murine cytomegalovirus (MCMV), large amounts of viral miRNAs are rapidly produced [58,176]. Recently, we reported that in addition to the expression of its own viral miRNAs, MCMV infection triggers the rapid degradation of two mature cellular miRNAs in various cell types, namely miR-27a and miR-27b [70]. These two cellular miRNAs show complete sequence identity but for the nineteenth nucleotide (“C” for miR-27a and “U” for miR-27b). As both miRNAs appeared to be similarly affected by MCMV, and because both quantitative RT-PCR (qRT-PCR) and northern blot analysis cannot properly distinguish miR-27a from miR-27b, we will refer indiscriminately to both miRNAs as miR-27. In detail, their degradation presented as a measurable decrease of the two mature miRNAs within 4 hours of infection, ultimately leading to an almost complete disappearance of miR-27 within two days of infection. Blocking viral gene expression in MCMV infected cells prevented miR-27 degradation [70]. It was thus tempting to speculate that this massive, apparently sequence-specific degradation of two cellular miRNAs was mediated by a viral transcript binding to the mature miRNAs, and subsequently targeting them for degradation *via* a yet to be discovered molecular mechanism. We decided to test this hypothesis by screening large deletion mutants to identify the gene responsible for this function. We started off with three MCMV mutants ($\Delta 1,6$; $\Delta 1,7$; $\Delta 6,7$) that we previously generated [177], each lacking two of the three gene blocks encompassing either MCMV genes m1–m16 (block 1), m144–m159 (block 6) or m159–m170 (block 7). It is important to note that none of these mutants shows any attenuation on NIH-3T3 fibroblasts *in vitro*, while all three show severe growth defects *in vivo* [177]. In order to ensure efficient infection of >99% of all cells, we always infected NIH-3T3 fibroblast with a multiplicity of infection (MOI) of 10 for 48 h, and determined changes in miR-27 expression levels relative to miR-24 by quantitative RT-PCR (qRT-PCR). We chose miR-24 for normalization as it is expressed from the same pri-miRNA transcript as miR-27. In addition, we found qRT-PCR C_T values for miR-24 to be virtually identical to miR-27 in uninfected cells, thus providing an ideal mean for normalization using the $\Delta\Delta C_T$ -method. In accordance with our previous observations [70], wild-type MCMV infection resulted in a ~30-fold reduction in miR-27 levels compared to miR-24 (Figure 12A). While miR-27 degradation was still apparent with the $\Delta 1,6$ mutant, both mutants lacking gene block 7 (m159–m170) completely lost their ability to target miR-

27 for degradation. Therefore, degradation of miR-27 indeed appeared to be mediated by a viral gene product. We thus generated and tested a second set of smaller deletion mutants ($\Delta 7S1$, $\Delta 7S2$ and $\Delta 7S3$, see Figure 12B), each lacking four MCMV genes of gene block 7. The results obtained with these three mutant viruses, following the same experimental setup as before, pinpointed the responsible viral gene to m167–m170 (Figure 12C). Finally, we generated and tested a third set of mutants ($\Delta m167$, $\Delta m168$, $\Delta m169$ and $\Delta m170$) lacking the predicted coding sequences (CDS) of the corresponding genes. Only the mutant lacking the predicted m168 CDS was no longer able to target miR-27 for degradation (Figure 12D). We thus looked for a putative binding site for miR-27 on either strand of the genome within the 389 nt deletion of m168 using RNA-hybrid [178]. Interestingly, this revealed a single binding site on the strand opposite to m168, within the predicted 3'-untranslated region (UTR) of m169. The binding site consists of a perfect match to the first 7 nt of miR-27a (6-mer seed match), a G-U pairing at the 8th position, a 5 vs. 6 nt bulge (known to prevent target degradation *via* Ago2 slicer activity), and a 7 nt perfect match to the 3'-end of the miRNA (including one G-U pairing adjacent to the bulge) (Figure 12E). The one nucleotide difference between miR-27a and miR-27b only results in a change from an A-U to a G-U pairing, which was predicted by RNA-hybrid to render the interaction to m169 slightly weaker for miR-27b than for miR-27a (mean free energy (mfe) = -23.5 kcal/mol vs. -25.7 kcal/mol). Markerless mutagenesis to introduce three single point mutations into the seed region of the predicted binding site (MCMV-m169-mut) (marked in Figure 12E) resulted in an almost complete loss of miR-27 degradation from ~30-fold, down to ~2-fold (Figure 12F). Degradation of miR-27 was completely restored for the revertant virus. However, it is important to note that only the middle one of these three point mutations actually disrupts seed pairing, as both A-U and G-U pairings are known to support RNA-RNA interactions, thus rendering the other two mutations less potent. Therefore, a G-U wobble at position 2, and a single mismatch in the middle of the seed region were sufficient to almost completely abolish miR-27 degradation.

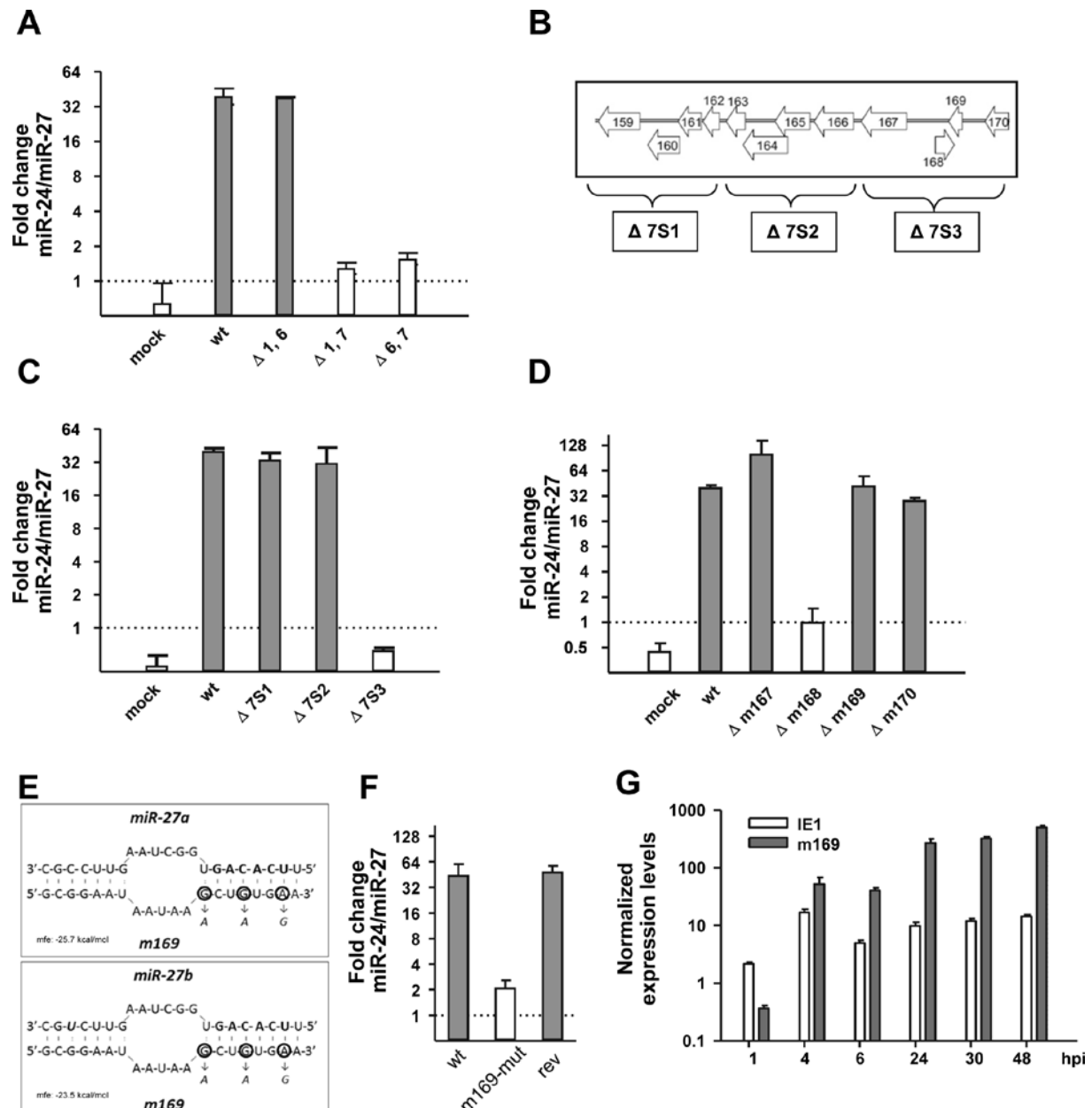


Figure 12. MCMV m169 transcript is targeting miR-27 via a single binding site in its predicted 3'-UTR
A. Gene block 7 (m149-m170) is crucial for miR-27 degradation. NIH-3T3 cells were infected with wild-type MCMV or three large deletion mutants each lacking two of the three gene blocks 1 (m01-m16), 6 (m144-m158) or 7 (m159-m170) at an MOI of 10. 48 h post infection total RNA was isolated and miR-27 levels were quantified relative to miR-24 by qRT-PCR. **B.** Genomic organization of gene block 7 and the three subdividing mutants. **C.** Degradation of miR-27 is mediated by a gene located in between m167 and m170. The effect of the indicated mutants on miR-27 expression was determined as described above. **D.** The genomic region encompassing the m168 coding sequence is essential for degradation of miR-27. The effect of the indicated mutants on miR-27 expression was determined as described above. This implicated either m168 or m169 to be implicated in miR-27 degradation. **E.** The binding site of m169 / miR-27a and miR-27b interactions. RNAhybrid predicted a single, well defined binding site for miR-27a/b in the predicted 3'-UTR of the m169 transcript showing a typical match-bulge-match structure. The three point mutations introduced by markerless mutagenesis to create MCMV-m169-mut are indicated. Only the middle one truly affects this interaction due to G:U ↔ A:U base pairing altered by the other two. In addition, the binding site to miR-27b is shown with the single nucleotide difference to miR-27a indicated in bold italics. The mean free energy (mfe) of the interactions was determined using RNAhybrid. **F.** Mutagenesis of the binding site abolished miR-27 degradation. The effect of the mutant virus and its revertant on miR-27 levels were determined as described above. **G.** Expression levels of m169 and IE1 transcripts. NIH-3T3 fibroblasts were infected with WT MCMV at an MOI of 10. At the indicated time points of infection total RNA was prepared. Expression levels of m169 and IE1 were determined by qRT-PCR and normalized for Lamin B receptor (LBR) mRNA levels

To get further insights into the characteristics of the m169 transcript, we made use of data generated by the Jonjic and Trgovcich laboratories, which performed a large scale cDNA cloning and sequencing study to comprehensively characterize the MCMV transcriptome (Lisnic *et al.*, manuscript in preparation). In this study, a ~1.7 kb transcript containing the m169 open reading frame (ORF) was identified (for transcript details see Figure 13). This analysis also revealed a novel intron of 78 nt, located close to the 3'-end of the putative m169 CDS. The miR-27 binding site is located 104 nt 3' of the m169 stop codon at the 5' end of the m169 transcript 3'-UTR. Quantitative RT-PCR revealed this transcript to be already expressed at high levels within the first hour of infection exceeding IE1 transcripts by >2-fold within 4 hours of infection and >20-fold at 48 hours post infection (hpi) (Figure 12G).



Figure 13. Annotated nucleotide sequence of the m169 transcript (Smith strain)

Degradation of miR-27 by the m169 transcript involves its 3'-tailing and -trimming

Recently, it was reported that extensive complementarity between a target RNA and a miRNA can result in post-transcriptional modifications of the miRNA, mainly addition of nucleotides at the 3' end of the small RNA (tailing), and shortening of the sequence from its 3' extremity (trimming) [158]. We therefore looked for post-transcriptional modifications of miR-27 at early times of infection prior to its degradation. We infected NIH-3T3 cells with wild-type MCMV at an MOI of 10 and collected cells to extract total RNA every hour from 1 to 5 hpi, and at 7, 9, 12, 24 and 48 hpi. We then performed high-resolution small RNA northern blot analysis on these RNA samples and probed for miR-27, miR-16 as well as the viral mcmv-miR-M23-2. As can be seen on Figure 14A, miR-27 accumulated as four distinct bands in the mock infected cells. During the first two to three hours of MCMV infection, the pattern of miR-27 bands did not change, but after four hours of infection additional bands started to appear, while conjointly the expression level of the major band started to decrease. The number of extra-bands visible on the miR-27 blot culminated at 7 hpi before gradually decreasing again, the quantification of the most prominent band showed that miR-27 was almost completely degraded by 48 hpi. The level of the control miRNA miR-16 was not affected throughout the time course, and the accumulation of the mcmv-miR-M23-2 occurred as expected [58]. At the same time, we also measured the accumulation of the viral transcript m169 and showed that it started to become detectable by northern blot at 2 hpi, and was abundantly expressed at 4 hpi, coinciding with the appearance of additional bands in the miR-27 blot (Figure 14B).

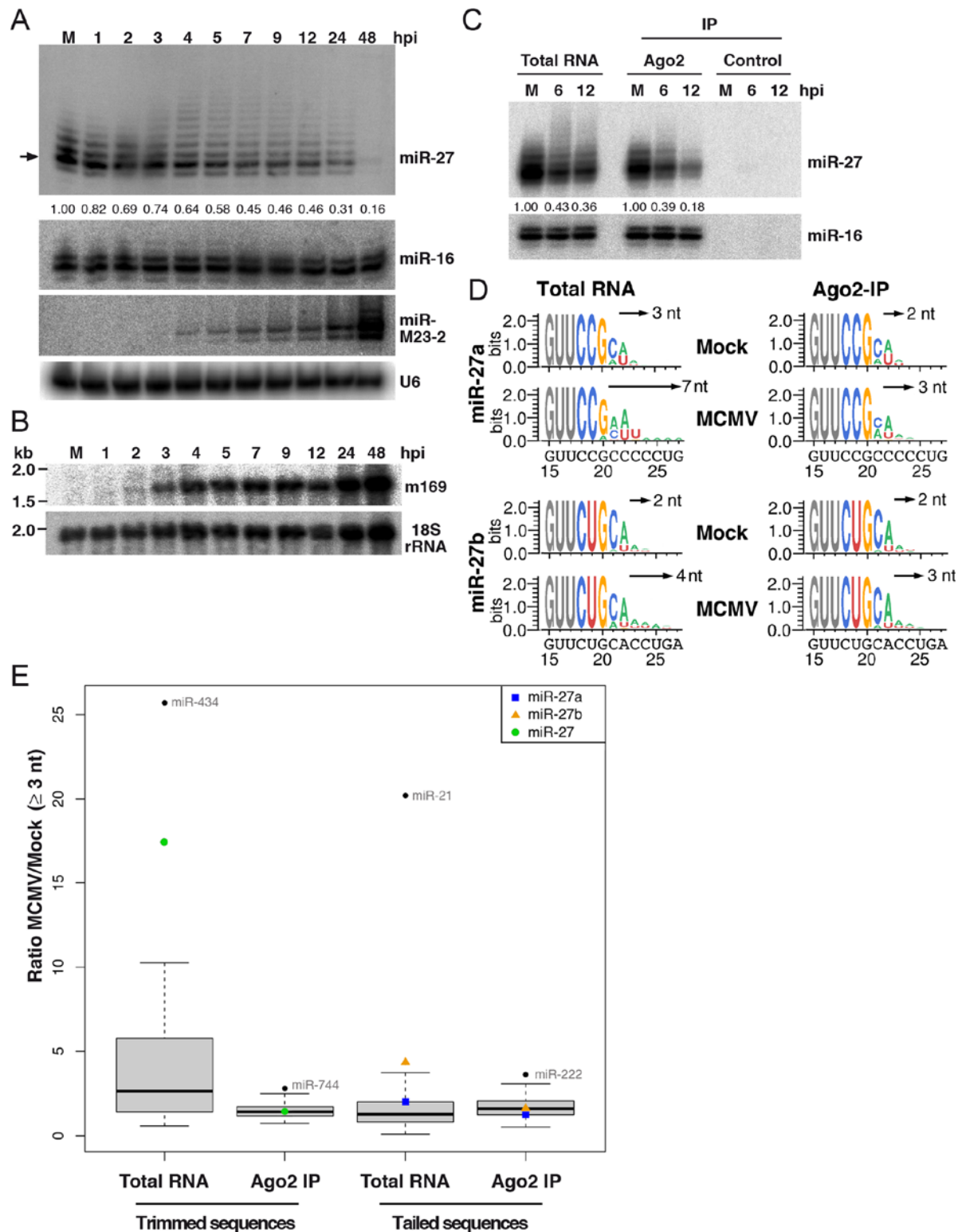


Figure 14. Degradation of miR-27 is linked to its 3'-tailing and -trimming

A. Northern blot analysis of miR-27, miR-16, miR-M23-2 in NIH-3T3 cells infected with wild type MCMV (MOI = 10). The arrow indicates the prominent band representing the mature miR-27, which is quantified relative to Mock (M) as indicated by the numbers below the blot. U6 snRNA was used as a loading control. **B.** Northern blot analysis of m169 transcript accumulation over time in the same MCMV-infected NIH-3T3 cells. 18S rRNA was used as a loading control. **C.** Accumulation of miR-27a and miR-27b in Ago2 IP and total RNA in mock (M) and from cells infected with MCMV for 6 and 12 hours. Signals were normalized to miR-16 and quantified relative to mock-infected cells. **D.** Sequence logo representations for tailed miR-27a and 27b retrieved from deep-sequencing analysis of total RNA or RNA extracted after Ago2 IP of mock or MCMV-infected cells (6 hpi). Only nucleotides 15 to 27 of miR-27 sequences presenting 3' addition are represented, nucleotides of interest are depicted in colour, and the sizes of the largest tails are indicated next to the arrows. The genomic

sequences of pre-miR-27a and b are indicated underneath the sequence logo representations. **E.** Boxplot representation of the trimmed and tailed MCMV/mock sequence ratios for the most abundant miRNAs shared by each library. Only sequences presenting with a 3'-trimming or a -tailing of ≥ 3 nt in total RNA or RNA extracted after Ago2 IP were considered. The outliers are indicated by black dots and miR-27a and b are indicated by a blue square and an orange triangle respectively. The green dot indicates sequences that could not be annotated as either miR-27a or 27b due to their trimming. The black bar indicates the median of all ratios.

In order to gain further insight into the level at which the degradation of miR-27 occurs, we then performed Ago2 immunoprecipitation (IP) of NIH-3T3 cells infected with MCMV at 6 and 12 hpi. We analyzed the accumulation of miR-27 in both the total RNA and RNA isolated after Ago2 IP. Although the resolution of this gel was not as good as in the previous northern blot, we could still see some tailing of miR-27 in the total RNA at 6 and 12 hpi (Figure 14C). Interestingly, the extent of tailing seemed to be lower in the RNA isolated from the Ago2 IP. In addition, miR-27 levels decreased significantly more rapidly in the Ago2 IP than in total RNA (Figure 14C), indicating that tailing of miR-27 might be accompanied by its displacement from Ago2 complexes subsequently followed by its degradation, or that extensive tailing occurred after displacement of miR-27 from Ago2.

We then set up to determine the nature of the modification of miR-27a and miR-27b by performing small RNA cloning and Illumina deep-sequencing using either total RNA extracted from mock-infected NIH-3T3 cells, or from cells infected with MCMV for 6 hours, as well as from RNA extracted after Ago2 IP from the same samples. The analysis of miR-27a and miR-27b sequences in the libraries revealed that in both mock- and MCMV-infected cells, addition of non-templated nucleotides could be detected at the 3' end, consistent with the northern blot data. Therefore, the additional bands seen for miR-27 by northern blot represent 3'-tailing with non-templated nucleotides, rather than processing isoforms. However, it is important to note that this feature was not unique to miR-27, but also seen for other cellular miRNAs. As can be seen in a sequence logo representation [179,180] of cloned miR-27a and b in total RNA extracted from MCMV-infected cells, the number of added nucleotides was greater for miR-27a (up to 3 nt in the mock vs. 7nt in the infected cells) than miR-27b (2 nt in mock vs. 4 nt MCMV infected cells respectively) (Figure 14D). The number of sequences presenting with longer tails, however, was lower for miR-27a than for miR-27b (Tables S4 and S5). The most prominent nucleotide added was an 'A', followed by a 'U'.

Intriguingly, in Ago2 IP the difference in tailing between mock and MCMV infected cells was neither evident for miR-27a nor miR-27b, indicative of displacement of extensively tailed miRNAs from Ago2, or conversely, tailing of miRNAs after displacement from Ago2. To estimate the significance of the modifications of miR-27 in MCMV infected cells, we extracted (for the most abundantly cloned cellular miRNAs) the number of sequences

presenting with a tail of ≥ 3 nt, and calculated the ratio of these values between MCMV and mock infected cells. Given that miRNA tailing has been associated with their trimming, we also performed the same analysis for sequences trimmed by at least 3 nt. We found that, in total RNA, miR-27b was significantly more tailed in MCMV infected cells compared to mock infected cells (4.35-fold) than any other cellular miRNA (median of ratio = 1.59) (Figure 14E). The ratio for miR-27a was 2.00, which is above the mean, but still inside the interquartile range. In addition, the enrichment of tailed miR-27b in MCMV infected cells was lost in Ago2 IP (Figure 14E). Only one other cellular miRNA, namely miR-21, showed significantly enhanced 3' tailing in MCMV infected cells (Figure 14E). As for miR-27b, this was only seen in total RNA but not in the Ago2 IP. Regarding the trimmed miRNAs, a strong enrichment (17.64-fold vs. a median ratio of 2.63) in MCMV infected cells compared to mock infected cells could be seen for miR-27 (due to the trimming, these sequences could not be attributed to either miR-27a or b). As for the tailed sequences, this enrichment was lost in the Ago2 IP. Only one other outlier, namely miR-434, showed an increased trimming in total RNA of MCMV vs. mock infected cells. Interestingly, this miRNA was also observed to be down-regulated in MCMV-infected cells (data not shown). We were unable to resolve trimming of miR-27 by northern blot. Finally, we also looked at miRNAs tailed or trimmed with ≥ 1 nt (Figure 15A), or ≥ 2 nt (Figure 15B), but did not find a significant difference between MCMV infected cells and non-infected cells for miR-27a and b. This is most probably due to the fact that both miRNAs already show the addition of up to 2 nucleotides in mock-infected cells, thereby introducing substantial variability and thus noise to our analysis. A global overview of all modifications observed for miR-27a and b can be found in Table S6.

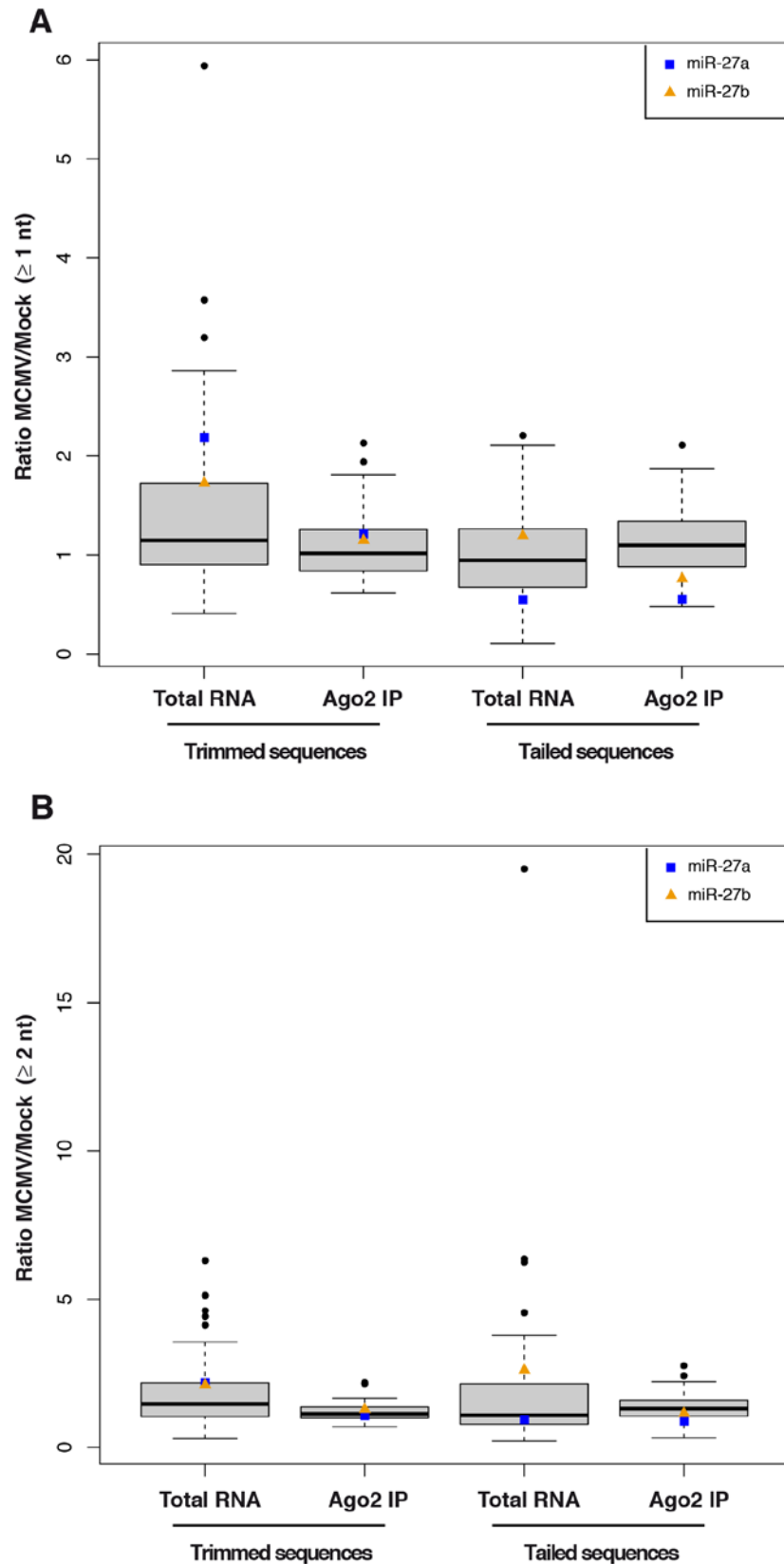


Figure 15. Boxplot representations of the trimmed and tailed MCMV/mock sequence ratios for the most abundant miRNAs common to all libraries

Only sequences trimmed or tailed by ≥ 1 nt (A) or ≥ 2 nt (B) in total RNA or RNA extracted after Ago2 IP were considered. The outliers are indicated by black dots and miR-27a and b are indicated by a blue square and an orange triangle, respectively. The black bar indicates the median of all ratios.

Retargeting of m169 to other cellular and viral miRNAs by target site replacement

In order to further characterize the mechanism of miR-27 degradation and obtain useful tools for further studies, we next tested whether we could retarget m169 to other cellular or viral miRNAs. We thus replaced the m169 binding site for miR-27 with a binding site for the ubiquitous cellular miR-16, or for the highly abundant viral miRNA mcmv-miR-M23-2 (Figure 16A). Binding sites were designed to mimic the natural match-bulge-match structure of the miR-27a binding site. We chose mcmv-miR-M23-2 as we recently found this miRNA (together with mcmv-miR-21-1) to be required for viral persistence in salivary glands [61]. After generating the mutant viruses (MCMV-m169-miR-16 and MCMV-m169-miR-M23-2) we performed a time-course of infection in NIH-3T3 cells with these viruses and performed northern blot analysis to probe for the effect of their retargeting on miR-27, miR-16 and mcmv-miR-M23-2 levels (Figure 16B). As expected, retargeting of m169 to other miRNAs by altering the miR-27 binding site completely abolished the ability of both mutants to mediate miR-27 degradation. In contrast, the MCMV-m169-mut still showed a slight reduction of miR-27 levels consistent with the ~2-fold reduction in miR-27 levels observed by qRT-PCR (see Figure 12F). Apparently, the single G-C to A-C change and the two A-U↔G-U changes to the seed region of the m169 binding site were not sufficient to completely abolish miR-27 binding. Most interestingly, this was accompanied by enhanced tailing of miR-27, represented by the appearance of additional bands on the northern blot. In contrast, complete disruption of this binding site by retargeting it to either miR-16 or mcmv-miR-M23-2 did not show this phenomenon. Together with the sequencing data shown in Figure 14D, these data provide strong evidence that miR-27 binding at this site mediates its tailing, either directly, or by displacing it from its Argonaute protein.

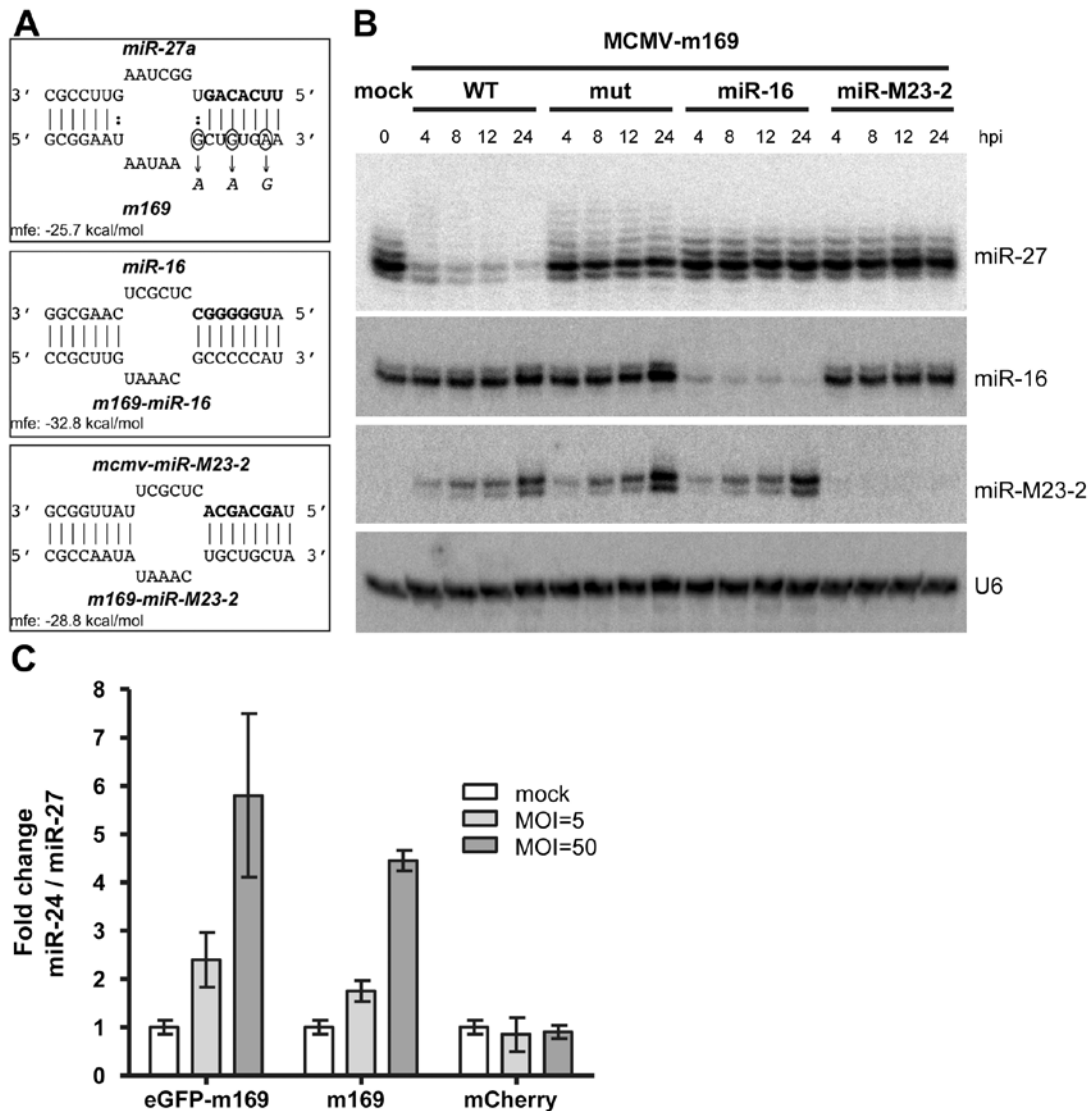


Figure 16. Retargeting of m169 to cellular and viral miRNAs

A. Schematic representation of the miR-27a/m169 binding site and the introduced mutated binding sites resulting in retargeting of m169 to either mmu-miR-16 or mcmv-miR-M23-2. Target site predictions were performed using RNAhybrid to design the retargeting of m169. **B.** Efficient retargeting of m169 to a cellular and a viral miRNA. NIH-3T3 cells were infected with the indicated viruses and total RNA isolated at different times of infection was analyzed by northern blot for miR-27, miR-16 and mcmv-miR-M23-2. U6 served as loading control. Retargeting of m169 to miR-16 and mcmv-miR-M23-2 abolished degradation of miR-27 but resulted in highly efficient degradation of the respective miRNAs. **C.** Expression of m169 3'-UTR is sufficient to mediate miR-27 degradation. Adenoviral vectors expressing either full-length m169 or its 3'-UTR fused to EGFP were used to transduce NIH-3T3 cells at an MOI of either 50 or 500. An adenoviral vector expressing mCherry was used as negative control. Two days post-transduction, total RNA was prepared and miR-24/miR-27 ratios were determined by qRT-PCR.

Infection with MCMV-m169-miR-16 resulted in the rapid degradation of miR-16 within the first four hours of infection. In addition, infection with MCMV-m169-miR-M23-2 completely abolished any detectable signal for mcmv-miR-M23-2 despite its strong expression and continuous accumulation during lytic MCMV infection (Figure 14B). Therefore, target site replacement of this single miRNA binding site in m169 is sufficient to efficiently target both cellular and viral miRNAs for rapid degradation.

Expression of m169 transcript alone is sufficient to target miR-27 for degradation

To test whether any other viral factors were involved in miR-27 degradation, we generated replication-deficient adenoviral vectors expressing either full-length m169 or its 3'-UTR fused to EGFP controlled by an EF1 promoter. An adenoviral vector expressing mCherry served as negative control. NIH-3T3 cells were transduced using an MOI of 50 or 500 (virus titers determined using HEK-293 cells) in the presence of TransMAX reagent to enhance transduction efficiency. Forty-eight hours after transduction of NIH-3T3 cells with these four adenoviruses, miR-27, miR-24 and m169 transcript levels were determined by qRT-PCR. Interestingly, expression of the 3'-UTR of m169 fused to EGFP was sufficient to mediate an MOI-dependent ~6-fold loss of miR-27 levels (Figure 16C). This is in accordance with m169 transcript levels being the highest in this condition but still 5- to 10-fold lower than those achieved by lytic MCMV infection as determined by qRT-PCR (data not shown). Therefore, expression of the 3'-UTR of m169 fused to a protein coding gene is sufficient to target a cellular miRNA for degradation and no other viral factors appear to be essential to this process.

As the 3'-UTR of m169 was apparently sufficient to mediate degradation of miR-27, we looked for additional motifs in it. We noticed a uridine-rich stretch located 69 nt 3' of the miR-27 binding site. Using markerless mutagenesis we mutated this stretch from 'UUUUUGUUUUUU' to 'AAGAAGAAAGAA' in the MCMV genome and reconstituted the mutant virus. However, this did not alleviate degradation of miR-27 following high MOI infection of NIH-3T3 fibroblasts (Figure 17).

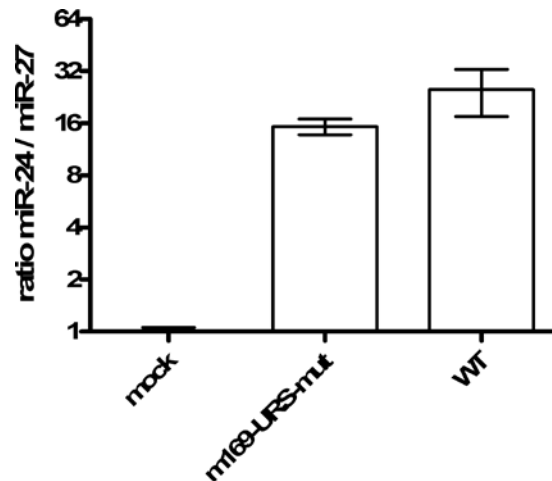


Figure 17. Mutagenesis of the pyrimidine-rich stretch close to the miR-27 binding site has no significant effect on miR-27 degradation

To generate MCMV-m169-URS-mut, the pyrimidine-rich stretch located 69 nt 3' of the miR-27 binding site was mutated from 'TTTTTGTTTTT' to 'AAGAAGAAAGAA' using markerless mutagenesis. The primers used to amplify the Kanamycin resistance gene encoded on the plasmid pEPKAN-S are included in Table 2. Following virus reconstitution, NIH-3T3 cells were infected with mock, m169-URS-mut or wild-type MCMV (WT) at an MOI of 10. At 48 hpi miR-24 and miR-27 levels were determined by q-RT-PCR. No significant difference in miR-27 degradation between m169-URS-mut and wild-type MCMV infection was observed.

m169 is a target of miR-27

While the m169 transcript obviously has a detrimental impact on miR-27 or any other miRNA binding to it in a miR-27-like manner, we needed to consider the option that the virus might simply utilize an abundant cellular miRNA to regulate expression of one of its genes. We thus investigated the effect of miR-27 on m169 RNA levels. First, we looked at m169 RNA levels following infection with wild-type MCMV, MCMV-m169-mut, its revertant, as well as the retargeted mutant MCMV-m169-miR-16. Expression levels of m169 mRNA at 24 and 48 hpi were determined relative to IE1 mRNA levels (to normalize for differences in infection) using qRT-PCR. The level of m169 mRNA was significantly greater (~2-fold, $p < 0.001$) for MCMV-m169-mut than for the other three viruses (Figure 18A). This is consistent with a partial loss of regulation of m169-mut by miR-27 (resulting in increased m169 levels) and an efficient retargeting of m169 by miR-16 which we found to be expressed at very similar levels as miR-27 using qRT-PCR (data not shown). At 48 hpi no differences in m169 transcript levels were observed anymore.

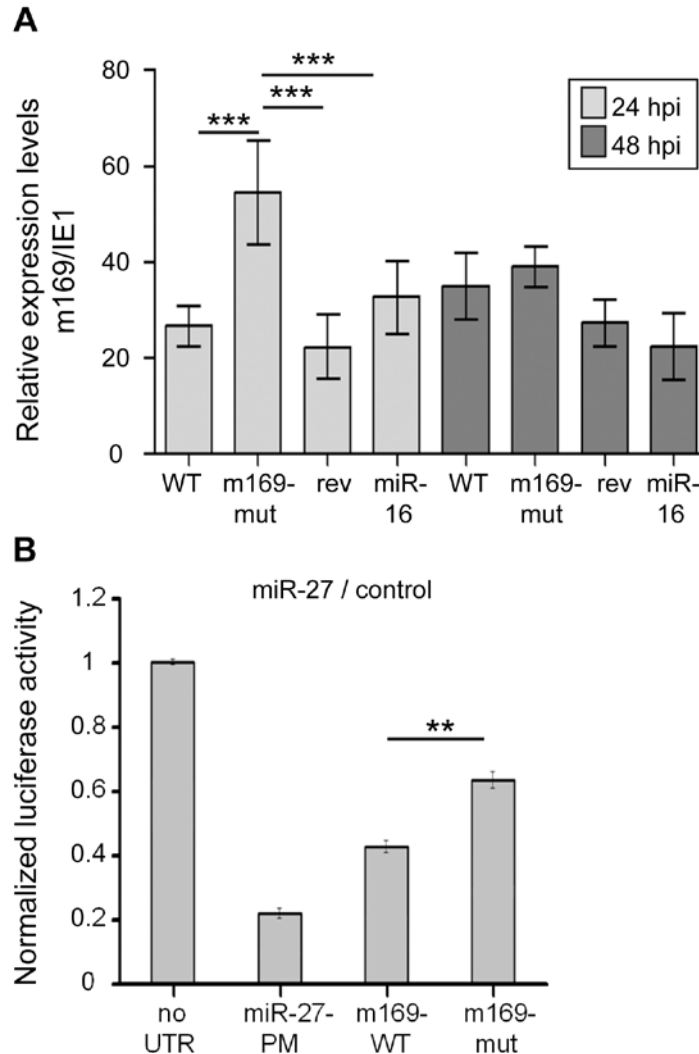


Figure 18. m169 is a target of miR-27.

A. Effect on m169 RNA levels. To assess the effect of the miRNA/m169 interaction on m169 transcript levels, NIH-3T3 cells were infected with wild-type MCMV, MCMV-m169-mut, its revertant as well as the retargeted mutant MCMV-m169-miR-16. At 24 and 48 hpi total RNA was prepared and m169 transcript levels were determined by qRT-PCR. In parallel IE1 RNA levels were quantified to normalize for dose of infection. Disruption of the miR-27 binding site (MCMV-m169-mut) resulted in significantly increased (One-way anova analysis followed by Tukey's multiple comparisons test: ***: $p < 0.0001$) m169 transcript levels at 24 hpi. This was restored when m169 was retargeted to miR-16 and no longer seen at 48 hpi. **B.** Dual-luciferase assay with psiCHECK2 constructs containing either no UTR, a perfect match (PM) binding site for miR-27, the wild type or the point mutant version of the m169 3'UTR. HeLa WS cells were co-transfected with the luciferase construct and a control miRNA mimic, or a miR-27a mimic. The ratios of normalized luciferase values for miR-27 and control mimics are indicated. ** $p < 0.001$.

We next assessed whether a luciferase sensor containing the m169 3'-UTR could be regulated by miR-27. We therefore generated psi-CHECK2 plasmids containing either a perfect match to miR-27, the full-length m169 3'UTR, or the point mutant version of the 3' UTR that was used in the virus infection experiment. These constructs were co-transfected into HeLa cells with control or miR-27 miRNA mimics (to prevent any possible down-regulation of the miRNA by these targets). As can be seen in Figure 18B, the perfect match sensor for miR-27 was 80% down-regulated by miR-27, while the m169 3'-UTR reporter showed a 60% down-

regulation. The insertion of the three point mutations in the m169'3'-UTR only partially alleviated its regulation by miR-27 to about 40%, which is consistent with the 2-fold effect of the respective mutant virus on miR-27 levels at 48 hpi. This indicates that the m169-mut transcript can no longer efficiently mediate miR-27 degradation, but is still partially regulated by miR-27. In summary, these data indicate a complex mutual interaction between miR-27 and m169.

The reciprocal interaction between miR-27 and m169 is important for *in vivo* infection

As the interaction between the m169 transcript and miR-27a appears to be mutual, the key question was whether the virus uses the m169 transcript to target an important cellular miRNA for degradation, or whether it simply uses an irrelevant but highly expressed cellular miRNA to reduce and delay protein expression of one of its genes. To address this question, we made use of our mutant and retargeted viruses and studied their phenotypes following 14 days of infection in mice. While we designed the three point mutations in MCMV-m169-mut such as not to alter the predicted m168 coding sequence, it is important to note that this was not possible for both MCMV-m169-miR-16 and MCMV-m169-miR-M23-2. For MCMV-m169-miR-M23-2 this altered six amino acids in m168. For MCMV-m169-miR-16 this resulted in a frame-shift and a premature stop codon 28 amino acids later (for details see Table 4). So far nothing is known about the function of m168, or whether it is expressed at all. However, we failed to detect any expression of the m168 transcript even at late time-points (both 24 and 48 hpi) of lytic MCMV infection of NIH-3T3 fibroblasts using next-generation sequencing (unpublished data). We thus infected BALB/c mice for 14 days with these viruses and determined virus titers in lungs. Interestingly, we observed a significant 3- to 12-fold attenuation of all three viruses, the greatest attenuation being observed for the m169-mut virus; no attenuation was observed for the revertant virus MCMV-m169-mut-rev (Figure 19A). This was also seen in BALB/c mice depleted for both CD4⁺ and CD8⁺ T-cells, indicating that the observed attenuation was independent of T-cell function. Next, we infected SCID BALB/c mice with wild-type MCMV, MCMV-m169-mut, or its revertant. At 14 days post infection (dpi) we again observed significant (~10-fold) attenuation of this mutant virus in both lungs and salivary glands (Figure 19B). We conclude that the quite striking role of miR-27 during lytic MCMV infection is independent of adaptive immunity. To test whether this phenotype would become apparent even at earlier stages of acute infection, we infected BALB/c mice for four days and compared virus titers in lung and spleen. While virus titers in lungs showed only a moderate, but consistent reduction in virus titers for all three mutants no

longer targeting miR-27, a strong 10- to 100-fold attenuation of all three mutants was observed in spleen (Figure 19C). Altogether, these data highlight that degradation of miR-27 by the MCMV m169 transcript, and presumably also the miRNA-mediated regulation of m169 protein expression are important factors during lytic virus infection *in vivo*.

Table 4. Changes in nucleotide sequence of the different mutants and their impact on the putative m168 coding sequence

WT-MCMV ggg act tct ttt cac agc tta tta ttc cgc aga tcg tcg tct G T S F H S L L F R R S S S
MCMV-m169-mut ggg act tct ttc cat agt tta tta ttc cgc aga tcg tcg tct G T S F H S L L F R R S S S
MCMV-m169-mut-rev ggg act tct ttt cac agc tta tta ttc cgc aga tcg tcg tct G T S F H S L L F R R S S S
MCMV-m169-miR-16 => G T S and then a frameshift and stop codon after about 28 aminoacids
MCMV-m169-miR-M23-2 ggg act ctt tat ggg ggc gtt tac aag cgg aga tcg tcg tct G T S Y G G V Y K R R S S S

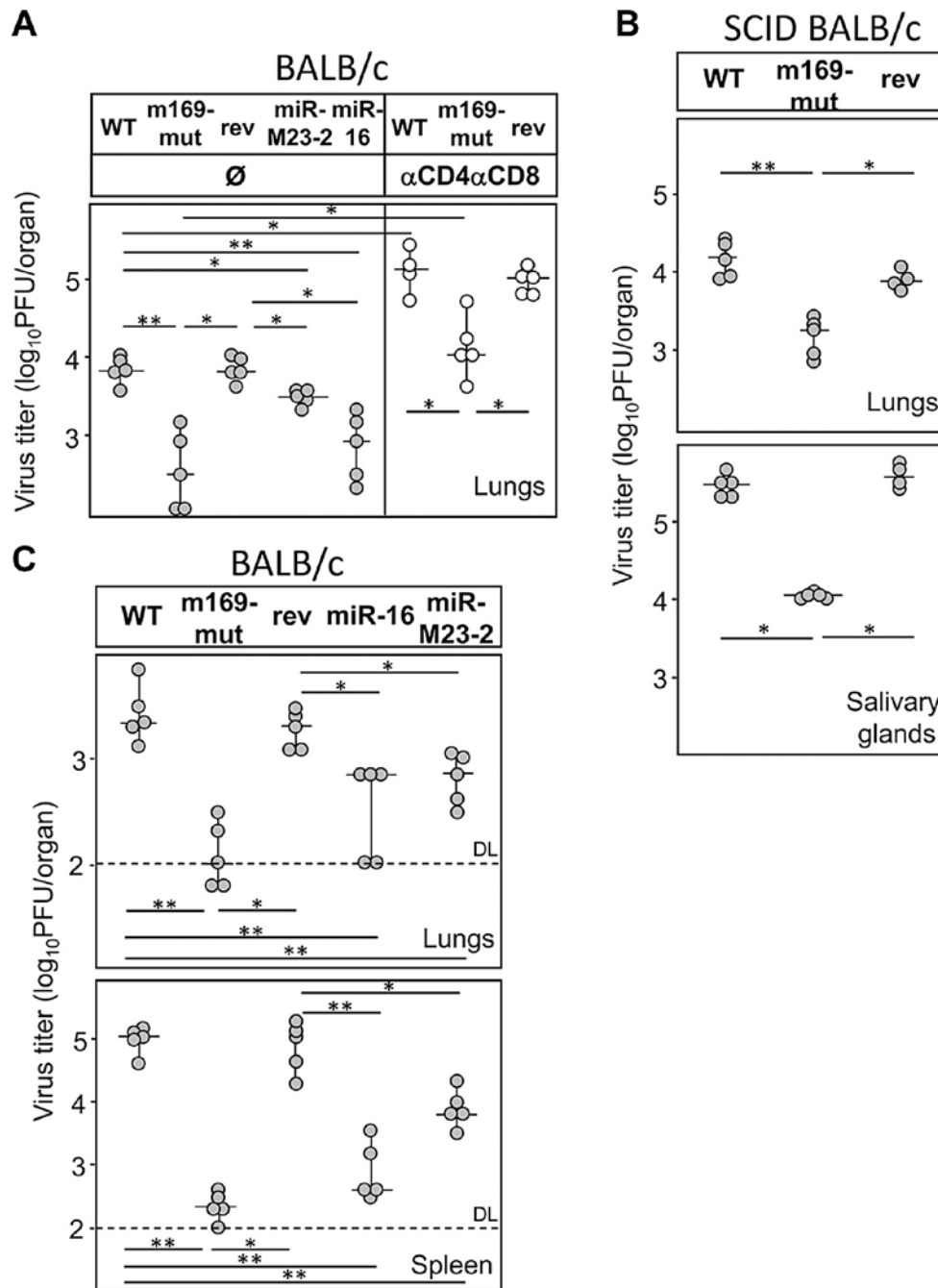


Figure 19. Degradation of miR-27 is important for efficient virus replication *in vivo*.

BALB/c (A) or SCID BALB/c (B) mice were injected intravenously (*i.v.*) with 1×10^5 PFU of wild-type (wt), MCMV-m169-mut, m169-mut-rev or the two retargeted viruses MCMV-m169-miR-16 and -miR-M23-2. Some of the BALB/c mice were depleted of CD4 and CD8 T cells. At 14 dpi organs were harvested and virus titers in lungs and salivary glands determined by standard plaque assay. C. BALB/c mice were injected *i.v.* with 1×10^5 PFU of indicated viruses. At 4 dpi organs were harvested and virus titers in lungs and spleen determined by standard plaque assay. Viral titers in organs of individual mice (circles) and median values (horizontal bars) are shown. DL = detection limit; * p<0.05; ** p<0.01.

III.4 Discussion

Besides expressing large amounts of viral miRNAs shortly after infection [58], MCMV also targets two cellular miRNAs for rapid degradation, namely miR-27a and b [70]. Using a set of deletion mutants and site directed mutagenesis, we show this effect to be mediated by a single binding site located within the 3'-UTR of a so far uncharacterized, highly abundant, spliced MCMV transcript, namely m169. We found this effect to be readily redirected to other cellular and viral miRNAs by target site replacement. Interestingly, expression of the m169 3'-UTR fused to EGFP by an adenoviral vector was sufficient to mediate degradation of miR-27, indicating that no other viral factors are essentially required in this process.

Recently, Ameres *et al.* reported on tailing and trimming of cellular miRNAs upon extensive base-pairing to their targets [158]. However, the underlying mechanism still remains to be determined. Thus, it is not known whether this is happening to miRNAs still bound by an Argonaute protein, or after their displacement from RISC. Upon wild-type MCMV infection, we observed extensive tailing of miR-27 by northern blot within the first few hours of infection, prior to its subsequent degradation. The tailing and degradation of miR-27 was not observed in cells infected with mutant viruses in which the miR-27/m169 RNA interaction was disrupted by retargeting m169 to either miR-16 or mcmv-miR-M23-2. This argues against a general effect of MCMV infection on miR-27 tailing. Despite the point mutations we introduced into the miR-27 binding site to generate MCMV-m169-mut, the m169-mut transcript was still able to bind miR-27, demonstrated by significant miR-27-mediated repression in dual-luciferase assays. In addition, it still resulted in a somewhat reduced but significant activity for miR-27 degradation (~2-fold instead of ~30-fold) as observed by both qRT-PCR and northern blot. Interestingly, we observed enhanced tailing of miR-27 following infection with MCMV-m169-mut compared to wild-type MCMV infection. Most likely, this is due to the larger amounts of miR-27 still present at 6–24 hpi. While these data thus provide strong hints that binding of miR-27 to this single binding site not only triggers its degradation but also its tailing, further studies are required to clarify the link between the two.

Consistent with the northern blot data, small RNA deep-sequencing revealed 3'-tailing with 1 to 3 non-template nucleotides for both miR-27a and miR-27b in uninfected cells. The presence of non-template tailing is a common feature of miRNAs, indicating that this is not unique to miR-27a/b. This was seen in both total RNA as well as Ago2 IP samples independent of MCMV infection. Upon MCMV infection, however, we observed both an enhanced tailing of miR-27b, as well as trimming of miR-27 (≥ 3 nt) in small RNA libraries

prepared from total RNA. Interestingly, this increased tailing and trimming of miR-27 was not detectable in small RNA isolated from Ago2 IP samples, which might indicate that these modifications occur after m169-mediated displacement of miR-27 from Ago2, or that the tailed and trimmed miR-27 forms are rapidly excluded from it. This is partially corroborated by the northern blot analysis, which showed a stronger MCMV-mediated down-regulation of miR-27 in Ago2 than in total RNA. The observation that miR-27b, and not miR-27a, showed enhanced tailing might be due to its slightly weaker interaction with m169, because a Watson-Crick base pair with the m169 transcript is replaced by a G-U pairing. It is thus tempting to speculate that we simply might have cloned and sequenced more tailed miR-27b in MCMV infected cells because it is less efficiently degraded than miR-27a – thereby either leaving less time for tailing of miR-27a following displacement from Ago2, or speeding up displacement of tailed miR-27a from Ago2 followed by its more rapid degradation. This would also explain the more rapid loss of both miR-16 and mcmv-miR-M23-2 following infection with the retargeted mutants, rendering tailing of these miRNAs below the detection limit of our northern blots. Studies are ongoing to address this important issue.

In a previous study [58], we already reported on extensive tailing of two viral miRNAs, namely mcmv-miR-m21-1 and mcmv-miR-M23-2, which was accompanied by a decrease of these miRNAs late in infection. As we found these two miRNAs to derive from a genomic locus transcribed from both the sense and antisense strand, tailing and degradation of these two miRNAs might result from binding to viral transcripts expressed from the antisense strand. Together with the data presented in this study, we therefore postulate that highly expressed transcripts, such as MCMV m169, can cause miRNA tailing (and trimming) followed by their degradation.

As m169 targets Argonaute-bound miR-27 for degradation, it was very reasonable to assume that m169 may also serve as a target for miR-27. Indeed we observed significantly higher m169 RNA levels following infection with MCMV-m169-mut than for wild-type MCMV, its revertant, or MCMV-m169-miR-16. Interestingly, this was only observed at 24 hpi, which was verified in three independent experiments. In contrast, at 48 hpi when wild-type MCMV infection has efficiently eliminated miR-27, its effect on m169 expression was relieved. As such, the mutual interaction between the m169 transcript and miR-27 is apparently complex. The key question really was whether the main function of m169 is to target an important cellular miRNA for degradation, or whether the virus simply uses an irrelevant but highly expressed cellular miRNA to reduce and delay protein expression of one of its genes. With the help of our retargeted viruses we were able to partially address this important question.

Interestingly, all three mutant viruses no longer able to efficiently target miR-27 for degradation were significantly attenuated at 4 and 14 dpi in all experiments we performed. This was particularly prominent in both spleen at 4 dpi, and in lungs at 14 dpi. It is, however, important to note that the generation of both MCMV-m169-miR-16 and MCMV-m169-miR-M23-2 (but not MCMV-m169-mut) resulted in alterations to the predicted m168 coding sequence. While we were unable to detect m168 expression by next-generation sequencing even at late times of infection (unpublished data; data not shown) this does not rule out that alterations in m168 may have contributed to the observed phenotype. In addition, we cannot exclude that degradation of miR-16 by MCMV-m169-miR-16 may have contributed to this phenotype. In contrast, we recently provided an extensive set of data showing that knock-out of mcmv-miR-M23-2 has no apparent effect on lytic virus replication in various organs at 4 dpi and in lungs at 14 dpi [61]. The knock-out (which also includes the knock-out of mcmv-miR-m21-1 which is generated from the antisense strand) only resulted in significantly lower virus titers in salivary gland at 14 dpi. In the course of the current study we decided to generate MCMV-m169-miR-M23-2 hoping to be able to further dissect the phenotype of the miR-m21-1/-M23-2 double miRNA knock-out virus in salivary gland [61]. However, as all three viruses no longer able to efficiently target miR-27 for degradation also showed significant attenuation in salivary gland at 14 dpi, this aim could not be achieved. In conclusion, it may thus well be that other factors than degradation of miR-27 contributed to the attenuation of the different mutants we observed. In particular the role of miR-27 in controlling the timing of m169 expression requires further studies. This and other factors are likely to have contributed to the attenuation of our three mutant viruses. However, as all three mutants deficient for miR-27 degradation were attenuated *in vivo* we believe this provides good evidence that degradation of miR-27 is indeed important during acute MCMV infection *in vivo*.

So far little is known about the function of miR-27. Our data provide strong evidence that miR-27 expression is harmful to productive MCMV infection. Interestingly, the Steitz laboratory recently showed that the oncogenic herpesvirus saimiri also uses one of its non-coding RNAs to target miR-27 for degradation [71]. This supports the interpretation of our data that degradation of miR-27 is indeed of importance for MCMV, and probably also for herpesvirus saimiri. The mechanism by which degradation of miR-27 aids lytic MCMV infection still remains elusive. To date, these two miRNAs have been implicated in pathways such as cell differentiation [181], adipogenesis [182], and angiogenesis [183]. Among the validated cellular targets, the tumor suppressor FOXO1, which is involved in controlling the

cell cycle through CDKN1C induction [184], might provide a link to the strong phenotype we observed during acute MCMV infection. Indeed, cytomegaloviruses are known for their manipulation of the cell cycle [185], and m169 may act by releasing the effects of miR-27 on cell cycle progression. Interestingly, recent reports showed that the level of the miR-16 family of miRNAs are efficiently destabilized in response to cell-cycle changes [186]. Therefore, rapid alterations in cellular miRNAs are likely to be of importance in the regulation of cell cycle progression.

Why does m169 so efficiently target miR-27 for degradation? We noted m169 to be expressed at extremely high levels within 4 h of infection, exceeding levels of IE1 by >20-fold at 24 h post infection. The number of m169 transcripts obviously matters. Mutagenesis of a uridine-rich motif, which we observed in close proximity to the miR-27 binding site, had no effect on miR-27 degradation. The shift from a classical miRNA-target interaction, where the miRNA regulates its target, and the opposite effect, *i.e.* miRNA degradation mediated by its RNA target, might thus simply be controlled by the relative abundance of the target RNA. When the m169 transcript reaches a certain level, it may thus start to trigger degradation of miR-27, ultimately avoiding its regulatory effect. Further studies are required to address this interesting question.

In conclusion, there is now increasing evidence that the expression of miRNAs is strongly regulated, and that these molecules are not as stable as they were once thought to be. They are part of a sophisticatedly tuned, complex reciprocal interaction network with the mRNA targets they regulate. The ability of cytomegalovirus to usurp the underlying cellular machinery by expressing decoy targets which bind to specific miRNAs and degrade them is yet another illustration of the fascinating dynamism of RNA-mediated regulation.

List of figures and tables

Figure 1. Establishment of 4sU-tagging for lytic MCMV infection	26
Figure 2. No effect of 1 h 200 μ M 4sU treatment on virus replication.....	27
Figure 3. Gene expression kinetics define distinct functional clusters	29
Figure 4. Validation of exemplary transcription factors	31
Figure 5. Identification of virus-specific regulation and counter-regulation using UV- inactivated virus.....	33
Figure 6. Real-time kinetics of viral gene expression.....	35
Figure 7. Temporal kinetics of MCMV replication	36
Figure 8. Regulation of viral gene expression following low and high MOI	38
Figure 9. Classification of reads aligned to mouse transcripts and genomic sequence	39
Figure 10. Analysis of MCMV gene expression by RNA-Seq.....	40
Figure 11. RNA-Seq data on MCMV gene expression using total RNA and unlabeled pre- existing RNA	41
Figure 12. MCMV m169 transcript is targeting miR-27 <i>via</i> a single binding site in its predicted 3'-UTR.....	60
Figure 13. Annotated nucleotide sequence of the m169 transcript (Smith strain).....	61
Figure 14. Degradation of miR-27 is linked to its 3' -tailing and -trimming	63
Figure 15. Boxplot representations of the trimmed and tailed MCMV/mock sequence ratios for the most abundant miRNAs common to all libraries	66
Figure 16. Retargeting of m169 to cellular and viral miRNAs.....	68
Figure 17. Mutagenesis of the pyrimidine-rich stretch close to the miR-27 binding site has no significant effect on miR-27 degradation	70
Figure 18. m169 is a target of miR-27.	71
Figure 19. Degradation of miR-27 is important for efficient virus replication <i>in vivo</i>	74
Table 1. All PCR primers used for qRT-PCR are shown.....	22
Table 2. List of all primers used for cloning	51
Table 3. List of all primers used for qRT-PCR.....	53
Table 4. Changes in nucleotide sequence of the different mutants and their impact on the putative m168 coding sequence.....	73
Table S1a. List of MCMV-regulated cellular genes.....	Appendix
Table S1b. List of MCMV-regulated genes with greater change in total RNA than in newly	

transcribed RNA.....	Appendix
Table S1c. Clusters of genes regulated with distinct kinetics.....	Appendix
Table S2. Statistics of RNA-seq data.....	Appendix
Table S3. TFM Explorer results.....	Appendix
Table S4. miR-27a Sequences from total RNA and Ago2-IP used to generate Figure 14D.....	Appendix
Table S5. miR-27b Sequences from total RNA and Ago2-IP used to generate Figure 14D.....	Appendix
Table S6. Modifications (Tailing/Trimming) of miR-27a and b sequences in total RNA and Ago2-IP.....	Appendix

List of abbreviations

4sU	4-thiouridine
Act-D	Actinomycin D
Ago	Argonaute protein
AP-1	activator protein 1
AP-4	activator protein 4
Aurkb	aurora kinase b
BAC	bacterial artificial chromosome
Bp	base pair
BrdU	Bromdesoxyuridin
BSA	bovine serum albumin
Bub1	budding uninhibited by benzimidazoles 1
CDKN1	cyclin-dependent kinase inhibitor 1
cDNA	complementary DNA
CDS	coding sequence
C/EBP	CCAAT/enhancer-binding-protein
ChIP	chromatin immunoprecipitation
CMV	Cytomegalovirus
DAPI	4',6-diamidino-2-phenylindole
dATP	desoxyadenosintriphosphat

List of abbreviations

DMEM	Dulbecco's Modified Eagle's Medium
DPBS	Dulbecco's Phosphate-Buffered Saline
DTT	dithiothreitol
EDTA	ethylenediaminetetraacetic acid
Elk-1	E twenty-six (ETS)-like transcription factor 1
ER	endoplasmatic reticulum
ERF	ethylene-responsive element-binding factor
Esp11	extra spindle pole bodies homolog 1
FOXO1	forkhead box protein O1
g	gram
Gadd45a	Growth arrest and DNA-damage-inducible protein alpha
GAPDH	glyceraldehyde-3-phosphate dehydrogenase
GEO	Gene expression Omnibus
GO	gene ontology
H	hour
HCl	hydrogen chloride
HCMV	human Cytomegalovirus
Herpud1	homocysteine-responsive endoplasmic reticulum- resident ubiquitin-like domain member 1 protein
hpi	hours post infection
IE	immediate early

List of abbreviations

Ifit1	interferon-induced protein with tetratricopeptide repeats1
IP	immunoprecipitation
IRF1	interferon regulatory factor 1
ISRE	IFN-stimulated response elements
IκBα	nuclear factor of kappa light polypeptide gene enhancer in B-cells inhibitor, alpha
JAK-STAT	janus kinase- signal transducer and activator of transcription
J	joul
Kcal	kilocalorie
Kb	kilo base pair
KCl	potassium chloride
Lamb1-1	Llminin, beta 1
Lbr	lamin b receptor
mA	milliampere
MCMV	murine Cytomegalovirus
mfe	mean free energy
MEF	murine embryonic fibroblast
MIEP	major immediate early promoter
min	minute
mRNA	messenger RNA

List of abbreviations

miRNA	microRNA
ml	milliliter
mpi	minutes post infection
MOI	multiplicity of infection
Mzf1	myeloid zinc finger 1
μ Ci	microCurie
μ g	microgram
μ l	microliter
μ M	micromolar
n	number
NaCl	sodium chloride
NaF	sodium fluoride
ND	nuclear domain
NF- κ B	nuclear factor of kappa light polypeptide gene
NF- κ B α	nuclear factor of kappa light polypeptide gene
E	enhancer in B-cells inhibitor, alpha
ng	nanogram
nm	nanometer
nM	nanomolar
nt	nucleotide
o/n	overnight

List of abbreviations

ORF	open reading frame
PAR-CLIP	Photoactivatable-Ribonucleoside-Enhanced Crosslinking and Immunoprecipitation
PBS	Phosphate-Buffered Saline
piRNA	piwiRNA
Pol	polymerase
PPR	proximal promoter region
pRB	retinoblastoma protein
PRRs	pattern recognition receptors
qRT-PCR	quantitative real-time PCR
rpm	rounds per minutes
RISC	RNA-induced silencing complex
RMA	Robust Multichip Average
RNA-Seq	RNA-Sequencing
RT	room temperature
SCP	small capsid protein
SD	standard derivation
SDS	sodium dodecyl sulfate
SP-1	Specificity Protein 1
TF	transcription factor
TFBs	transcription factor binding site

List of abbreviations

TFM	transcription factor matrix
Top2 α	topoisomerase (DNA) II alpha
TSS	transcription start site
UTR	untranslated region
UV	ultra violett
wt	wild type
w/v	weight/volume
YY1	ying yang protein 1

References

1. Roizman B, Carmichael LE, Deinhardt F, De-The G, Nahmias AJ, et al. (1981) Herpesviridae. Definition, provisional nomenclature, and taxonomy. The Herpesvirus Study Group, the International Committee on Taxonomy of Viruses. *Intervirology* 16: 201–217.
2. Mocarski E, Shenk T, Pass R (2007) Cytomegaloviruses. In: Knipe DM, Howley PM, editors *Fields Virology*, Vol2, pp 2701-2772 Lippincott Williams & Wilkins, Philadelphia.
3. Radtke K, Döhner K, Sodeik B (2006) Viral interactions with the cytoskeleton: a hitchhiker's guide to the cell. *Cellular microbiology* 8: 387–400.
4. Mettenleiter TC, Klupp BG, Granzow H (2009) Herpesvirus assembly: an update. *Virus research* 143: 222–234.
5. Sinclair J, Sissons P (2006) Latency and reactivation of human cytomegalovirus. *The Journal of general virology* 87: 1763–1779.
6. Roizman B, Knipe DM, Whitley RJ (n.d.) Herpes Simplex Viruses. In: Knipe DM, Howley PM, editors *Fields Virology*, Vol2, pp 2501-2602 Lippincott Williams & Wilkins, Philadelphia.
7. Paulus C, Nevels M (2009) The human cytomegalovirus major immediate-early proteins as antagonists of intrinsic and innate antiviral host responses. *Viruses* 1: 760–779.
8. Stinski MF, Isomura H (2008) Role of the cytomegalovirus major immediate early enhancer in acute infection and reactivation from latency. *Medical microbiology and immunology* 197: 223–231.
9. Wright E, Bain M, Teague L, Murphy J, Sinclair J (2005) Ets-2 repressor factor recruits histone deacetylase to silence human cytomegalovirus immediate-early gene expression in non-permissive cells. *The Journal of general virology* 86: 535–544.
10. Weill L, Shestakova E, Bonnefoy E (2003) Transcription factor YY1 binds to the murine beta interferon promoter and regulates its transcriptional capacity with a dual activator/repressor role. *Journal of virology* 77: 2903–2914.
11. Ioudinkova E, Arcangeletti MC, Rynditch A, De Conto F, Motta F, et al. (2006) Control of human cytomegalovirus gene expression by differential histone modifications during lytic and latent infection of a monocytic cell line. *Gene* 384: 120–128.
12. Murphy JC, Fischle W, Verdin E, Sinclair JH (2002) Control of cytomegalovirus lytic gene expression by histone acetylation. *The EMBO journal* 21: 1112–1120.
13. Wathen MW, Stinski MF (1982) Temporal patterns of human cytomegalovirus transcription: mapping the viral RNAs synthesized at immediate early, early, and late times after infection. *Journal of virology* 41: 462–477.
14. Lukac DM, Manuppello JR, Alwine JC (1994) Transcriptional activation by the human cytomegalovirus immediate-early proteins: requirements for simple promoter structures and interactions with multiple components of the transcription complex. *Journal of virology* 68: 5184–5193.
15. Compton T, Feire A (2007) Early events in human cytomegalovirus infection. In: Arvin A, Campadelli-Fiume G, Mocarski E, Moore PS, Roizman B, Whitley R, Yamanishi K, editors *Source Human Herpesviruses: Biology, Therapy, and Immunoprophylaxis* Cambridge: Cambridge University Press; 2007 Chapter 16.
16. Anders D, Kerry J (2007) DNA synthesis and late viral gene expression. In: Arvin A, Campadelli-Fiume G, Mocarski E, Moore PS, Roizman B, Whitley R, Yamanishi K,

- editors Source Human Herpesviruses: Biology, Therapy, and Immunoprophylaxis Cambridge: Cambridge University Press; 2007 Chapter 16.
17. Isaacson MK, Juckem LK, Compton T (2008) Virus entry and innate immune activation. *Current topics in microbiology and immunology* 325: 85–100.
 18. Browne EP, Wing B, Coleman D, Shenk T (2001) Altered cellular mRNA levels in human cytomegalovirus-infected fibroblasts: viral block to the accumulation of antiviral mRNAs. *J Virol* 75: 12319–12330.
 19. Montag C, Wagner J, Gruska I, Hagemeyer C (2006) Human cytomegalovirus blocks tumor necrosis factor alpha- and interleukin-1beta-mediated NF-kappaB signaling. *Journal of virology* 80: 11686–11698.
 20. Fliss PM, Jowers TP, Brinkmann MM, Holstermann B, Mack C, et al. (2012) Viral Mediated Redirection of NEMO/IKK γ to Autophagosomes Curtails the Inflammatory Cascade. *PLoS Pathogens* 8: e1002517.
 21. Stinski MF, Isomura H (2008) Role of the cytomegalovirus major immediate early enhancer in acute infection and reactivation from latency. *Medical microbiology and immunology* 197: 223–231.
 22. Caposio P, Lugini A, Bronzini M, Landolfo S, Gribaudo G (2010) The Elk-1 and serum response factor binding sites in the major immediate-early promoter of human cytomegalovirus are required for efficient viral replication in quiescent cells and compensate for inactivation of the NF-kappaB sites in proliferating cells. *Journal of virology* 84: 4481–4493.
 23. Liu R, Baillie J, Sissons JG, Sinclair JH (1994) The transcription factor YY1 binds to negative regulatory elements in the human cytomegalovirus major immediate early enhancer/promoter and mediates repression in non-permissive cells. *Nucleic acids research* 22: 2453–2459.
 24. Sambucetti LC, Cherrington JM, Wilkinson GW, Mocarski ES (1989) NF-kappa B activation of the cytomegalovirus enhancer is mediated by a viral transactivator and by T cell stimulation. *The EMBO journal* 8: 4251–4258.
 25. Netterwald J, Yang S, Wang W, Ghanny S, Cody M, et al. (2005) Two gamma interferon-activated site-like elements in the human cytomegalovirus major immediate-early promoter/enhancer are important for viral replication. *Journal of virology* 79: 5035–5046.
 26. Wiebusch L, Hagemeyer C (1999) Human cytomegalovirus 86-kilodalton IE2 protein blocks cell cycle progression in G(1). *Journal of virology* 73: 9274–9283.
 27. Hertel L, Chou S, Mocarski ES (2007) Viral and cell cycle-regulated kinases in cytomegalovirus-induced pseudomitosis and replication. *PLoS pathogens* 3: e6.
 28. Jault FM, Jault JM, Ruchti F, Fortunato EA, Clark C, et al. (1995) Cytomegalovirus infection induces high levels of cyclins, phosphorylated Rb, and p53, leading to cell cycle arrest. *Journal of virology* 69: 6697–6704.
 29. Gaspar M, Shenk T (2006) Human cytomegalovirus inhibits a DNA damage response by mislocalizing checkpoint proteins. *Proceedings of the National Academy of Sciences of the United States of America* 103: 2821–2826.
 30. Goldmacher VS, Bartle LM, Skaletskaya A, Dionne CA, Kedersha NL, et al. (1999) A cytomegalovirus-encoded mitochondria-localized inhibitor of apoptosis structurally unrelated to Bcl-2. *Proceedings of the National Academy of Sciences of the United States of America* 96: 12536–12541.
 31. Skaletskaya A, Bartle LM, Chittenden T, McCormick AL, Mocarski ES, et al. (2001) A cytomegalovirus-encoded inhibitor of apoptosis that suppresses caspase-8 activation. *Proceedings of the National Academy of Sciences of the United States of America* 98: 7829–7834.

32. Brune W, Nevels M, Shenk T (2003) Murine cytomegalovirus m41 open reading frame encodes a Golgi-localized antiapoptotic protein. *Journal of virology* 77: 11633–11643.
33. Friedel CC, Dölken L (2009) Metabolic tagging and purification of nascent RNA: implications for transcriptomics. *Molecular bioSystems* 5: 1271–1278.
34. Raghavan A, Ogilvie RL, Reilly C, Abelson ML, Raghavan S, et al. (2002) Genome-wide analysis of mRNA decay in resting and activated primary human T lymphocytes. *Nucleic acids research* 30: 5529–5538.
35. Wang Y, Liu CL, Storey JD, Tibshirani RJ, Herschlag D, et al. (2002) Precision and functional specificity in mRNA decay. *Proceedings of the National Academy of Sciences of the United States of America* 99: 5860–5865.
36. Dölken L, Ruzsics Z, Rädle B, Friedel CC, Zimmer R, et al. (2008) High-resolution gene expression profiling for simultaneous kinetic parameter analysis of RNA synthesis and decay. *RNA (New York, NY)* 14: 1959–1972. doi:10.1261/rna.1136108.
37. Miller MR, Robinson KJ, Cleary MD, Doe CQ (2009) TU-tagging: cell type-specific RNA isolation from intact complex tissues. *Nature methods* 6: 439–441.
38. Rabani M, Levin JZ, Fan L, Adiconis X, Raychowdhury R, et al. (2011) Metabolic labeling of RNA uncovers principles of RNA production and degradation dynamics in mammalian cells. *Nature biotechnology* 29: 436–442.
39. Miller C, Schwab B, Maier K, Schulz D, Dümcke S, et al. (2011) Dynamic transcriptome analysis measures rates of mRNA synthesis and decay in yeast. *Molecular systems biology* 7: 458.
40. Friedel CC, Dölken L, Ruzsics Z, Koszinowski UH, Zimmer R (2009) Conserved principles of mammalian transcriptional regulation revealed by RNA half-life. *Nucleic acids research* 37: e115.
41. Bartel DP (2009) MicroRNAs: target recognition and regulatory functions. *Cell* 136: 215–233.
42. Kozomara A, Griffiths-Jones S (2011) miRBase: integrating microRNA annotation and deep-sequencing data. *Nucleic acids research* 39: D152–D157.
43. Friedman RC, Farh KK-H, Burge CB, Bartel DP (2009) Most mammalian mRNAs are conserved targets of microRNAs. *Genome research* 19: 92–105.
44. Carthew RW, Sontheimer EJ (2009) Origins and Mechanisms of miRNAs and siRNAs. *Cell* 136: 642–655.
45. Chendrimada TP, Gregory RI, Kumaraswamy E, Norman J, Cooch N, et al. (2005) TRBP recruits the Dicer complex to Ago2 for microRNA processing and gene silencing. *Nature* 436: 740–744.
46. Cullen BR (2004) Transcription and processing of human microRNA precursors. *Molecular cell* 16: 861–865.
47. Fabian MR, Sonenberg N, Filipowicz W (2010) Regulation of mRNA translation and stability by microRNAs. *Annual review of biochemistry* 79: 351–379.
48. Kim J, Inoue K, Ishii J, Vanti WB, Voronov SV, et al. (2007) A MicroRNA feedback circuit in midbrain dopamine neurons. *Science (New York, NY)* 317: 1220–1224.
49. Paroo Z, Ye X, Chen S, Liu Q (2009) Phosphorylation of the human microRNA-generating complex mediates MAPK/Erk signaling. *Cell* 139: 112–122.
50. Hagan JP, Piskounova E, Gregory RI (2009) Lin28 recruits the TUTase Zcchc11 to inhibit let-7 maturation in mouse embryonic stem cells. *Nature structural & molecular biology* 16: 1021–1025.
51. Li J, Yang Z, Yu B, Liu J, Chen X (2005) Methylation protects miRNAs and siRNAs from a 3'-end uridylation activity in Arabidopsis. *Current biology* □: CB 15: 1501–1507.

52. Johnston M, Geoffroy M-C, Sobala A, Hay R, Hutvagner G (2010) HSP90 protein stabilizes unloaded argonaute complexes and microscopic P-bodies in human cells. *Molecular biology of the cell* 21: 1462–1469.
53. Pfeffer S, Zavolan M, Grässer FA, Chien M, Russo JJ, et al. (2004) Identification of virus-encoded microRNAs. *Science (New York, NY)* 304: 734–736.
54. Grey F, Antoniewicz A, Allen E, Saugstad J, McShea A, et al. (2005) Identification and characterization of human cytomegalovirus-encoded microRNAs. *Journal of virology* 79: 12095–12099.
55. Tang S, Bertke AS, Patel A, Wang K, Cohen JI, et al. (2008) An acutely and latently expressed herpes simplex virus 2 viral microRNA inhibits expression of ICP34.5, a viral neurovirulence factor. *Proceedings of the National Academy of Sciences of the United States of America* 105: 10931–10936.
56. Pfeffer S, Sewer A, Lagos-Quintana M, Sheridan R, Sander C, et al. (2005) Identification of microRNAs of the herpesvirus family. *Nature methods* 2: 269–276.
57. Umbach JL, Kramer MF, Jurak I, Karnowski HW, Coen DM, et al. (2008) MicroRNAs expressed by herpes simplex virus 1 during latent infection regulate viral mRNAs. *Nature* 454: 780–783.
58. Dölken L, Perot J, Cognat V, Alioua A, John M, et al. (2007) Mouse cytomegalovirus microRNAs dominate the cellular small RNA profile during lytic infection and show features of posttranscriptional regulation. *Journal of virology* 81: 13771–13782.
59. Tuddenham L, Jung JS, Chane-Woon-Ming B, Dölken L, Pfeffer S (2012) Small RNA deep sequencing identifies microRNAs and other small noncoding RNAs from human herpesvirus 6B. *Journal of virology* 86: 1638–1649.
60. Dölken L, Malterer G, Erhard F, Kothe S, Friedel CC, et al. (2010) Systematic analysis of viral and cellular microRNA targets in cells latently infected with human gamma-herpesviruses by RISC immunoprecipitation assay. *Cell host & microbe* 7: 324–334.
61. Dölken L, Krmpotic A, Kothe S, Tuddenham L, Tanguy M, et al. (2010) Cytomegalovirus microRNAs facilitate persistent virus infection in salivary glands. *PLoS pathogens* 6: e1001150.
62. Umbach JL, Kramer MF, Jurak I, Karnowski HW, Coen DM, et al. (2008) MicroRNAs expressed by herpes simplex virus 1 during latent infection regulate viral mRNAs. *Nature* 454: 780–783.
63. Skalsky RL, Corcoran DL, Gottwein E, Frank CL, Kang D, et al. (2012) The viral and cellular microRNA targetome in lymphoblastoid cell lines. *PLoS pathogens* 8: e1002484.
64. Gottwein E, Corcoran DL, Mukherjee N, Skalsky RL, Hafner M, et al. (2011) Viral microRNA targetome of KSHV-infected primary effusion lymphoma cell lines. *Cell host & microbe* 10: 515–526.
65. Suffert G, Malterer G, Hausser J, Viiliäinen J, Fender A, et al. (2011) Kaposi's sarcoma herpesvirus microRNAs target caspase 3 and regulate apoptosis. *PLoS pathogens* 7: e1002405.
66. Nachmani D, Stern-Ginossar N, Sarid R, Mandelboim O (2009) Diverse herpesvirus microRNAs target the stress-induced immune ligand MICB to escape recognition by natural killer cells. *Cell host & microbe* 5: 376–385.
67. Stern-Ginossar N, Elefant N, Zimmermann A, Wolf DG, Saleh N, et al. (2007) Host immune system gene targeting by a viral miRNA. *Science (New York, NY)* 317: 376–381.
68. Grey F, Meyers H, White EA, Spector DH, Nelson J (2007) A human cytomegalovirus-encoded microRNA regulates expression of multiple viral genes involved in replication. *PLoS pathogens* 3: e163.

69. Wang F-Z, Weber F, Croce C, Liu C-G, Liao X, et al. (2008) Human cytomegalovirus infection alters the expression of cellular microRNA species that affect its replication. *Journal of virology* 82: 9065–9074.
70. Buck AH, Perot J, Chisholm MA, Kumar DS, Tuddenham L, et al. (2010) Post-transcriptional regulation of miR-27 in murine cytomegalovirus infection. *RNA* (New York, NY) 16: 307–315.
71. Cazalla D, Yario T, Steitz JA, Steitz J (2010) Down-regulation of a host microRNA by a Herpesvirus saimiri noncoding RNA. *Science* (New York, NY) 328: 1563–1566.
72. Mocarski E, Shenk T, Pass R (2007) Cytomegaloviruses. In: Knipe DM, Howley PM, editors *Fields Virology*, Vol2, pp 2701-2772 Lippincott Williams & Wilkins, Philadelphia. Available:about:blank. Accessed 25 January 2012.
73. Yurochko AD, Hwang ES, Rasmussen L, Keay S, Pereira L, et al. (1997) The human cytomegalovirus UL55 (gB) and UL75 (gH) glycoprotein ligands initiate the rapid activation of Sp1 and NF-kappaB during infection. *Journal of virology* 71: 5051–5059.
74. Simmen K a, Singh J, Luukkonen BG, Lopper M, Bittner A, et al. (2001) Global modulation of cellular transcription by human cytomegalovirus is initiated by viral glycoprotein B. *Proceedings of the National Academy of Sciences of the United States of America* 98: 7140–7145.
75. Browne EP, Shenk T (2003) Human cytomegalovirus UL83-coded pp65 virion protein inhibits antiviral gene expression in infected cells. *Proceedings of the National Academy of Sciences of the United States of America* 100: 11439–11444.
76. Zhu H, Cong JP, Mamtora G, Gingeras T, Shenk T (1998) Cellular gene expression altered by human cytomegalovirus: global monitoring with oligonucleotide arrays. *Proceedings of the National Academy of Sciences of the United States of America* 95: 14470–14475.
77. Kenzelmann M, Muhlemann K (2000) Transcriptome analysis of fibroblast cells immediate-early after human cytomegalovirus infection. *J MolBiol* 304: 741–751.
78. Simmen KA, Singh J, Luukkonen BG, Lopper M, Bittner A, et al. (2001) Global modulation of cellular transcription by human cytomegalovirus is initiated by viral glycoprotein B. *ProcNatlAcadSciUSA* 98: 7140–7145.
79. Hertel L, Mocarski ES (2004) Global analysis of host cell gene expression late during cytomegalovirus infection reveals extensive dysregulation of cell cycle gene expression and induction of Pseudomitosis independent of US28 function. *J Virol* 78: 11988–12011.
80. Challacombe JF, Rechtsteiner A, Gottardo R, Rocha LM, Browne EP, et al. (2004) Evaluation of the host transcriptional response to human cytomegalovirus infection. *Physiological genomics* 18: 51–62. doi:10.1152/physiolgenomics.00155.2003.
81. Ishov AM, Maul GG (1996) The periphery of nuclear domain 10 (ND10) as site of DNA virus deposition. *The Journal of cell biology* 134: 815–826.
82. Maul GG (1998) Nuclear domain 10, the site of DNA virus transcription and replication. *BioEssays* □: news and reviews in molecular, cellular and developmental biology 20: 660–667.
83. Everett RD, Chelbi-Alix MK (n.d.) PML and PML nuclear bodies: implications in antiviral defence. *Biochimie* 89: 819–830.
84. Wu WS, Vallian S, Seto E, Yang WM, Edmondson D, et al. (2001) The growth suppressor PML represses transcription by functionally and physically interacting with histone deacetylases. *Molecular and cellular biology* 21: 2259–2268.
85. Li H, Chen JD (2000) PML and the oncogenic nuclear domains in regulating transcriptional repression. *Current opinion in cell biology* 12: 641–644.
86. Hollenbach AD, McPherson CJ, Mientjes EJ, Iyengar R, Grosveld G (2002) Daxx and histone deacetylase II associate with chromatin through an interaction with core

- histones and the chromatin-associated protein Dek. *Journal of cell science* 115: 3319–3330.
87. Hofmann H, Sindre H, Stamminger T (2002) Functional interaction between the pp71 protein of human cytomegalovirus and the PML-interacting protein human Daxx. *Journal of virology* 76: 5769–5783.
 88. Ishov AM, Vladimirova OV, Maul GG (2002) Daxx-mediated accumulation of human cytomegalovirus tegument protein pp71 at ND10 facilitates initiation of viral infection at these nuclear domains. *Journal of virology* 76: 7705–7712.
 89. Tang Q, Maul GG (2003) Mouse Cytomegalovirus Immediate-Early Protein 1 Binds with Host Cell Repressors To Relieve Suppressive Effects on Viral Transcription and Replication during Lytic Infection. *Journal of virology* 77: 1357–1367.
 90. Maul GG, Negorev D (2008) Differences between mouse and human cytomegalovirus interactions with their respective hosts at immediate early times of the replication cycle. *Medical microbiology and immunology* 197: 241–249.
 91. Marchini A, Liu H, Zhu H (2001) Human cytomegalovirus with IE-2 (UL122) deleted fails to express early lytic genes. *Journal of virology* 75: 1870–1878.
 92. Heider JA, Bresnahan WA, Shenk TE (2002) Construction of a rationally designed human cytomegalovirus variant encoding a temperature-sensitive immediate-early 2 protein. *Proceedings of the National Academy of Sciences of the United States of America* 99: 3141–3146.
 93. Sciortino M-teresa, Suzuki M, Taddeo B, Roizman B (2001) RNAs Extracted from Herpes Simplex Virus 1 Virions: Apparent Selectivity of Viral but Not Cellular RNAs Packaged in Virions. *Society* 75: 8105–8116. doi:10.1128/JVI.75.17.8105.
 94. Sarcinella E, Brown M, Tellier R, Petric M, Mazzulli T (2004) Detection of RNA in purified cytomegalovirus virions. *Virus research* 104: 129–137.
 95. Terhune SS, Shenk T (2004) RNAs Are Packaged into Human Cytomegalovirus Virions in Proportion to Their Intracellular Concentration. *Society* 78: 10390–10398. doi:10.1128/JVI.78.19.10390.
 96. Bechtel J, Grundhoff A, Ganem D (2005) RNAs in the virion of Kaposi's sarcoma-associated herpesvirus. *Journal of virology* 79: 10138–10146.
 97. Groves IJ, Reeves MB, Sinclair JH (2009) Lytic infection of permissive cells with human cytomegalovirus is regulated by an intrinsic “pre-immediate-early” repression of viral gene expression mediated by histone post-translational modification. *The Journal of general virology* 90: 2364–2374.
 98. Cuevas-Bennett C, Shenk T (2008) Dynamic histone H3 acetylation and methylation at human cytomegalovirus promoters during replication in fibroblasts. *Journal of virology* 82: 9525–9536.
 99. Nevels M, Paulus C, Shenk T (2004) Human cytomegalovirus immediate-early 1 protein facilitates viral replication by antagonizing histone deacetylation. *Proceedings of the National Academy of Sciences of the United States of America* 101: 17234–17239.
 100. Yang E, Van NE, Zavolan M, Rajewsky N, Schroeder M, et al. (2003) Decay rates of human mRNAs: correlation with functional characteristics and sequence attributes. *Genome Res* 13: 1863–1872.
 101. Bresnahan WA, Shenk T (2000) A subset of viral transcripts packaged within human cytomegalovirus particles. *Science* 288: 2373–2376.
 102. Schwanhäusser B, Busse D, Li N, Dittmar G, Schuchhardt J, et al. (2011) Global quantification of mammalian gene expression control. *Nature* 473: 337–342.
 103. Rupp B, Ruzsics Z, Sacher T, Koszinowski UH (2005) Conditional cytomegalovirus replication in vitro and in vivo. *Journal of virology* 79: 486–494.

104. R Development Core Team (2007) A language and environment for statistical computing. ISBN 3-900051-07-0 [http://wwwR-project.org](http://www.R-project.org) 2007.
105. Benjamini Y, Hochberg Y (2007) Controlling the False Discovery Rate: A Practical and Powerful Approach to Multiple Testing.
106. Defrance M, Touzet H (2006) Predicting transcription factor binding sites using local over-representation and comparative genomics. *BMC bioinformatics* 7: 396.
107. Munger J, Bajad SU, Coller H a, Shenk T, Rabinowitz JD (2006) Dynamics of the cellular metabolome during human cytomegalovirus infection. *PLoS pathogens* 2: e132. doi:10.1371/journal.ppat.0020132.
108. Kenzelmann M, Maertens S, Hergenahm M, Kueffer S, Hotz-Wagenblatt A, et al. (2007) Microarray analysis of newly synthesized RNA in cells and animals. *Proc Natl Acad Sci USA* 104: 6164–6169.
109. Griboaud G, Ravaglia S, Guandalini L, Cavallo R, Gariglio M, et al. (1996) The murine cytomegalovirus immediate-early 1 protein stimulates NF-kappa B activity by transactivating the NF-kappa B p105/p50 promoter. *Virus research* 45: 15–27.
110. Mack C, Sickmann A, Lembo D, Brune W (2008) Inhibition of proinflammatory and innate immune signaling pathways by a cytomegalovirus RIP1-interacting protein. *Proceedings of the National Academy of Sciences of the United States of America* 105: 3094–3099.
111. Gilmore TD (2006) Introduction to NF-kappaB: players, pathways, perspectives. *Oncogene* 25: 6680–6684.
112. Dang CV, Resar LM, Emison E, Kim S, Li Q, et al. (1999) Function of the c-Myc oncogenic transcription factor. *Experimental cell research* 253: 63–77.
113. Grandori C, Cowley SM, James LP, Eisenman RN (2000) The Myc/Max/Mad network and the transcriptional control of cell behavior. *Annual review of cell and developmental biology* 16: 653–699.
114. Gupta S, Seth A, Davis RJ (1993) Transactivation of gene expression by Myc is inhibited by mutation at the phosphorylation sites Thr-58 and Ser-62. *Proceedings of the National Academy of Sciences of the United States of America* 90: 3216–3220.
115. Hagemeyer C, Walker SM, Sissons PJG, Sinclair JH (1992) The 72K IE1 and 80K IE2 proteins of human cytomegalovirus independently trans-activate the c-fos, c-myc and hsp70 promoters via basal promoter elements. *Journal of General Virology* 73: 2385–2393.
116. Le VTK, Trilling M, Zimmermann A, Hengel H (2008) Mouse cytomegalovirus inhibits beta interferon (IFN-beta) gene expression and controls activation pathways of the IFN-beta enhanceosome. *The Journal of general virology* 89: 1131–1141. doi:10.1099/vir.0.83538-0.
117. Hollander MC, Alamo I, Jackman J, Wang MG, McBride OW, et al. (1993) Analysis of the mammalian gadd45 gene and its response to DNA damage. *The Journal of biological chemistry* 268: 24385–24393.
118. Smith GB, Mocarski ES (2005) Contribution of GADD45 family members to cell death suppression by cellular Bcl-xL and cytomegalovirus vMIA. *Journal of virology* 79: 14923–14932.
119. Kokame K, Agarwala KL, Kato H, Miyata T (2000) Herp, a new ubiquitin-like membrane protein induced by endoplasmic reticulum stress. *The Journal of biological chemistry* 275: 32846–32853.
120. Qian Z, Xuan B, Gualberto N, Yu D (2011) HCMV protein pUL38 suppresses ER stress-mediated cell death independent of its ability to induce mTORC1 activation. *Journal of virology* 85: 9103–9113.
121. Timpl R, Brown JC (1994) The laminins. *Matrix biology*: journal of the International Society for Matrix Biology 14: 275–281.

122. Wang JC (1996) DNA topoisomerases. *Annual review of biochemistry* 65: 635–692.
123. Scrivano L, Esterlechner J, Mühlbach H, Ettischer N, Hagen C, et al. (2010) The m74 gene product of murine cytomegalovirus (MCMV) is a functional homolog of human CMV gO and determines the entry pathway of MCMV. *Journal of virology* 84: 4469–4480.
124. Popa M, Ruzsics Z, Lötzerich M, Dölken L, Buser C, et al. (2010) Dominant negative mutants of the murine cytomegalovirus M53 gene block nuclear egress and inhibit capsid maturation. *Journal of virology* 84: 9035–9046.
125. MacDonald MR, Burney MW, Resnick SB, Virgin HW IV (1999) Spliced mRNA encoding the murine cytomegalovirus chemokine homolog predicts a beta chemokine of novel structure. *Journal of virology* 73: 3682–3691.
126. Maninger S, Bosse JB, Lemnitzer F, Pogoda M, Mohr CA, et al. (2011) M94 is essential for the secondary envelopment of murine cytomegalovirus. *Journal of virology* 85: 9254–9267.
127. Fleming P, Davis-Poynter N, Degli-Esposti M, Densley E, Papadimitriou J, et al. (1999) The murine cytomegalovirus chemokine homolog, m131/129, is a determinant of viral pathogenicity. *Journal of virology* 73: 6800–6809.
128. Akter P, Cunningham C, McSharry BP, Dolan A, Addison C, et al. (2003) Two novel spliced genes in human cytomegalovirus. *The Journal of general virology* 84: 1117–1122.
129. Babić M, Krmpotić A, Jonjić S (2011) All is fair in virus-host interactions: NK cells and cytomegalovirus. *Trends in molecular medicine* 17: 677–685.
130. Dimova DK, Dyson NJ (2005) The E2F transcriptional network: old acquaintances with new faces. *Oncogene* 24: 2810–2826.
131. Attwooll C, Lazzerini Denchi E, Helin K (2004) The E2F family: specific functions and overlapping interests. *The EMBO journal* 23: 4709–4716.
132. Schmit F, Korenjak M, Mannefeld M, Schmitt K, Franke C, et al. (2007) LINC, a human complex that is related to pRB-containing complexes in invertebrates regulates the expression of G2/M genes. *Cell cycle (Georgetown, Tex)* 6: 1903–1913.
133. Knight AS, Notaridou M, Watson RJ (2009) A Lin-9 complex is recruited by B-Myb to activate transcription of G2/M genes in undifferentiated embryonal carcinoma cells. *Oncogene* 28: 1737–1747.
134. Kalejta RF, Bechtel JT, Shenk T (2003) Human cytomegalovirus pp71 stimulates cell cycle progression by inducing the proteasome-dependent degradation of the retinoblastoma family of tumor suppressors. *Molecular and cellular biology* 23: 1885–1895.
135. Kalejta RF, Shenk T (2003) Proteasome-dependent, ubiquitin-independent degradation of the Rb family of tumor suppressors by the human cytomegalovirus pp71 protein. *Proceedings of the National Academy of Sciences of the United States of America* 100: 3263–3268.
136. Song YJ, Stinski MF (2002) Effect of the human cytomegalovirus IE86 protein on expression of E2F-responsive genes: a DNA microarray analysis. *Proc Natl Acad Sci USA* 99: 2836–2841.
137. Wiebusch L, Neuwirth A, Grabenhenrich L, Voigt S, Hagemeyer C (2008) Cell cycle-independent expression of immediate-early gene 3 results in G1 and G2 arrest in murine cytomegalovirus-infected cells. *J Virol* 82: 10188–10198.
138. Wathen MW, Stinski MF (1982) Temporal patterns of human cytomegalovirus transcription: mapping the viral RNAs synthesized at immediate early, early, and late times after infection. *Journal of virology* 41: 462–477.
139. Geballe AP, Mocarski ES (1988) Translational control of cytomegalovirus gene expression is mediated by upstream AUG codons. *Journal of virology* 62: 3334–3340.

140. Geballe AP, Spaete RR, Mocarski ES (1986) A cis-acting element within the 5' leader of a cytomegalovirus beta transcript determines kinetic class. *Cell* 46: 865–872.
141. Sinclair J (n.d.) Chromatin structure regulates human cytomegalovirus gene expression during latency, reactivation and lytic infection. *Biochimica et biophysica acta* 1799: 286–295.
142. Woodhall DL, Groves IJ, Reeves MB, Wilkinson G, Sinclair JH (2006) Human Daxx-mediated repression of human cytomegalovirus gene expression correlates with a repressive chromatin structure around the major immediate early promoter. *The Journal of biological chemistry* 281: 37652–37660.
143. Netterwald J, Yang S, Wang W, Ghanny S, Cody M, et al. (2005) Two gamma interferon-activated site-like elements in the human cytomegalovirus major immediate-early promoter/enhancer are important for viral replication. *Journal of virology* 79: 5035–5046.
144. Meier JL, Stinski MF (2006) Major immediate-early enhancer and its gene products. In: Reddehase, M J, editor *Cytomegaloviruses: Molecular Biology and Immunology* pp 151-166 Norfolk, UK: Caister Academic Press.
145. Krol J, Loedige I, Filipowicz W (2010) The widespread regulation of microRNA biogenesis, function and decay. *Nature reviews Genetics* 11: 597–610.
146. Kozomara A, Griffiths-Jones S (2011) miRBase: integrating microRNA annotation and deep-sequencing data. *Nucleic acids research* 39: D152–D157.
147. van Rooij E, Sutherland LB, Qi X, Richardson JA, Hill J, et al. (2007) Control of stress-dependent cardiac growth and gene expression by a microRNA. *Science (New York, NY)* 316: 575–579.
148. Hafner M, Landthaler M, Burger L, Khorshid M, Hausser J, et al. (2010) Transcriptome-wide identification of RNA-binding protein and microRNA target sites by PAR-CLIP. *Cell* 141: 129–141.
149. Konig J, Zarnack K, Rot G, Curk T, Kayikci M, et al. (2011) iCLIP--transcriptome-wide mapping of protein-RNA interactions with individual nucleotide resolution. *Journal of visualized experiments* □: JoVE.
150. Kishore S, Jaskiewicz L, Burger L, Hausser J, Khorshid M, et al. (2011) A quantitative analysis of CLIP methods for identifying binding sites of RNA-binding proteins. *Nature methods* 8: 559–564.
151. Hagan JP, Piskounova E, Gregory RI (2009) Lin28 recruits the TUTase Zcchc11 to inhibit let-7 maturation in mouse embryonic stem cells. *Nature structural & molecular biology* 16: 1021–1025.
152. Heo I, Joo C, Cho J, Ha M, Han J, et al. (2008) Lin28 mediates the terminal uridylation of let-7 precursor MicroRNA. *Molecular cell* 32: 276–284.
153. Lehrbach NJ, Armisen J, Lightfoot HL, Murfitt KJ, Bugaut A, et al. (2009) LIN-28 and the poly(U) polymerase PUP-2 regulate let-7 microRNA processing in *Caenorhabditis elegans*. *Nature structural & molecular biology* 16: 1016–1020.
154. Yang Z, Ebright YW, Yu B, Chen X (2006) HEN1 recognizes 21-24 nt small RNA duplexes and deposits a methyl group onto the 2' OH of the 3' terminal nucleotide. *Nucleic acids research* 34: 667–675.
155. Li J, Yang Z, Yu B, Liu J, Chen X (2005) Methylation protects miRNAs and siRNAs from a 3'-end uridylation activity in *Arabidopsis*. *Current biology* □: CB 15: 1501–1507.
156. Kirino Y, Mourelatos Z (2007) The mouse homolog of HEN1 is a potential methylase for Piwi-interacting RNAs. *RNA (New York, NY)* 13: 1397–1401.
157. Saito K, Sakaguchi Y, Suzuki T, Suzuki T, Siomi H, et al. (2007) Pimet, the *Drosophila* homolog of HEN1, mediates 2'-O-methylation of Piwi-interacting RNAs at their 3' ends. *Genes & development* 21: 1603–1608.

158. Ameres SL, Horwich MD, Hung J-H, Xu J, Ghildiyal M, et al. (2010) Target RNA-directed trimming and tailing of small silencing RNAs. *Science (New York, NY)* 328: 1534–1539.
159. Leung AKL, Sharp PA (2010) MicroRNA functions in stress responses. *Molecular cell* 40: 205–215.
160. Pfeffer S, Sewer A, Lagos-Quintana M, Sheridan R, Sander C, et al. (2005) Identification of microRNAs of the herpesvirus family. *Nature methods* 2: 269–276.
161. Lecellier C-H, Dunoyer P, Arar K, Lehmann-Che J, Eyquem S, et al. (2005) A cellular microRNA mediates antiviral defense in human cells. *Science (New York, NY)* 308: 557–560.
162. Cullen BR (2011) Viruses and microRNAs: RISCy interactions with serious consequences. *Genes & Development* 25: 1881–1894.
163. Otsuka M, Jing Q, Georgel P, New L, Chen J, et al. (2007) Hypersusceptibility to vesicular stomatitis virus infection in Dicer1-deficient mice is due to impaired miR24 and miR93 expression. *Immunity* 27: 123–134.
164. Santhakumar D, Forster T, Laqtom NN, Fragkoudis R, Dickinson P, et al. (2010) Combined agonist-antagonist genome-wide functional screening identifies broadly active antiviral microRNAs. *Proceedings of the National Academy of Sciences of the United States of America* 107: 13830–13835.
165. Wagner M, Koszinowski UH (2004) Mutagenesis of viral BACs with linear PCR fragments (ET recombination). *Methods in molecular biology (Clifton, NJ)* 256: 257–268.
166. Wagner M, Jonjic S, Koszinowski UH, Messerle M (1999) Systematic excision of vector sequences from the BAC-cloned herpesvirus genome during virus reconstitution. *Journal of virology* 73: 7056–7060.
167. Tischer BK, von Einem J, Kaufer B, Osterrieder N (2006) Two-step red-mediated recombination for versatile high-efficiency markerless DNA manipulation in *Escherichia coli*. *BioTechniques* 40: 191–197.
168. Jordan S, Krause J, Prager A, Mitrovic M, Jonjic S, et al. (2011) Virus progeny of murine cytomegalovirus bacterial artificial chromosome pSM3fr show reduced growth in salivary Glands due to a fixed mutation of MCK-2. *Journal of virology* 85: 10346–10353.
169. Leung AKL, Young AG, Bhutkar A, Zheng GX, Bosson AD, et al. (2011) Genome-wide identification of Ago2 binding sites from mouse embryonic stem cells with and without mature microRNAs. *Nature structural & molecular biology* 18: 237–244.
170. Pall GS, Hamilton AJ (2008) Improved northern blot method for enhanced detection of small RNA. *Nature protocols* 3: 1077–1084.
171. Pfeffer S (2007) Identification of virally encoded microRNAs. *Methods in enzymology* 427: 51–63.
172. Morgulis A, Gertz EM, Schäffer AA, Agarwala R (2006) A fast and symmetric DUST implementation to mask low-complexity DNA sequences. *Journal of computational biology*: a journal of computational molecular cell biology 13: 1028–1040.
173. Langmead B, Trapnell C, Pop M, Salzberg SL (2009) Ultrafast and memory-efficient alignment of short DNA sequences to the human genome. *Genome biology* 10: R25.
174. Brune W, Hengel H, Koszinowski UH (2001) A mouse model for cytomegalovirus infection. *Current protocols in immunology / edited by John E Coligan [et al] Chapter 19: Unit 19.7.*
175. Cobbold SP, Jayasuriya A, Nash A, Prospero TD, Waldmann H (n.d.) Therapy with monoclonal antibodies by elimination of T-cell subsets in vivo. *Nature* 312: 548–551.
176. Buck AH, Santoyo-Lopez J, Robertson KA, Kumar DS, Reczko M, et al. (2007) Discrete clusters of virus-encoded micrnas are associated with complementary

- strands of the genome and the 7.2-kilobase stable intron in murine cytomegalovirus. *Journal of virology* 81: 13761–13770.
177. Cicin-Sain L, Bubić I, Schnee M, Ruzsics Z, Mohr C, et al. (2007) Targeted deletion of regions rich in immune-evasive genes from the cytomegalovirus genome as a novel vaccine strategy. *Journal of virology* 81: 13825–13834.
 178. Rehmsmeier M, Steffen P, Hochsmann M, Giegerich R (2004) Fast and effective prediction of microRNA/target duplexes. *RNA (New York, NY)* 10: 1507–1517.
 179. Crooks GE, Hon G, Chandonia J-M, Brenner SE (2004) WebLogo: a sequence logo generator. *Genome research* 14: 1188–1190.
 180. Schneider TD, Stephens RM (1990) Sequence logos: a new way to display consensus sequences. *Nucleic acids research* 18: 6097–6100.
 181. Feng J, Iwama A, Satake M, Kohu K (2009) MicroRNA-27 enhances differentiation of myeloblasts into granulocytes by post-transcriptionally downregulating Runx1. *British journal of haematology* 145: 412–423.
 182. Lin Q, Gao Z, Alarcon RM, Ye J, Yun Z (2009) A role of miR-27 in the regulation of adipogenesis. *The FEBS journal* 276: 2348–2358.
 183. Zhou Q, Gallagher R, Ufret-Vincenty R, Li X, Olson EN, et al. (2011) Regulation of angiogenesis and choroidal neovascularization by members of microRNA-23~27~24 clusters. *Proceedings of the National Academy of Sciences of the United States of America* 108: 8287–8292.
 184. Myatt SS, Wang J, Monteiro LJ, Christian M, Ho K-K, et al. (2010) Definition of microRNAs that repress expression of the tumor suppressor gene FOXO1 in endometrial cancer. *Cancer research* 70: 367–377.
 185. Kalejta RF, Shenk T (2002) Manipulation of the cell cycle by human cytomegalovirus. *Frontiers in bioscience*: a journal and virtual library 7: d295–d306.
 186. Rissland OS, Hong S-J, Bartel DP (2011) MicroRNA Destabilization Enables Dynamic Regulation of the miR-16 Family in Response to Cell-Cycle Changes. *Molecular Cell* 43: 993–1004.